UNIVERSITY OF OKLAHOMA

GRADUATE COLLEGE

TARGETED GENE DELIVERY TO MESENCHYMAL STEM CELLS USING

NANOPARTICLES

A DISSERTATION

SUBMITTED TO THE GRADUATE FACULTY

in partial fulfillment of the requirements for the

Degree of

DOCTOR OF PHILOSOPHY

By

DONGDONG WANG
Norman, Oklahoma
2016

TARGETED GENE DELIVERY TO MESENCHYMAL STEM CELLS USING
NANOPARTICLES

A DISSERTATION APPROVED FOR THE
DEPARTMENT OF CHEMISTRY AND BIOCHEMISTRY

BY

_____
Dr. Chuanbin Mao, Chair

_____
Dr. Ann H. West

_____
Dr. Wai Tak Yip

_____
Dr. Charles V. Rice

_____
Dr. Scott D. Russell

Acknowledgements

I would like to thank Dr. Chuanbin Mao for his kind guidance and support during my Ph.D study. Dr. Mao has offered me great academic freedom to pursue my research interests and encouraged me to learn pragmatic research techniques. My research ideas and inspirations are full-blown in this lab and this research experience will greatly benefit me in the long run.

I would also like to express my sincere appreciation to my committee members Dr. Wai Tak Yip, Dr. Ann H. West, Dr. Scott D. Russell and Dr. Charles V. Rice for valuable suggestions, discussions and strong support for my continued study towards my Ph.D degree. Dr. Philip E. Klebba, Dr. Paul F. Cook, Dr. Binil Starly and Dr. Jun Li used to be my committee members and I would like to thanks them for kind support.

I also like to thank Gregory W. Strout, Dr. Preston Larson, Dr. Ben Smith and Scott D. Russell from Noble Electron Microscopy Laboratory (SRNEML) at University of Oklahoma (OU). Their patient training and guidance greatly assisted me in my research. Their excellent expertise and professional dedication set a good example for my future career.

Table of Contents

List of Tables

List of Figures

Chapter 3:

Abstract

Stem cells hold great potential for the regenerative medicine and tissue engineering. Controlling the fate of stem cell in a reliable method still remains a problem. The strategies for directing the fate of stem cells include biophysical cues (e.g. matrix stiffness, topography, and extracellular forces), biochemical cues (e.g. growth factors, cytokines and chemokines) and cellular reprogramming (e.g. gene delivery). Controlled delivery of specific genes, such as transcription factor encoding genes, to stem cells is a promising strategy for stem-cell based therapy.

Gene delivery methods include two major categories: viral vectors and non-viral vectors. Non-viral gene delivery vectors hold great promise for gene therapy due to the safety concerns with viral vectors. However, the application of non-viral vectors is hindered by their low transfection efficiency. Herein, in order to tackle this challenge, we endeavored to develop non-viral vectors with efficient gene delivery and low toxicity to hard-to-transfect MSCs.

First, we focused on the identification and characterization of novel MSCs-targeting peptides using phage libraries. A peptide (VTAMEPGQ) that can home to rat mesenchymal stem cells (rMSCs) was identified. This VTAMEPGQ peptide demonstrated high affinity and specificity to rMSCs.

When integrated into liposome protamine/DNA lipoplex (LPD) system, the peptide significantly enhanced gene transfection efficiency to rMSCs.

Second, we focused on developing efficiently and chemically-defined LPD-based gene delivery system to rMSCs. We employed three-folds reiterated VTAMEPGQ peptides, nuclear localization signal and liposome/protamine complex to delivery vascular endothelial growth factor (VEGF) reporter gene to rMSCs. The developed LPD gene delivery complex demonstrated high transfection efficiency and long-lasting gene expression profile.

Third, we developed Glutathione (GSH) cleavable magnetic/silica nanoclusters integrating MSC-homing major coat protein (pVIII) for targeted gene delivery. pVIII proteins were purified from the VTAMEPGQ-sequence bearing phage identified by phage display technique. The intracellular GSH is responsible for cleaving the S-S bond to dissociate the nanoclusters to release DNA. The as-synthesized gene delivery complex also showed satisfactory gene transfection result to rMSCs.

Finally, we studied the role of cell-binding peptides in directing the stem cell differentiation. We take advantage of the three peptides, which are selected by phage display and show different binding affinities against MSCs, to investigate the osteogenic differentiation of MSCs. Surprisingly,

we discovered that the peptide (VTAMEPGQ) with the highest MSC-binding affinity induced the osteogenic differentiation of MSCs most efficiently. We propose that the MSC-binding peptides may bind to the bone morphometric protein (BMP) receptors to initiate the osteogenic differentiation pathway.

Chapter 1　Introduction

1.1 Stem cell

Stem cells hold promising potential for the regeneration of injured, diseased and aged tissues. There are three main types of stem cells: embryonic stem cells (ESCs), induced pluripotent stem cells (iPSCs) and adult stem cells (ASCs). Embryonic stem cells, which are derived from inner cell mass of blastocysts, could differentiate to generate all three embryonic germ layers, that is, ectoderm, endoderm, and mesoderm[1,2]. Induced pluripotent stem cells, which have all the characteristics of embryonic stem cells, were first developed by introducing four defined factors into somatic fibroblast cells[3]. ESCs and iPSCs have unlimited self-renewal potential in culture, but the lack of reliable methods to pattern these cells into a tissue specific lineage limits their uses in clinics. iPSCs are extremely advantageous because they show high immune compatibility and avoid ethical issues faced by ESCs. Adult stem cells (for example mesenchymal stem cells) lack the plasticity of ESCs and iPSCs. However, ASCs can efficiently differentiate into specialized cell types.

1.1.1 Stem cell niche

In the body, adult stem cells reside in a special microenvironment termed the "niche," which supports and regulates stem cells to maintain tissue homeostasis. Extrinsic signals, including secreted factors, cell-cell interactions and ECM, regulate stem cell fate collectively. Transforming growth factor beta (TGF-β) superfamily, including TGF-β proteins, growth differentiation factors (GDFs) and bone morphogenetic proteins (BMPs), regulates various biological effects by binding to targeting cell surface receptors[4]. For example, bone morphogenetic protein 2 (BMP2) was demonstrated to induce the basic helix-loop-helix protein MASH1 and neurogenesis in neural crest stem cells.[5].

Various intrinsic factors also contribute to stem cell self-renewal and differentiation. Cell fate in development is delicately regulated by transcription factors that act as molecular switches to turn on or inactivate specific gene expression[6]. The POU domain transcription factor Oct3/4 is essential for the pluripotency in embryo and ESCs in vitro[7]. Multipotent cell lineages in early development are governed by SRY (sex determining region Y)-related HMG (high-mobility group)-box transcription factor Sox2[8,9]. Also, The homeoprotein Nanog a critical factor underlying pluripotency in both inner cell mass and ESCs[10]. Oct4-Sox2-Nanog

network together maintains cell pluripotency while repressing genes that induce differentiation[11]. By introducing defined factors including Oct3/4 and Sox 2, mouse and human somatic cells can be reprogrammed to ESCs-like iPSCs[3,12].

The niche concept was first proposed by Schofield in 1978[13]. Stem cells in the niche are exposed to complex biochemical mixtures of soluble factors including cytokines, chemokines, and growth factors, as well as insoluble factors including extracellular matrix (ECM) and transmembrane receptors[14]. Upon injury or disease, stem cells in the niche are induced to proliferate and differentiate into target cell types and restore damaged tissue. Niche system also regulates stem cells through biophysical cues including matrix topography, density and mechanical properties[15,16]. Furthermore, the niche prevents tumorigenesis by controlling stem cells in the arrested state and maintaining the balance between self-renewal and differentiation[17].

The niche hypothesis had been verified by a variety of co-culture and transplantation experiments[18-21]. In contrast to the fruitful research on invertebrate niches, the relative vastness of mammalian tissues and the complicated anatomic structure make it much more difficult to characterize individual stem cells in vivo[17,22]. Among mammalian tissues,

3

epithelial stem cells reside in the bulge of hair follicles of the skin[23,24]. Neural stem cells (NSCs) reside in the subventricular zone (SVZ) of lateral ventricle in the brain[25]. Muscle stem cells reside among satellite cells beneath the basal lamina of myofibers[21]. Hematopoietic stem cells reside in multiple niches, including bone marrow and sinusoidal endothelium in diverse tissues[26]. MSCs also reside within bone marrow.[27]

Stem cells are defined by their ability to self-renew and differentiate into different mature cell types. Therefore, stem cells hold great promise for regenerative medicine therapies. However, the stem cell therapy is hindered by limitations including immuno-incompatibility, teratoma risk and so on. Overcoming the obstacles requires designing biomaterials that better mimic stem cell niche where stem cells reside in inside biological body. Ideally, an artificial niche (Figure 1.1) would include cell-extracellular matrix (ECM) interactions, cell-cell interactions, soluble biochemical factors and biophysical cues[28]. Although remarkable accomplishments had been made towards these needs, great efforts still need to be made to improve the clinical application of artificial niche.
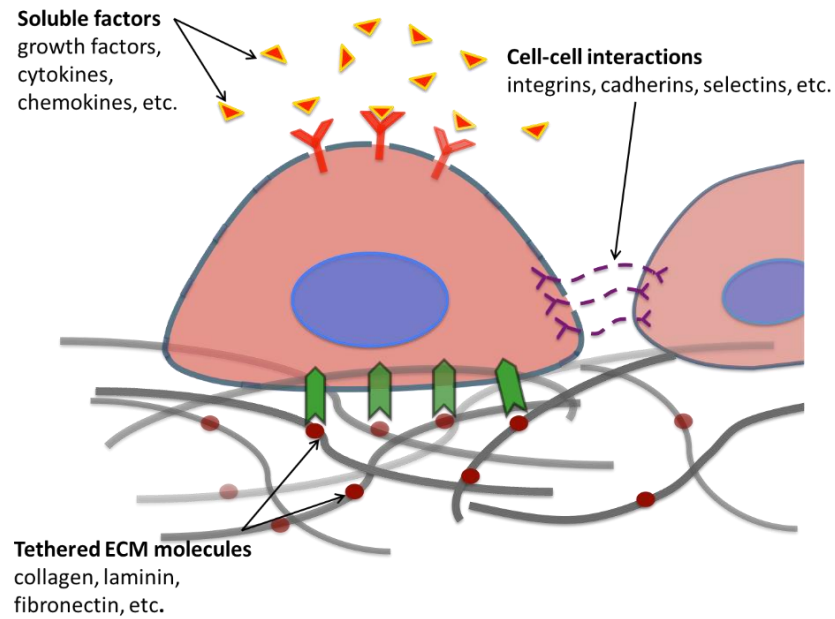
Figure 1.1 Schematic illustration of artificial stem cell niche. An ideal niche includes cell-tethered ECM molecules (collagen, laminin, fibronectin and so on), molecules for cell-cell interactions (integrins, cadherins, selectins and so on), and cell-soluble factors (growth factors, cytokines, chemokines and so on). (Figure adapted with permission from reference 28)

1.1.2 Mesenchymal stem cells

Mesenchymal stem cells (MSCs) have the capacity to differentiate into cells of mesodermal lineages, including osteogenic, chondrogenic, myogenic and adipogenic lineages. This differentiation capacity makes

the use of MSCs an attractive treatment for tissue regeneration and engineering. Furthermore, they are relatively easy to isolate, manipulate and culture, show significant expansion capability. These characteristics make MSCs excellent candidates for the regenerative medicine.

Friedenstein *et al* found that the cells isolated from bone marrow can differentiate into fibroblast-like mesenchymal stem cells[29,30]. They first isolated the whole bone marrow from mouse and cultured in plastic dishes. Then the non-adherent cells (hematopoietic cells) are discarded after 4 hours. The remaining adherent cells were initially heterogeneous in morphology, while most of the cells were spindle-shaped. The adherent cells remained slow growth for 2-4 days and then the growth rate increased rapidly. After several passages, the cells became more homogeneously and are fibroblast-like. Their study also found that these cells could differentiate into colonies similar to bone or cartilage deposits. Other groups continued to explore the characterization of bone-marrow developed adherent cells from Friedenstein's method and they demonstrated that the cells were multipotential and could differentiate into osteoblasts(bone cells), chondrocytes (cartilage cells), adipocytes (fat cells), and even myoblasts (muscle cells)[31,32]. These cells were named mesenchymal stem cells (MSCs), because their potential to differentiate into mesenchymal-type cells. Besides bone marrow, MSCs have also

been isolated from various locations including adipose tissue, fetal blood, liver, amniotic fluid, etc[33,34].

Osteoblasts differentiation of MSCs can be induced by biochemical cues including ascorbic acid, dexamethasone and beta-glycerophosphate for around 2 weeks. The osteogenic induced MSCs can form nodules and alkaline phosphatase activity increases[35]. Also, the calcium deposit can be observed over time and these calcium nodules will be stained positively by alizarin red. To induce the adipogenic differentiation, MSCs will be treated with insulin, isobutyl methyl xanthine, dexamethasone, and indomethacin. The differentiated cells show enrichment of lipid rich vacuoles. Adipogenic markers such as lipoprotein lipase, and the fatty acid-binding protein aP2 can be detected. Oil red O staining is used to evaluate the Accumulation of lipid in cell vacuoles. For chondrogenic differentiation, MSCs are exposed to transforming growth factor-beta[36]. The differentiated MSCs demonstrate strong staining by toluidine blue, which indicates glycosaminoglycans accumulation within the extracellular matrix. To promote myoblastic differentiation, 5-azacytidine and amphotericin B were used to treat MSCs[37]. Study also found that MSCs can be induced to be neuron-lineage specific efficiently[38]. The MSCs were gene transfected with Notch intracellular domain and then exposed with basic fibroblast growth

factor, forskolin and ciliary neurotrophic factor. Neural stem cells specific markers were observed after gene transfection. Induced neuronal cells were also verified after growth factor introduction.

Overall, MSCs are multipotent and have capacity to differentiate into specialized cell types. MSCs can go through numerous cell divisions while maintaining the potency. Also, MSCs can be easily obtained from bone marrow or adipose tissue and can be easily expanded in vitro. All these advantages make MSCs attractive candidate for regenerative medicine and biomedical engineering.

1.2 Gene delivery to stem cells

Gene therapy is the treatment of disease by delivery of genetic information into specific target cells[39]. The completion of Human Genome Project and the advances in biotechnology as well as molecular biology has contributed to the discovery of numerous disease-related genes. Gene therapy can be realized by direct replacement of abnormal genes to treat diseases such as muscular dystrophy[40] or cystic fibrosis[41], etc. By delivering therapeutic genes to alter the gene expression of current genomes, diseases such as neurological[42,43], cardiovascular[44] or cancer[45] can be treated.

Due to the great therapeutic potential the gene therapy could bring, gene therapy has been heavily investigated for the last decade. In 2000, by treatment of two infants with severe combined immunodeficiency-X1 disease, Cavazzana-Calvo *et al.* reported the first successful clinical trial of gene therapy[46].

1.2.1 Gene therapy strategies

Overall there are two types of gene therapy strategies: direct gene delivery and cell-based gene delivery[47]. An ideal gene therapy method should present following features: efficient encapsulation and protection of DNA, high transfection efficiency, minimum non-specific interactions with circulation system such as blood, non-immunogenic and nontoxic, etc.

The direct gene delivery indicates delivering therapeutic genes containing vectors directly to the location of injury[48]. Under this condition, a scaffold will be used for controlled release or direct injection of gene-containing vector to the target organ. However, the cells adjacent to the targeting area may also be transfected, which lowers the overall transfection efficiency. To tackle this problem, a transfection system with targeting functionality may be used. Another problem with this strategy is: some vectors can only transfect cells that are actively dividing.

It is during the cell dividing phase that the cell nucleus member disappears and the genes have the opportunity to integrate with the cell genome. For instance, heart or brain is mostly composed of non-dividing cells. It would be difficult to use vectors directly to transfect these organs. This problem limits the application of direct gene delivery.

For cell-based gene delivery, most often a type of stem cell will be used as target cell. The gene-containing vectors are introduced into the target cells in vitro. During the in vitro process the transfected cells can be cultured in dishes or already in a three-dimensional (3D) environment. Then the transfected cells are allowed to proliferate to enough amounts and finally introduced to injury sites of patients. Study showed that stem cell, such as MSCs, can be used for cell-based gene delivery and thus serve as invaluable source for understanding the molecular mechanisms underlying tissue/organ regeneration and repair[49,50].

1.2.2 Gene delivery methods

Broadly, gene delivery methods include two major categories: viral vectors and non-viral vectors.

The typical method to deliver a therapeutic gene into cells involves the use of viral vectors, such as retrovirus, adenovirus, lentivirus (for example, HIV), adeno-associated virus, etc. The virus in nature, for

the purpose of self-replication, have developed skill to efficiently enter target cell, transport to the cell nucleus and promote expression of the virus genome. The virus gene delivery is termed "infection". Viruses have evolved so sophisticated over nature's selection as gene-delivery vectors, the recombinant viral vectors are essentially very efficient to allow stable gene expression. As a result, majority of gene-therapy research reported in the literature and clinical trials have used viral vectors as subjects[51].

However, Due to the inherent problem such as immune responses induction and oncogenic risk, the viral gene delivery application is hindered[52,53]. Moreover, the viral vector's packaging capacity of foreign DNA is limited and their large-scale production is onerous. There is also possibility that the viral vector may revert to a wild-type, which is pathogenic to host system. All these facts necessitate the development of alternative non-viral gene transfection systems.

Non-viral vectors give rise to improved safety, higher flexibility and more facile scalability. Ideal non-viral vectors can electrostatically bind gene into compact nanometer size particles and protect genes from degradation, show low immunogenicity and low transmission disease risk[52,53]. The extensively studied non-viral vectors include cationic polymers and lipids. They are also known as polyplexes and lipoplexes,

respectively. However, the study of non-viral vectors for gene delivery present problem comparing with viral vectors, such as lower transfection efficiency[54], unpredictability and transfection efficiency strongly depend on cell type, in vivo instability and tend to be degraded or removed by host circulation system and possible high toxicity, etc. For instance, primary cells, e.g. MSCs, are hard to transfection by non-viral vectors[55].

Non-viral delivery method can only delivery genes passively to cells during cell division phase when cell nuclear membrane transiently disappeared. Thus, non-viral delivery strictly dependent on cell division process to facilitate DNA delivery into cell nucleus. Since most primary cells divide quite slowly or do not divide at all, it is very difficult to transfect primary cells using non-viral method.

Cationic lipids are the most extensively studied non-viral vectors due to their high transfection efficiency. The first reported use of cationic lipids for gene delivery is by Felgner in 1987[56]. Cationic lipids can self-assemble into liposomes by having non-polar tails and positive polar heads[57]. The positively charged liposome can bind to anionic DNA to form "lipoplexes". The DNA can be either bound to liposome surface or be encapsulated in the internal aqueous phase. After endocytosis into cells, the lipoplex will disrupt the endosomal membrane to release DNA into cell cytoplasm[58]. Commercially available liposome-based

transfection vectors, such as Lipofectamine® 2000, FuGENE™ 6 and Effectene™ have been developed for cell gene transfection[59-62]. These commercially available products are also often used as reference vectors as comparison to newly developed gene delivery materials. 'Lipofection' has also been widely used in in vivo gene delivery studies as well as many gene-therapy clinical trials. However, liposome-based gene delivery method suffers limitations, including cellular toxicity and particle stability upon systemic administration.

Cationic polymers are versatile molecules that were studied as gene delivery vectors[63,64]. The polymers vectors can include linear, branched and dendritic structures. Variations in polymer design comprise molecular weight, chemical composition, degree of branching and density. Cationic polymers usually contain high level of DNA-binding moieties functional groups (e.g. primary, secondary, tertiary and quaternary amines) and other positively charged groups such as amidines. Due to the flexibility of polymer chemistries, it is possible to offer multiple-functionality for efficient gene delivery while maintaining stable formulation, biocompatibility and easy production. The cationic polymers can interact with negatively charged DNA to from polyplexes. "Polyfection" is termed as gene transfection mediated by polymers. Polyethylenimine (PEI), a type of cationic polymers, is often used as a

reference in gene transfection studies. PEI can be either linear or branched. After entering cell, PEI escapes from endosomes through a "proton-sponge" mechanism[65]. PEI over a wide range of molecular weights had been studied as a gene delivery vectors. Molecular weights between 12-70 kDa demonstrated the highest transfection efficiency[66,67]. Ahn *et al* used pDNA/PEI polyplexes and reported a 10% transfection efficiency to bone marrow derived MSCs[68]. The study also showed that optimal transfection efficiency was obtained at an N/P ratio (N is moles of primary amines in the PEI; P is moles of phosphate groups in the DNA backbone) of 16.

1.2.3 Gene delivery barriers

1.2.3.1 DNA encapsulation

Naked DNA delivered to cells is degraded by DNase within minutes. Thus a vector is necessary to encapsulate DNA to protect DNA from nucleolytic enzyme degradation. Hosam *et al* showed that DNA encapsulated in polyamidoamine dendrimers were stable for hours[69]. The study showed that the protection is related to the structural morphology of the formed dendrimer-DNA complex, which is dependent on time allowed for complex formation and the dendrimer loading. Through electrostatic interactions between the positive charges on vector and the

negative charges on DNA backbone (phosphates groups), gene delivery carriers interact and condense DNA into compact particles (Figure 1.2). It is an entropically driven process and the mixed DNA and vector should form complex spontaneously. It is noticeable that researchers need to make a balance between strong binding to encapsulate DNA and efficient DNA release in cell cytoplasm. A strong binding make also prevent the gene transcription[70].

.
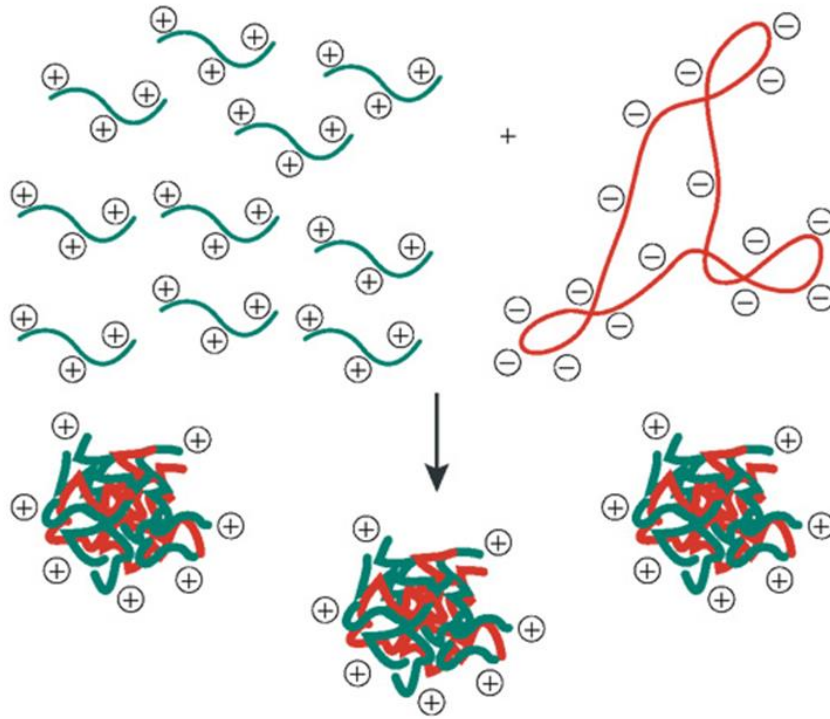
Figure 1.2 DNA-vector complexes are formed by electrostatic interactions between polycations and DNA. (Figure adapted with permission from reference 39). When aqueous solutions of a polycation and DNA are mixed, polyplexes form spontaneously. The interaction is entropically driven. For gene delivery, an excess of polycation is typically used, which generates particles with a positive surface charge.

1.2.3.2 In vivo stability

It is crucial that the DNA-vector complex is stable in vivo after injection. Neutral complexes in physiological conditions quickly form large aggregates due to the hydrophobic effect. Thus it is an ineffective gene-delivery method and could even be toxic. In comparison, positively charged particles can remain relative stable in solution. Higher positively charged particles can also absorb serum albumin as well as more negatively charged proteins to form larger aggregates. The large aggregates can bind to cell membrane and disrupt the membrane to induce toxicity. It also might lead to rapid clearance by phagocytic cells and the reticuloendothelial system[71]. When the vector particles are conjugated with hydrophilic polymers such as polyethylene glycol (PEG), the particles can resist protein or salt induced interference[72,73]. It is presumed that the enhanced stability is due to the steric effects that lead to diminished particle–protein and particle–particle interactions.

1.2.3.3 Cell-targeting vectors

The most challenging question in gene or drug delivery system is efficient targeted delivery of gene materials, otherwise the majority of the effective agents are wasted during the pathway. Generally, targeting moieties are conjugated to gene delivery vectors to provide cell-targeting

functionality. The cell specific vectors can target specific cell receptors and enter cell via receptor-mediated endocytosis. Study reported that galactosylated vectors can specifically target hepatocyte and enhanced the transfection efficiency[74,75] . Folate-bearing vectors were used to transfect genes into receptor-bearing HeLa and IGROV cell lines[76]. Other specific agents, including antibodies[77], epidermal growth factor[78], RGD sequence[79] targeting integrin were also used for cell specific gene delivery. Various conjugation methods have been used to bind targeting motifs to vectors, such as disulfide bond or biotin–streptavidin interaction.

1.2.3.4 Endocytosis and Endosome escape.

The vector-DNA particles typically are internalized by endocytosis to be encapsulated in endosomes (Figure 1.3). Endosomes are the membrane "bubbles" that originates from the cell plasma membrane. The particles can be fused to lysosomes, the acidic cell organelle filled with hydrolytic enzymes capable of degrading all kinds of biomolecules[80]. The particles need to escape from these vesicles into the cytoplasm and be trafficked into cell nucleus for gene expression. The particles without targeting motif bind electrostatically to the cell membrane and are typically internalized via adsorptive pinocytosis[81]. The particles with targeting motifs are often internalized a by receptor-mediated endocytosis

18

mechanism. The particles in the early endosome are then transformed into late endosomes. Due to ATPase proton-pump activated proton influx, late endosomes rapidly acidify to pH around 5–6. The late endosomes subsequently fused to lysosomes, with further activated proton influx to lower the pH to approximate 4.5. Most DNA-bearing particles are trapped in these cell compartments and are degraded and recycled. The optimal gene delivery vectors need to escapes from these vesicles to get into cell nucleus.
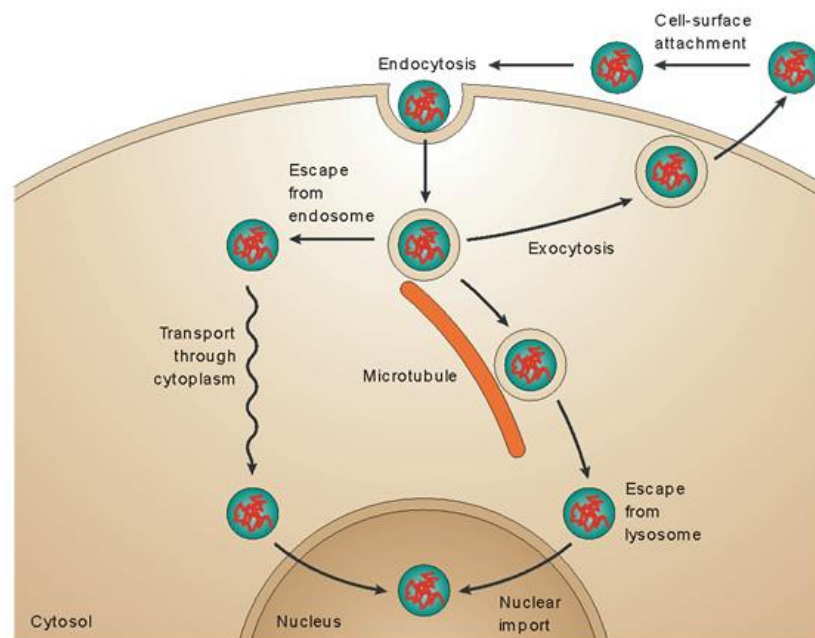
Figure 1.3 Barriers to intracellular trafficking of polyplexes. Polyplexes needs to attach to cell surface and then enter cell by endocytosis, escape

from endolysosomes, move through the cytoplasm toward the nucleus and cross the nuclear membrane. Alternative pathways exist for several of these steps. (Figure adapted with permission from reference 39).

One strategy for escape from the cellular compartment is the proton-sponge mechanism[65]. Polymers such as polyethylenimine (PEI)[82,83] and polyamidoamine (PAMAM) dendrimers contain a high density of primary, secondary and tertiary amines. These amine groups can accept the protons pumped into cell vesicles to prevent pH decrease. As a result, more protons are pumped in for the purpose of reaching the desired acidic pH. The accumulation of protons in the vesicle needs to be balanced by another influx of negative charged ions, such as chloride. The increased ion concentration inside the vesicle will induce more influx of water molecules and ultimately results in osmotic breakdown of endosome vesicle to release the DNA into the cytoplasm.

1.2.3.5 Nucleus transport

After particles bearing DNA escape from endosome, they need to migrate through the cytoplasm to the cell nucleus for gene expression. However, the cytoplasm contains organelles, cellular proteins and microtubules, etc. All these obstacles may hinder particle movement. In addition, the presence of cytosolic nucleases in the cytoplasm would

degrade all unprotected DNA[84], which exert another barrier for successful gene transfection.

The cell nucleus is protected by a double-bilayer membrane which tightly regulates the transport of specific type of biomolecules. Virus-based vectors have evolved to take advantage of cell-nuclear import machinery to transport vectors to the cell nucleus[85]. However, it is a formidable obstacle for non-viral vectors to transport through cell nuclear membrane of non-dividing cells, as non-viral vectors don't have the capacity to utilize cell nuclear import machinery. To overcome this obstacle, nuclear localization signal (NLS) peptides could be used to facilitate the transport of non-viral vectors into cell nucleus. The NLS consists of sequences of positively-charged lysine or arginine amino acids[86]. The NLS is recognized by importin to initiate cell nucleus translocation. Maria *et al* reported that transfection efficiency was enhanced by 10- to 1,000-fold to different cell types after the single nuclear localization signal peptide (PKKKRKVEDPYC) was incorporated in gene delivery[87].

1.3 Designing biomaterials to regulate stem cell fate.

Two-dimensional (2D) systems are advantageous to identify and characterize the effects of individual niche factors on stem cell fate. In

21

vitro, stem cell research is performed frequently with cells cultured on flat substrates coated with collagen, laminin or feeder-cell layers. The effect of soluble or tethered ECM molecules had been explored both individually and collectively. In one example, human neural precursor cells were exposed to a mixture of ECM components and other recombinant signaling molecules[88]. The study revealed that Wnt signaling and Notch signaling could synergistically maintain the cells in an undifferentiated state, whereas BMP 4 signaling could induce a differentiated phenotype characterized by co-expression of glial and neuronal markers. Diseased tissues are often related to altered organization of ECM components such as laminin, resulting in substantial changes to the stiffness of the matrix. Natural and synthetic materials can be engineered to be cell culture matrices with controlled stiffness. For example, mesenchymal stem cells (MSCs) were demonstrated to specify lineage and phenotypes with extreme sensitivity to matrix stiffness. Soft matrices induced neurogenic, stiffer matrices showed myogenic, and rigid matrices are proven osteogenic[89].

In 2D scaffolds, cells are typically cultured on a flat surface at the basal side and liquid medium on the apical surface. In 3D scaffolds, stem cells can be encapsulated into a sophisticated microenvironment that is more comparable to cells grown in vivo. When cultured on 3D materials,

many aspects of cell behaviors, including adhesion, proliferation, migration and differentiation showed variability compared with cells cultured on 2D substrates. In general, biomaterials used for 3D scaffolds should have the following characteristics: biocompatibility, biodegradability, reproducibility, high porosity and high immunocompatibility[90]. Furthermore, it is also highly desirable that the scaffold has the ability to promote ECM secretion and to deliver bioactive signals. It is important that the 3D environment has interconnected pores, which facilitates the free flow of air and nutrients. In one example, Human embryonic stem cells (hESCs) were cultured in a three-dimensional porous natural polymer scaffold comprised of chitosan and alginate[91]. The results demonstrated biocompatibility and biodegradability of the polymer scaffold, and provide a strategy for the direct implantation of stem cell populated scaffolds. The physical barriers that impede cell proliferation, migration and morphogenesis should also be overcome[14]. One promising approach is to use polymer gels that contain chemically cross-linked substrates that are degradable when exposed to proteases secreted by cells. This feature allows a dynamic interplay between the cells and the scaffold, which would facilitate the infiltration of cells and thus the re-homogeneity of the matrices. For instance, matrix metalloproteinase (MMP) degradable hydrogels have been demonstrated to promote cell migration through

proteolytic degradation and to support cell growth both in vitro and in vivo[92,93].

The different components that make up the ECM provide an insight for designing scaffolds based on protein and peptide biomaterials[94]. The proteins and protein derivatives play critical roles in vivo and thus make such materials attractive for tissue engineering applications. Furthermore, their natural origin means that these materials often contain motifs for cellular adhesion and tend to be biocompatible. Engineered protein and peptide materials can uniquely meet the desire for a bioactive scaffold that is versatile and tunable[95]. Protein and peptide material design offers advantages in structure, cellular interaction, cellular signaling and specific cell targeting and binding. Designing these protein biomaterials molecularly provides engineers flexibility and reproducibility. In addition, a protein or peptide molecule is composed of a polymer backbone made of amino acids, which are inherently biocompatible, biodegradable and bioactive. The amino acid sequences can be derived from natural protein, through high-throughput screening or computational design to obtain multi-functionalities. The intrinsic properties of proteins and peptides provide tunable mechanical, chemical, and biological functionalities in the design of biomaterials.

Phage display technique provides a promising means for identifying novel peptide ligands against a variety of targets without prior knowledge about their molecular properties[96]. Homing peptide sequences with high specificity and affinity to cells or tissues have been successfully discovered by phage display technique[97,98]. It is plausible that targeting ligands that bind diverse classes of receptors could exert effects on cell growth and differentiation. To provide insight into such novel ligands, the Kiessling lab employed phage display to identify novel peptides that bind to embryonal carcinoma (EC) pluripotent cells[99]. When fused to self-assembled monolayers (SAMs) of alkanethiols on gold, six selected peptides sequences mediated EC cell adhesion. Further study showed synthetic surfaces displaying phage-display derived peptides maintained the proliferation of undifferentiated human ESCs. When these cells were cultured on SAMs presenting the sequence LTTAPKLPKVTR or TVKHRPDALHPQ in culture medium, they showed pluripotency expression at levels similar to the cells on Matrigel. In another study, Caprini et al utilized phage display technique on murine NSCs and isolated a peptide, KLPGWSG, associated with stem cell maintenance and differentiation[100]. This study concluded that KLPGWSG peptide sequence and the functionalized self-assembling peptide Ac-KLP (KLPGWSG acetylated at the N-terminus) can be used in stem cell therapies for nerve

regeneration. The Bush lab showed a collagen sponge scaffold niche modified with peptides derived from in vivo phage biopanning promoted repair of bone defects, whereas the control scaffold without peptides was less effective[101]. Treatment of MSCs increased alkaline phosphatase activity, enhanced nodule formation by the MSCs, and up-regulated the expression of genes for osteocalcin, osterix, bone sialoprotein, and runx2. Further study demonstrated that MSCs treated with peptides in vitro differentiate towards osteogenesis and the collagen sponge niche modified with peptides promoted the repair of unicortical defects. All these studies indicate that the phage screening strategy is a promising avenue towards the generation of functional peptide ligands that control the fate of stem cells.

Chapter 2 Synergetic Targeted Delivery of Sleeping-Beauty Transposon System to Mesenchymal Stem Cells Using LPD Nanoparticles Modified with a Phage-Displayed Targeting Peptide

2.1 Introduction

For decades, the goal of gene therapy has been the development of an optimal gene delivery system. Foreign DNA must penetrate three cellular barriers, including cell membrane, nucleus trafficking, and chromosomal integration for successful gene expression. Basically, gene delivery to mammalian cells can be categorized into two main methods: viral and non-viral. Viral vectors efficiently deliver genes to target cells as a part of their natural ability.[102] However, clinical outcomes in several gene therapy trials have served to highlight key problems of carcinomatous mutation in their therapeutic application.[39,103] Non-viral vectors alternatives to viral vectors are often less effective because integration of single genes into chromosomes requires efficiently penetrating the above three barriers.[104,105]

Transposable elements can be considered as natural, non-viral gene delivery vehicles capable of efficient genomic insertion. The plasmid-

based transposon system of Sleeping Beauty (SB) combines the advantages of viruses and naked DNA molecules. In contrast to plasmid vectors, transposons can integrate into host chromosomes through a precise, recombinase-mediated mechanism, providing long-term expression of the gene of interest in cells. The advantages of transposons in comparison to viral systems include their simplicity and improved safety concerns.

Phage display is a promising technique to find interacting peptide ligands to certain targets without any prior knowledge about their molecular properties.[96] In vitro and in vivo phage display applications have been successfully conducted by a large number of research groups to identify homing peptide ligands targeting various cells or tissues.[106,107] In this work, a peptide was screened by phage display to increase the targeting delivery of transposon to rat mesenchymal stem cells (rMSCs). In order to overcome the nuclear membrane, a nuclear localization signal (NLS) was used to enhance nuclear translocation of gene materials.

Mesenchymal stem cells (MSCs) have the capacity to differentiate into cells of mesodermal lineages, including osteogenic, chondrogenic, myogenic and adipogenic lineages. This differentiation capacity makes MSCs an attractive candidate for tissue regeneration and engineering.

Furthermore, MSCs are relatively easy to isolate, manipulate and culture. In addition, MSCs show significant expansion capability in vitro.[108,109] These characteristics make them attractive candidates for the delivery of exogenous genes. We suggested that a novel rMSC-homing peptide by phage display screening, in combination with NLS, could enable novel preparation of efficient gene carriers. The resultant nanoparticle complex could promote the delivery of transposon into rMSC specifically. The peptide of nuclear localization signal (NLS) is derived from the simian virus 40 large tumor antigen (DKKKRKV) which mediates binding of the karyophilic protein to importin α. And the NLS peptide was found vital in achieving the high levels of gene expression.[87] In conclusion, we used phage display technique to identify an rMSC-homing peptide ligand and then integrated the identified homing peptide and the reported NLS into a peptide-combined liposome-based carrier for development of an effective transposon gene delivery system.

2.2 Methods and experiments

2.2.1 Plasmid Development

The original SB transposon pT2/SVNeo and transposase pSB11 were a gift from Dr. Perry B. Hackett (University of Minnesota). The neomycin resistance gene in pT2/SVNeo was converted into the EGFP

gene by restriction digestion with Bcl I and BstB I (New England Biolabs, Inc. MA, USA). The fragment excised by the two restriction enzymes from pT2/SVNeo plasmids was discarded and replaced by a PCR fragment of pEGFP-N1 with a similar restriction digestion. The sequence of primer 1 is GCGGTGATCATATGGTGAGCAAGGGC; the primer 2 is GCGGTTCGAACTTTACTTGTACAGCT. After the appropriate fragments were gel purified and recovered, the EGFP fragment was cloned by ligation into the pT2/SVNeo, giving rise to pT2/EGFP constructs. pT2/EGFP and pSB11 plasmid were purified using the EndoFree Plasmid Max Kit (Qiagen, CA, USA). Rhodamine-labeling for pDNA was performed using a ITTM-Rhodamine labeling kit (Mirus, Madison, WI, USA) according to the manufacturer's protocol.

2.2.2 Phage selection

The phage display screening procedure followed the previous protocol with a slight modification.[110] We used a major coat displayed phage library, namely landscape phage library, to perform the biopanning. This library contains billions of fd-tet phage clones and in each phage clone the foreign peptide is displayed on the N-terminal end of each copy of major coat protein of fd-tet phage. Briefly, the landscape phage library was first depleted with culture flask at 37°C for 1 h to remove the phages

that specifically bound to the culture flask. The depleted phage library was incubated with target rMSCs at room temperature for 1 h. The rMSCs were washed 10 times with bovine serum albumin (BSA)/Tween washing buffer to remove the unbound phages. The cell bound phages were eluted with low pH elution buffer (0.1N HCl, 1 mg/mL BSA and pH adjusted to 2.2 with glycine) for 10 min. The eluate was neutralized by 1 M Tris-HCl (pH = 9.1) immediately. The first-round eluate was concentrated by using a Centricon 100 kDa Ultrafilter (Amicon, USA). The concentrated eluate was transfected to the starved cells and incubated for 15 min at room temperature. The phage-infected cells were added to NZY medium with tetracycline (0.2μ g/mL) and incubated for 45 min at 37°C with shaking. The tetracycline concentration was increased to 20μ g/mL, and the shaking of the flask was continued for 24 h at 37°C. The rMSC-internalized phage clones were recovered using the cell lysis buffer (2% sodium deoxycholate, 10 mM Tris-HCl, 2 mM EDTA, pH 8.0). The cells were centrifuged at 130 g for 10 min. The supernatant was removed and the cell lysis buffer was added to the pellet. The phages were used for amplification and further selection as stated above. The purified phage after each round was used as an input library for the next round of selection, which proceeded similarly to the first round as described above. After the third round of the selection, the eluted phages

were titrated and 40 random colonies were picked up for sequencing in order to determine the sequence of rMSC-binding peptides.

2.2.3 Binding Assessment by Phage Capture ELISA

The binding ability and specificity of the selected phages to rMSCs were measured by enzyme linked immunosorbent assay (ELISA). Confluent cells in 24-well plate (Corning Inc., MA, USA) were fixed by 4% paraformaldehyde (Sigma-Aldrich Co. LLC, USA) for 15 min, blocked with 0.1% BSA for 1 h at room temperature, and washed three times with PBS. Subsequently, 2×10^9 cfu purified phages in blocking buffer were added and incubated for 1 h at room temperature. The plate was subsequently washed three times with PBS containing 0.5% Tween 20, and washed another three times with PBS. This was followed by incubation with anti-fd bacteriophage IgG conjugated with alkaline phosphatase (Abcam, MA, USA) for 1 h at room temperature. After a final washing step, alkaline phosphatase substrate, p-nitrophenyl phosphate, was added to the wells and the absorbance was measured at 405 nm using a plate reader (Gen5, BioTek Instruments, Inc. USA).

2.2.4 Peptide-Affinity Assay

The peptide-affinity assay was performed according to the method mentioned previously with minor modifications.[111,112] The cells were cultured until 70–90% confluence, and then incubated with 1 and 10 μM FITC-labeled targeting peptide for 4 h at 37°C to allow cell binding. The cells were fixed with 4% paraformaldehyde for 30 min at 4°C. The rat fibroblastic cells and rat smooth muscle cells were used as control cells. They were incubated with 10 μM FITC-labeled targeting peptide for 4 h at 37°C to investigate the specificity of peptide. The nuclei were then counterstained with DAPI. The cells were observed under a Nikon fluorescence microscope.

2.2.5 Competitive Binding Using Synthetic Peptide

For specific competitive blocking of peptide, rMSCs (Invitrogen, USA) were cultured with targeting peptide or control peptide (GCVKYMVM) without FITC at a concentration of 10 μM for 2 h. After incubation, 10 μM of FITC-labeled targeting peptide was added and incubated for another 4 h. Then the cells were then examined by fluorescence microscopy.

2.2.6 The Preparation and Physico-Chemical Properties of Liposome Protamine/DNA Lipoplexes (LPD)

LPD was prepared according to the method reported previously with some modifications.[113-115] First, the liposomes consisting of DOTAP, DOPE and cholesterol (1:1:1 molar ratio) (Avanti Polar Lipids, Inc. USA) were prepared by thin film hydration. Second, protamine (0.5 mg/mL) (Sigma-Aldrich Co. LLC, USA), various peptides (0.5 mg/mL), and the Sleeping Beauty system (pDNA, a mixture of transposon and transposase gene at a mass ratio of 2:1) were mixed at various weight ratios. The resultant protamine/pDNA complex was allowed to stand at room temperature for 20 min. The above liposome was then added into the protamine/pDNA complex followed by vortexing. The resultant mixture was kept at room temperature for another 20 min to form LPD.

Protamine/pDNA particles were prepared at different weight ratios, and LPD was prepared with various liposome and peptide concentrations. The samples were electrophoresed on a 0.8% (w/v) agarose gel in TAE buffer at 90 V for 40 min, and analyzed on a UV illuminator to show the location of the DNA.

The size and zeta-potential values of protamine/pDNA particles and LPD were determined by dynamic light scattering (DLS) (Zeta Potential Analyzer, Brook haven Instruments Corporation, Holtsville, NY). The final concentration of pDNA was 20 μg/mL in HEPES buffer for assay.

The morphology of LPD was observed using TEM (Carl Zeiss, Germany). One drop of LPD was placed on a copper grid and stained with 2% uranyl acetate for 3 min. The grid was allowed to dry further for 20 min and then examined with the electron microscope.

2.2.7 Gene Transfection

For the transfection experiments, rMSCs were seeded in the 24-well plate at a density of 1×10^5 cells/well and incubated overnight. The pDNA was made of a mixture of transposon pT2/EGFP and transposase pSB11 with a mass ratio of 2:1 as described in an earlier report[116]. The LPD with various peptides in low glucose DMEM was added, and Lipofectamine2000 (Invitrogen, USA) was used as a control. The cells were incubated for 4 h at 37°C. The transfection medium was then replaced with a fresh culture medium and the cells were further incubated for up to 72 h. Inverted fluorescent microscopy was also used to observe the GFP expression. The transfected cells was digested by trypsin and fixed in a 4% paraformaldehyde for 30 min at 4°C to prepare single-cell suspensions. The percentage of cells positive for GFP was determined by flow cytometry (Becton-Dickinson Biosciences, Franklin Lakes, NJ, USA) by setting a gate according to the control and 1×10^4 cells were evaluated in each experiment.

2.2.8 Confocal Microscopy

LPD was prepared by carboxyfluorescein-labeled DOPE (Avanti Polar Lipids, Inc. USA), and the pDNA was labeled with rhodamine as mentioned above. The rMSCs were grown on glass cover slips in 12-well plates and incubated at 37°C for a day. The cells were then transfected by labeled LPD and pDNA complexes. The cells were then incubated for 4 h at 37°C. The transfection medium was then replaced with a fresh medium. After 5 h, the cells were fixed with 4% paraformaldehyde for 30 min. To stain the cell nuclei, the cells were incubated with DAPI for 30 min at 4°C, and then the cover slips were mounted on glass slides. The fluorescence was examined with a confocal laser scanning microscope (Leica TCS NT, Germany).

2.2.9 Cytotoxicity Assay

Cytotoxicity of LPD was assayed using MTT reagent. Briefly, rMSCs were seeded at 1×10^4 cells per well in 96-well plates. One day later, the cells were transfected by LPD with various peptides at different liposome concentration. The Lipofectamine 2000 was used as the control. The cells were incubated for another 12 h at 37°C. The medium was replaced with 80 μL of fresh medium without serum and 20 μL of MTT (5 mg/mL) (Sigma-Aldrich Co. LLC, USA) solution, and incubated for

an additional 4 h. Subsequently, the medium was removed and 100 µL of dimethyl sulfoxide (DMSO) was added. The absorbance at 570 nm was measured by using a microplate reader.

2.2.10 Osteogenesis Assay

1×10^5 transfected or untransfected MSCs/well were seeded in a 24-well plate in triplicate. After 24 h, medium was removed and 500 µL of HyClone osteogenic differentiation medium (Thermo Fisher Scientific Inc., USA) was added. Medium was changed every 3 days. Cultures were harvested at day 14. To analyze osteopontin expression, cells were fixed with 4% paraformaldehyde. Cells were saturated with 5% BSA for 30 min. 300 µL of anti-osteopontin antibody (ab 8448-200, Abcam, MA, USA), which was diluted 1:300 in phosphate buffered saline (PBS) containing 5% BSA, was added and incubated overnight at 4°C. The cells were then washed with PBS/5% BSA and incubated with a secondary, tetramethylrhodamine goat anti-rabbit IgG (H+C) (Molecular probes, Invitrogen, USA) for 60 min at room temperature. The nuclei were stained by DAPI. The cells were observed with a fluorescence microscope.

2.2.11 Statistics analysis

For statistical analysis, one-way analysis of variance (ANOVA) was carried out by SPSS 11 software, and a p values < 0.05 were considered statistically significant.

2.3 Results

2.3.1 Identification of rMSC-Homing Phage Clones

rMSC-homing phage clones were isolated from a major coat displayed phage library after three rounds of panning. The major coat displayed phage library, also termed landscape phage library, is made of billions of fd-tet phage clones with each phage clone fully displaying a unique foreign peptide on the major coat. Namely, for each phage clone, the foreign peptide is fused to each of the ≈3900 copies of major coat protein of fd-tet phage. Phages that were bound to rMSCs in the initial selection procedure were amplified separately by infecting bacteria and used as an input for the next round of affinity selection. After the three rounds of affinity selection, 51 clones were randomly picked and sequenced. The cell-binding peptides and their frequencies are shown in Table 2.1. No cell internalized phages were detected after cell lysate amplification and phage titering. The cell-binding phage clones with a sequence of VTAMEPGQ demonstrated the highest affinity to rMSCs.

Phage capture ELISA also indicated that the selected cell-binding phage with sequence VTAMEPGQ has high affinity against rMSCs (Figure 2.1).

Motif ID	Motif Sequence	Frequency
#1	VTAMEPGQ	28
#2	AFNPEPGQ	11
#3	VTALEPGQ	7
#4	DTPPGWDQ	5

Table 2.1 Peptide sequences displayed by selected rMSC-binding phage clones and their occurrence frequencies.
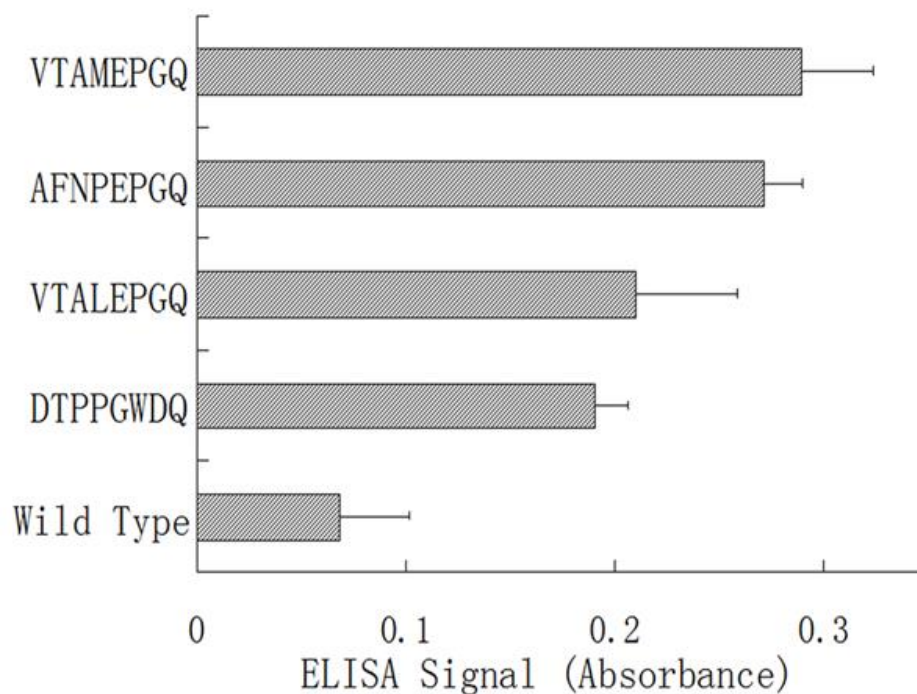
Figure 2.1 Binding of control wild type phage and affinity selected phages to rMSCs evaluated by ELISA. The *x* axis indicates the absorbance of ELISA signal and the *y* axis shows the affinity selected peptide sequences displayed on the major coat of phage.

2.3.2 rMSC-affinity and specificity of the identified peptide.

The identified peptide (VTAMEPGQ) was designated as peptide 1 (Table 2.1). A randomly scrambled peptide (GCVKYMVM, peptide 4) was used as the negative control. The rMSCs were incubated with FITC labeled peptide 1 or 4, and observed using a fluorescence microscope.

When incubated with 10 uM FITC-peptide 1, strong fluorescent signals were observed in rMSCs (Figure 2.2b), whereas a weak FITC signal was detected of 1 μM FITC-peptide 1 (Figure 2.2a). When incubated with 1μM and 10 μM FITC-labeled scrambled peptide 4, no specific fluorescence signal was observed from rMSCs at both concentrations (Fig. 2.2c and 2.2d). This result suggests that peptide 1 can bind with rMSCs in a concentration dependent way. But scrambled peptide 4 is not able to bind to rMSCs specifically.
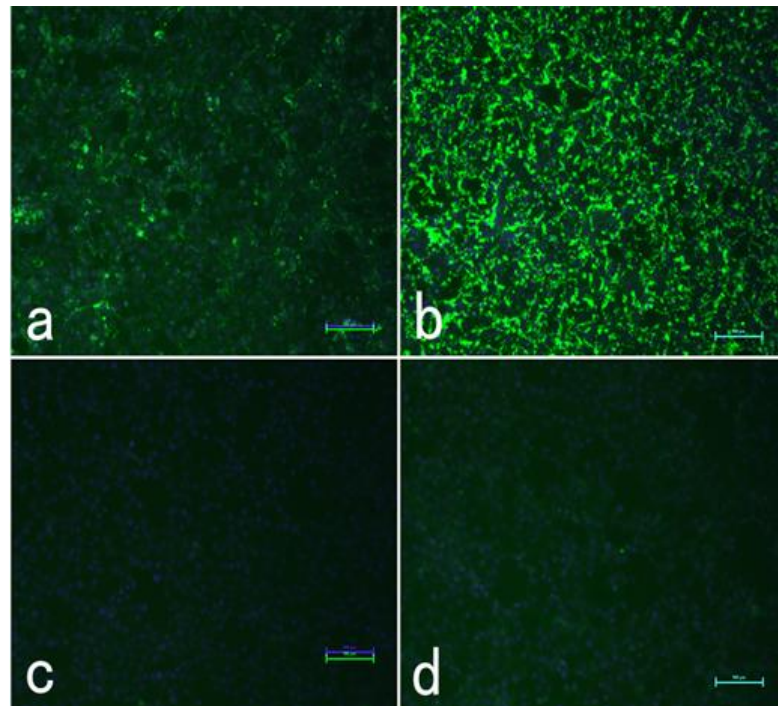
Figure 2.2 Cellular affinity of peptide 1 with rMSCs. Strong fluorescence signals were visualized, indicating that plenty of 10 μM FITC-labeled

peptide 1 located in rMSCs (*b*). Weak fluorescence was detected from 1 μM FITC-labeled peptide 1 in rMSCs (*a*). No specific fluorescence signal was observed from both 1 and 10 μM FITC-labeled peptide 4 (*c*, *d*). The nucleus was stained with DAPI. Scale bar: 100 μm.

2.3.3 Competitive Binding Using Synthetic Peptide.

In order to verify whether internalization of peptide 1 takes place through a VTAMEPGQ recognition motif, competitive assay was performed by pre-binding of peptide 1 or 4 without FITC to rMSCs. Peptide 1 or 4 was incubated with the cells prior to the incubation of FITC-labeled peptide 1. Figure 2.3 shows that pre-incubation with un-labled peptide 1 reduced the binding of FITC-labeled peptide 1 to the rMSCs, but the pre-incubation with peptide 4 didn't affect the binding of FITC-labeled peptide 1 with rMSCs. This fact confirms that FITC-labeled peptide 1 is competitively inhibited in the presence of peptide 1, but not of peptide 4.
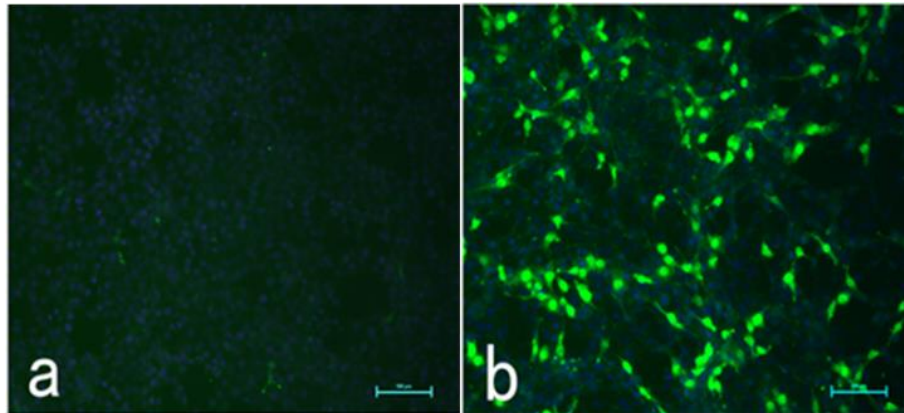
Figure 2.3 Blocking binding to rMSCs in the presence of peptide 1 or 4. rMSCs were pre-incubated with 10 μM peptide 1 (a) or 4 (b) without FITC followed by incubation with 10 μM FITC-labeled peptide 1. Fluorescence microscopy confirmed that rMSCs preincubated with peptide 4 displayed much stronger fluorescence signals (b) than those preincubated with peptide 1 (a). The nucleus was stained with DAPI. Scale bar: 100 μm.

2.2.4 Preparation and Physico-Chemical Properties of Liposome Protamine/DNA Lipoplexes (LPD)

To construct the LPD, we used a two-step packaging technology employing a multilayering method. First, the DNA was packaged into a condensed core via electrostatic interactions with protamine. The targeting peptide with slightly positive potential was also added and interacted with the plasmid to form a negatively charged particle. Second,

positively-charged DOTAP/DOPE/Chol liposome was added to form a complex with negative protamine/DNA particle, leading to the formation of LPD (Figure 2.4).

The formation of LPD was verified via gel electrophoresis and zeta potential measurement. According to the results of gel electrophoresis, DNA migration started to be retarded when the weight ratio of protamine to pDNA reached 1.5:1 for the protamine to condense the DNA (Figure 2.5). Thus, the protamine/pDNA particle was prepared at a weight ratio of 1:1 to ensure that its zeta potential was negative to favor its integration with the DOTAP/DOPE liposome.

The results of dynamic light scattering (DLS) showed that the zeta potential of the protamine/pDNA complex was negative and 245.7 nm in size at the weight ratio of 1:1 (Table 2.2), which was consistent with the result of gel electrophoresis. At a weight ratio of 1.5:1, the particle of protamine/pDNA became positive in potential and 118.5 nm in size, which indicates that pDNA was condensed by protamine to form a more compact particle.

Figure 2.4 Schematic illustration of targeting LPD modified with rMSC-homing peptide and NLS peptide.

	Size [nm]	Zeta-potential [mV]
Protamine:pDNA = 1:1	245.7 ± 6.47	-27.55 ± 3.33
Protamine:pDNA = 1.5:1	118.5 ± 4.99	26.25 ± 2.99
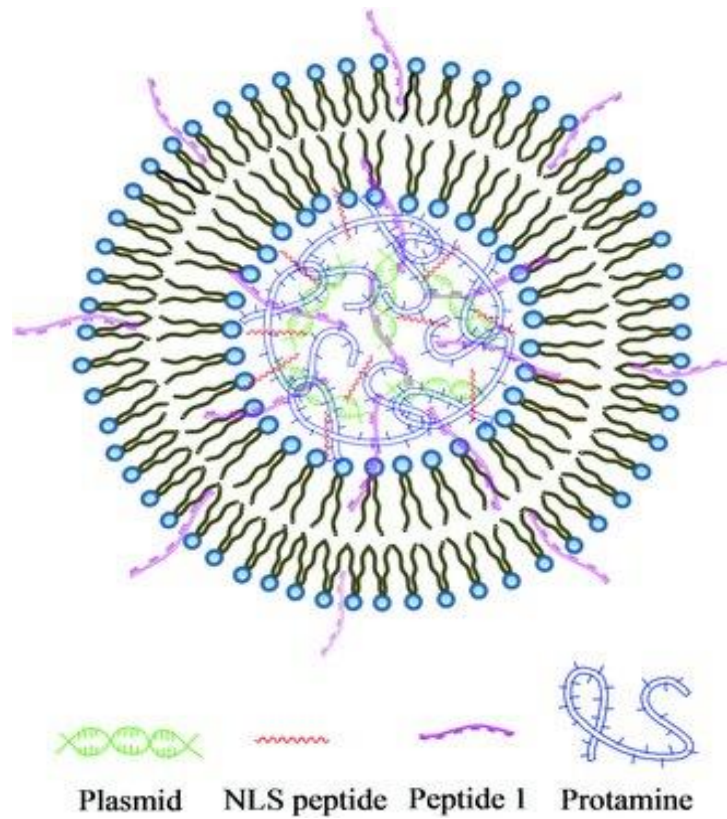
	Size [nm]	Zeta-potential [mV]
LPD (10 mM liposome)	245.1 ± 5.65	20.74 ± 1.89

Table 2.2 Particle size and zeta potential of protamine/pDNA particles and LPD. The pDNA concentration was 20 μg/mL. The concentration of liposome is denoted by the concentration of DOTAP in LPD.
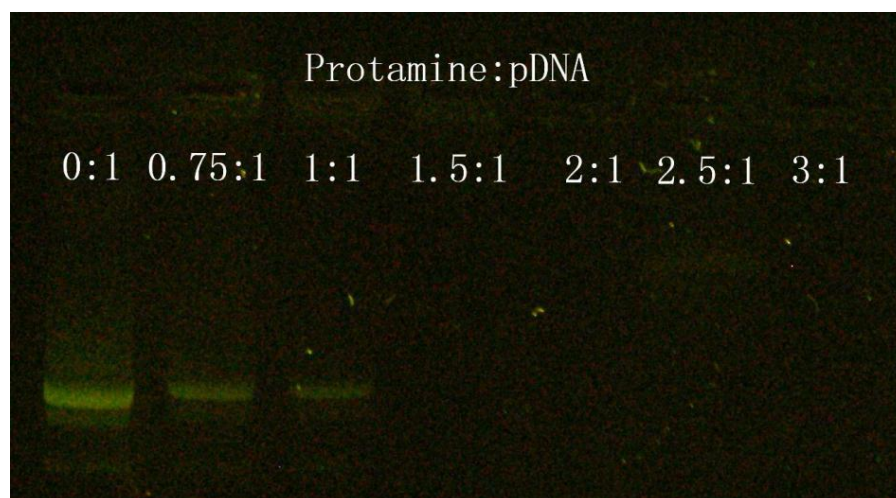
Figure 2.5 Agarose gel electrophoresis retardation assay of protamine/pDNA polyplexes at various weight ratios. The mixtures were incubated at room temperature for 20 min, subject to electrophoresis on a 0.8% (W/V) agarose gel and stained with ethidium bromide.

The LPD was then prepared with various concentrations of liposome. The gel electrophoresis and DLS were both performed to verify the formation of the LPD. With the increasing concentration of liposome, DNA migration was retarded gradually (Figure 2.6). The protamine/pDNA particles could be complexed completely with DOTAP/DOPE liposome at a concentration of 10 mM DOTAP. The results of DLS were consistent with those of the gel electrophoresis. After being incorporated with the DOTAP/DOPE liposome, LPD had a zeta potential of positive 20.74 mV, and was 245.1 nm in size (Table 2.2). The size of the LPD was confirmed by TEM (Figure 2.7)
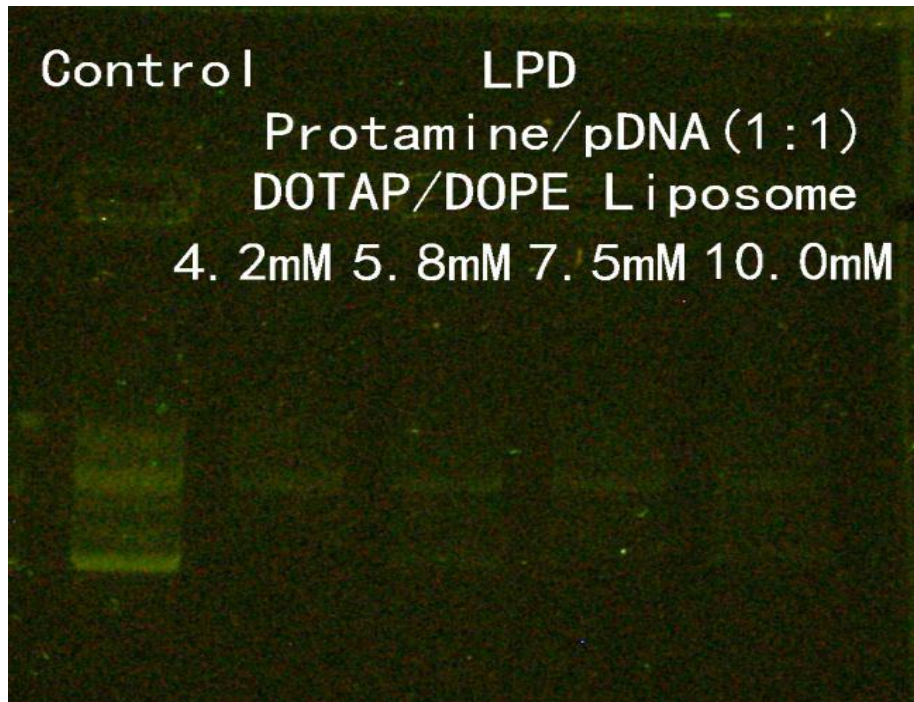
Figure 2.6 Gel assay of LPD at various liposome concentrations (protamine/pDNA = 1:1), using pDNA as a control. The protamine and pDNA were mixed at weight ratios of 1:1 and the complex was incubated for 20 min at room temperature. Then, the DOTAP/DOPE/Chol liposome was added into the complex followed by mixing and standing at room temperature for 20 min and electrophoresis on 0.8% (W/V) agarose gel. In this study, liposomes were prepared from synthetic phospholipids. Their main components include DOTAP and DOPE. The molecular weight of DOTAP and DOPE is 758.19 Da and 744.03 Da, respectively. The molecular ratio between them is 1:1. The concentration of liposomes was denoted by the concentration of DOTAP in LPD.
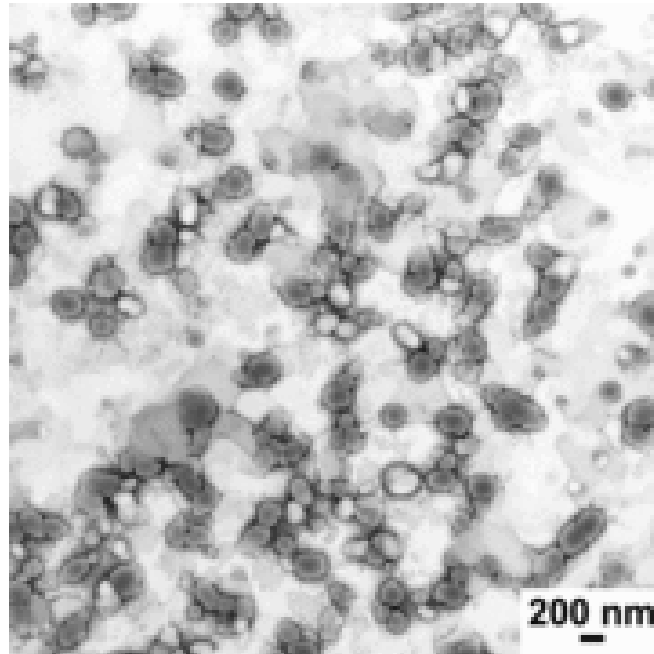
Figure 2.7 Morphology of LPD observed by transmission electron microscope. The particles were negatively stained by 2% uranyl acetate for 3 min.

2.3.5 Transfection Efficiency

To investigate the peptide-enabled targeted delivery efficiency, we performed the transfection efficiency study using LPD with the synthetic targeting peptide 1. Lipofectamine 2000 served as a control (Figure 2.8A). The result showed that the transfection efficiency of LPD with peptide 1 was 3.24- and 1.41-fold higher than Lipofectamine2000 and LPD without peptide, respectively, showing enhanced targeted gene delivery to rMSCs.

This indicates that peptide 1 enhanced transgenic expression by means of targeting to rMSCs. This demonstrated the great potential of peptide 1 as a ligand in rMSCs targeting.

To further enhance the nuclear translocation efficiency of SB transposon system, three-fold reiterated NLS motif (DPKKKRKVDPKKKRKVDPKKKRKV, peptide 2) of SV40 T large antigen was employed to promote the nuclear translocation and gene expression of LPD.[117] To investigate the effect of fused peptide, an LPD with a fusion peptide (DPKKKRKVDPKKKRKVDPKKKRKVVTAMEPGQ, peptide 3) from peptides 1 and 2 was compared to the LPD containing unfused peptides 1 and 2. The results showed that LPD with fusion peptide 3 did not demonstrate a better gene expression than sole peptide 1 or 2. This means that after fusion, peptides 1 and 2 did not produce an improved effect. However, LPD with both unfused peptides 1 and 2 integrated could obtain the highest gene expression among all the peptide combinations. This indicates that a synergetic effect could be realized by encapsulating both peptides 1 and 2 in LPD. The fluorescence microscopy results also confirmed this synergetic effect (Figure 2.8B).
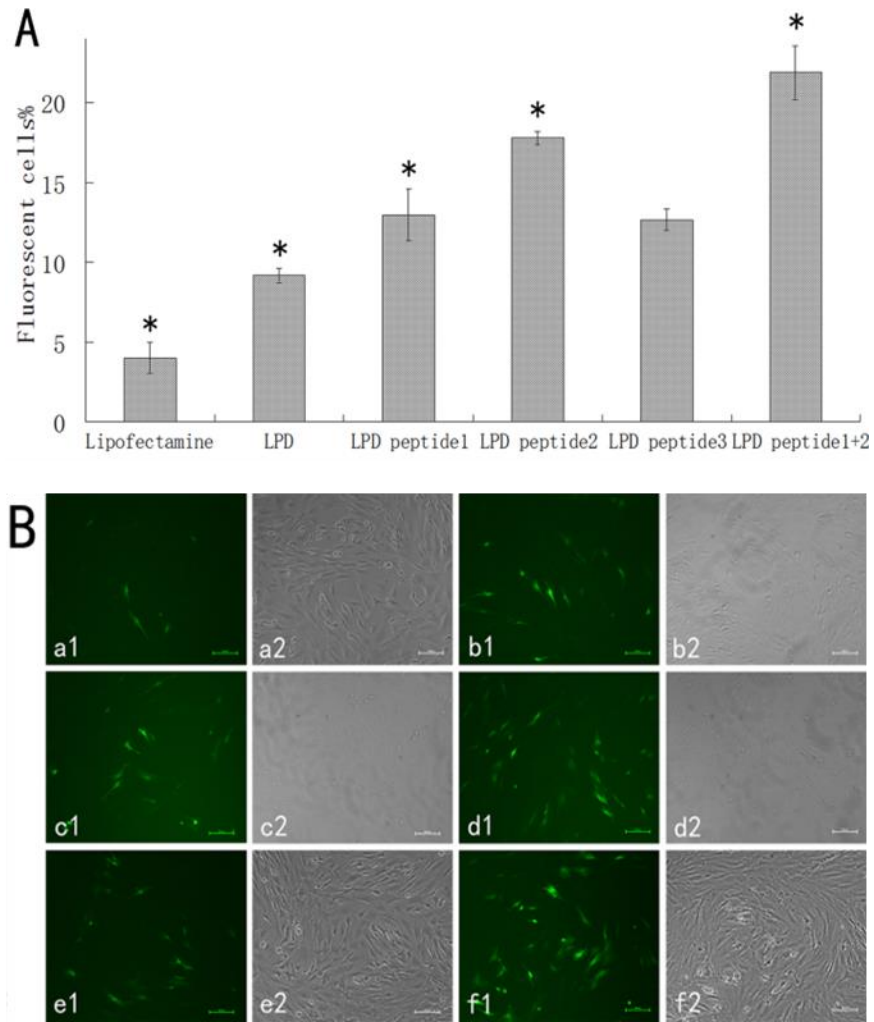
Figure 2.8 Transfection efficiency of LPD in rMSCs. Lipofectamine 2000 was used as the control. A) EGFP expression after transfection by LPD with various peptides was examined by flow cytometry. LPD with both unfused peptides 1 and 2 integrated could obtain the highest gene expression among all peptides tested. Fusion peptide 3 (fused from peptides 1 and 2) did not display a better gene expression. The percentage

of EGFP positive cells is shown as the mean ± standard deviation of triplicate measurements. (*) indicates a statistically significant difference ($p < 0.05$). B) Comparison of transfection expression of EGFP mediated by Lipofectamine2000 (a), LPD (b), and LPD with peptide 1 (c), peptide 2 (d), peptide 3 (e), peptide 1 + 2 (f) in rMSCs using the transposon containing EGFP reporter gene. Image 1 in (a–f) shows GFP expression and image 2 is the corresponding bright-field light image. Scale bar: 100 µm.

The LPD with various combinations among the peptides 1, 2, and 3 was then investigated for a higher transgenic efficiency (Figure 2.9A). The result showed that the combination of peptides 1 and 2 was still better than the other two combinations. The effects of varying peptide/plasmid weight ratio on transfection efficiencies into rMSCs were determined to ascertain an optimal dosage. Using a 3:1 peptide to plasmid ratio resulted in the best gene expression among all examined peptide/plasmid ratios (Figure 2.9B). A decreased transfection efficiency of LPD was observed at ratios higher or lower than the 3:1 of peptide/plasmid ratio. It was therefore concluded that using a 3:1 peptide/plasmid ratio was optimal for further use.

To verify the effect of peptides 1 and 2, the random peptide (GCVKYMVM, peptide 4) was utilized as a substitution and combined with either peptide 1 or 2 in LPD for gene transfection. The results showed that compared to peptides 1 and 2, the random peptide did not increase any transfection efficiency of LPD in rMSCs (Figure 2.9C). After being combined with peptide 1 or 2, peptide 4 still did not result in an improved transfection efficiency. It further confirmed that there was a synergetic effect between peptides 1 and 2, i.e., between rMSC-homing and NLS peptide. These two peptides should be co-existing (but without forming fusion peptide) to maximize the transfection efficiency of LPD.

A time course of gene expression was then performed for SB transposon system (made of pT2/EGFP and pSB11 at a mass ratio of 2:1) and pEGFP-N1 genes with expression levels measured up to 168 h (Figure 2.9D). After 96 h, the transgenic expression level of SB transposon system in rMSCs reached its maximum, which was referred to as 100%. After 24 h, relatively low SB transposon system and pEGFP-N1 transfection rates of only about 50% of maximum of transposon transfection were observed. Transfection of pEGFP-N1 reached its maximum at 72 h, which was only about 70% of the transposon system's maximum, and with no further significant increase seen at 96 h. The transfection rates of pEGFP-N1 then decreased significantly to

approximately 50% after 144 and 168 h. The transposon system did not show obvious decreases in transfection levels at 120, 144, and 168 h, which are all maintained at about 90% of the maximum.
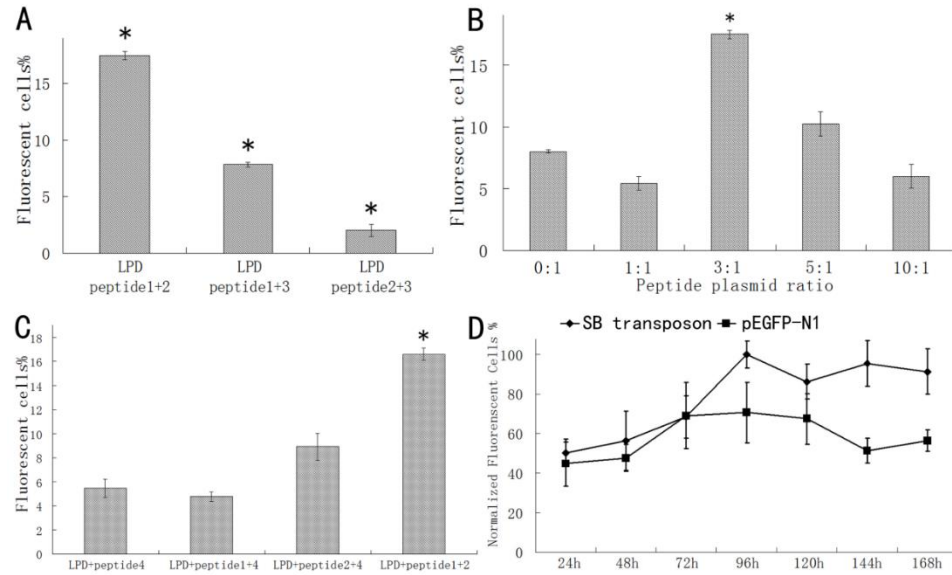
Figure 2.9 Comparison of gene transfection efficiencies. A) The EGFP expression level of LPD with different combinations of the peptides 1, 2, and 3. The combination of peptides 1 and 2 was superior to the other two combinations. B) The transfection efficiency of LPD with the various peptide/plasmid weight ratios. LPD with peptide/plasmid ratio of 3:1 was optimal for gene expression. C) A control peptide (peptide 4) was utilized to verify the synergetic effect between peptides 1 and 2. Peptide 4 did not promote transfection of LPD neither solely nor combining with peptide 1 or 2. D) Percentage of EGFP positive cells in rMSCs after varying the

duration of transgene expression. The highest transfection levels were observed at 96 h with the SB transposon system gene, which was set as 100%. SB transposon system maintained about 90% of its maximum after 168 h. However, pEGFP-N1 showed obvious decreases in transfection levels at that time. Each assay was shown as means ± standard deviation (n = 3). (*) Indicates a statistically significant difference (p < 0.05).

2.3.6 Confocal Microscopy

For investigating the intracellular localization of LPD with or without NLS peptide, carboxyfluorescein labeled DOPE was used to prepare liposome. The pDNA was labeled with rhodamine. The cells were scanned with a confocal fluorescence microscope. After the cells were transfected with LPD containing the NLS peptide, rhodamine-labeled pDNA colocalized with the nuclei as indicated by white arrows in Figure 2.10A(d). However, LPD without the NLS peptide rarely translocated pDNA into the nuclei (Figure 2.10B). This result indicates that the NLS peptide guides the nuclear translocation of pDNA efficiently. This efficient translocation into the nucleus may be responsible for the high transfection efficiency of LPD.
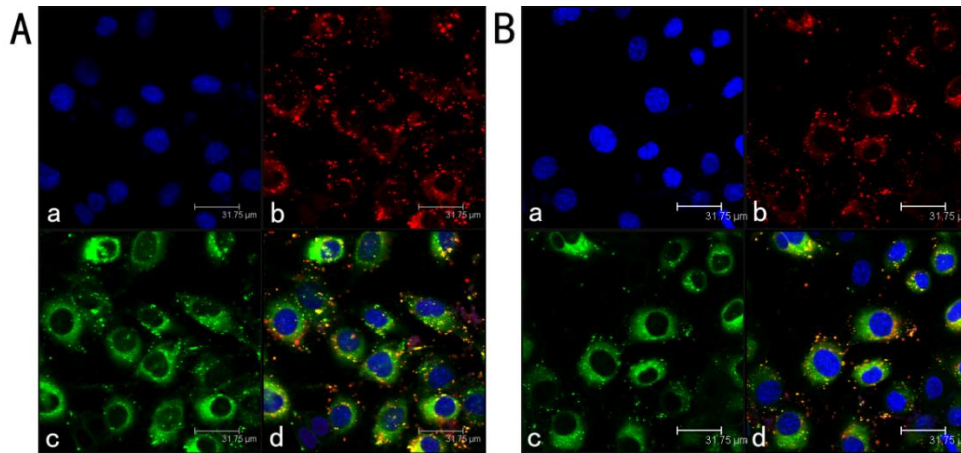
Figure 2.10 Subcellular distribution of LPD with and without NLS peptide 2 (A and B, respectively) was visualized by confocal microscopy in rMSCs. a: DAPI labeled nuclei (blue); b: rhodamine labeled pDNA (red); c: carboxyfluorescein labeled liposome (green); d: merged images of a, b, and c. Guided with NLS peptide, LPD and rhodamine-labeled pDNA could colocalize in the nuclei. However, without NLS peptide, LPD and pDNA rarely appeared into the nuclei. Scale bar: 31.75 μm. White arrows in A(d) are used to indicate that rhodamine-labeled pDNA colocalized with the nuclei.

2.3.7 Cytotoxicity

In vitro cytotoxicity of various concentrations of LPD and Lipofectamine 2000 was investigated with rMSCs after 12 h incubation at 37°C by MTT assay (Figure 2.11). At Lipofectamine 2000 concentrations

over 40 mM, cell viability was lower than 80%, indicating that it has obvious toxicity at these higher concentrations. Cell viability was slightly reduced at higher concentrations of LPD, but still higher than 80%. This fact demonstrates that LPDs with peptides show low cytotoxicity with good biocompatibility. Furthermore, there was no significant difference in the toxicity of different formulation at all given concentrations ($p < 0.05$).
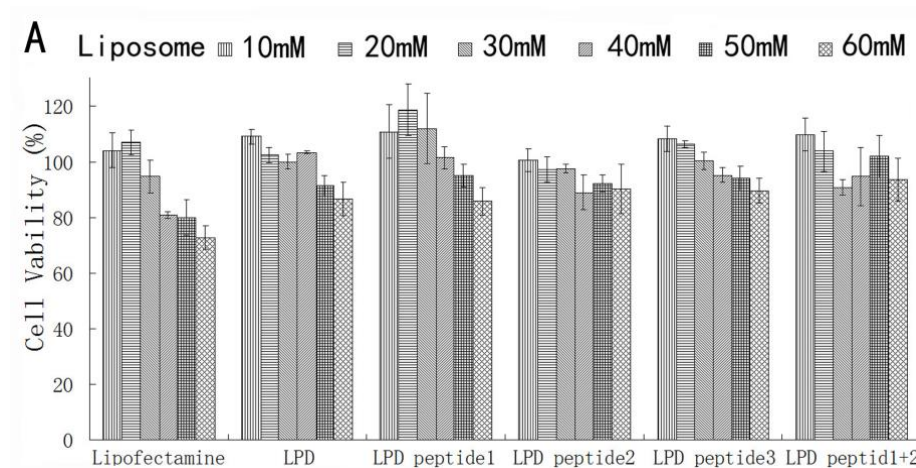
Figure 2.11 MTT assay for evaluating cytotoxicity of LPD with various peptides at different liposome concentrations. Lipofectamine 2000 was used as a control. The cell viability of samples with LPD with peptides at all liposome concentrations was higher than 80%. Lipofectamine 2000 had obvious toxicity at concentrations over 40 mM. The concentration of

liposome is denoted by the concentration of DOTAP in LPD. The data points represent the mean ± standard deviation of three experiments.

2.3.8 Cell Differentiation test

Osteogenesis of rMSCs after transfected by LPD was determined by the production of LPD after 14 days in an osteogenic medium. Osteopontin is a bone marker protein and its expression by osteoblasts differentiated from rMSCs was used as a marker to verify the osteoblastic differentiation of rMSCs. Similar to untransfected rMSC (Figure 2.12B) but unlike the undifferentiated control (Figure 2.12C), LPD-transfected rMSCs (Figure 2.12A) retained the ability of rMSCs to differentiate along the osteogenic lineage.
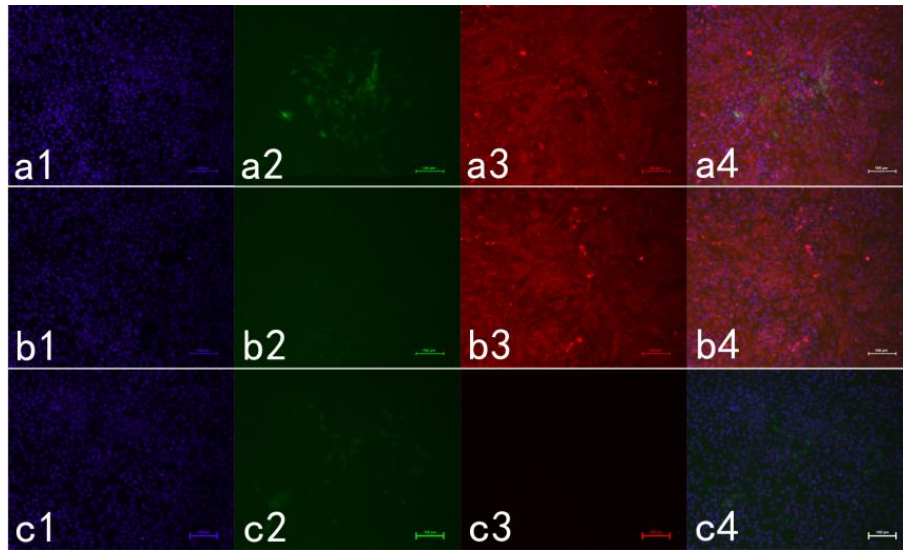
Figure 2.12 Osteogenic differentiation assays of rMSCs. A) Differentiation of LPD-transfected rMSCs in an osteogenic medium. B) Differentiation of untransfected rMSCs in an osteogenic medium. C) The undifferentiated rMSC was tested as a control. Image 1 in (A–C) shows cell nuclei using DAPI stain (blue); image 2 is GFP expression (green); image 3 shows immunofluorescence staining of osteopontin-positive cells (red); image 4 is merged from images 1, 2, and 3. No differences in osteogenic differentiation were observed between transfected and untransfected rMSCs, but the differentiation of both transfected and untransfected rMSCs was different from the undifferentiated control. Scale bar: 100 μm.

2.4 Discussion

MSCs are multipotent cells, which hold a tremendous promise for the construction and regeneration of tissues. However, MSCs by themselves have exhibited limited efficacy in terms of tissue regeneration and differentiation to the desired cell types. Therefore, genetic engineering has been proposed as a method to enhance the efficacy of MSC-based therapies. Genetic modification of stem cells by transposons to obtain sustained gene expression may further enhance their therapeutic efficacy.

Sleeping Beauty (SB) is a Tc1/mariner-like transposon system, artificially reconstructed by site-directed mutagenesis from an inactive salmonid transposable element.[118] After expression in a cell, SB transposases bind to the SB inverted/direct repeat elements (IRs/DRs) in a substrate-specific manner and induce transposition by a ''cut-and-paste'' mechanism, inserting a transposon into a new genomic location containing TA dinucleotides.[118,119] Transposon integration occurs with little preference for the transcriptional status or genetic identity of the sequence into which the SB transposon integrates.[119-122] Since its introduction, the SB transposon system has been tested in numerous model organisms to correct several genetic deficiencies.[123]

Although proof-of-principle studies using non-viral gene delivery have established the potential of SB-mediated insertion into the host genome for long-term gene correction,[124] the delivery is nonselective. Thus, an efficient cell type-specific targeting system is desirable to fully investigate the potential of SB and other vertebrate transposon vector systems for gene therapy.

We constructed LPD for a targeted transposon delivery. This structure is advantageous in terms of integrating various functional devices for controlling intracellular trafficking into one nanoparticle. The LPD was a nanoparticle formed solely by charge-charge interactions, specifically, between preformed cationic liposomes, and an anionic complex of protamine, targeting peptides and anionic nucleic acids. First, the plasmid was condensed by protamine into a negatively charged compact core. The complex should only contain the required amount of protamine that can provide sufficient concentration but keep the complex negatively charged. Then, the complex interacted with the cationic liposome to form the LPD. Again, the LPD should only contain a slight excess of lipids that allow full coating of the complex with the cationic lipids.

According to the result of zeta-potential measurement, protamine/pDNA particle at a 1:1 weight ratio had a negative potential. After being incorporated with DOTAP/DOPE/Chol liposome, the zeta potential of particles was shifted to positive, which confirmed the formation of LPD. The gel electrophoresis, which was consistent with zeta potential measurement, also demonstrated the shift of zeta-potential. The highly positively charged surface of LPD (zeta potential $\approx$20 mV) would favor the strong charge-charge interaction with the cells, which could increase the association with the cells during gene transfection. The diameter of LPD was approximately 200 nm, which would facilitate its endocytosis by cells.[125]

Three rounds of consecutive phage display panning were conducted to select peptide ligands which can target rMSCs specifically. After panning, four peptide sequences were identified from randomly selected individual recombinant phages. Based on the recovery efficiency and phage capture ELISA results, we categorized the peptide VTAMEPGQ as the best binder to rMSCs under stringent conditions. rMSCs-affinity assay showed that as the concentration of peptide increases, more FITC-labeled peptide 1 was located in rMSCs, but neither high nor low concentrations of control peptide 4 induced localization into rMSCs. Furthermore, the affinity between dye-labeled peptide 1 and rMSCs was

competitively inhibited in the presence of peptide 1. However, the affinity of dye-labeled peptide 1 for rMSCs was not affected by control peptide 4. After the FITC-labeled peptide 1 was interacted with two different control cells (rat fibroblastic cells and rat smooth muscle cells) separately, we found that peptide 1 did not bind any of the two control cells. These facts confirm that peptide 1 has high targeting specificity and affinity against rMSCs. Thus, we selected peptide 1 as rMSCs-homing peptide candidate for the rest of our study.

The transfection experiment showed that transgenic activity of LPD could be promoted by either peptide 1 or 2. This indicates that peptide 1 could target to rMSCs and enhance the endocytosis of LPD mediated by receptor. The peptide 2 could direct plasmid into the nuclei to improve the interaction between the exogenous gene and the host genome. Peptide 3 is fused from peptides 1 and 2 and did not display better action than the original sequences. It is assumed that the function of the two peptides might be degraded by steric hindrance after being fused together, thus resulting in their inactivity.

After being combined with both unfused peptides 1 and 2, LPD mediated a higher gene expression. It was suggested that LPD could firstly home to and enter the rMSCs by means of peptide 1, and then, be

guided by peptide 2 to translocate into the nuclei and achieve efficient gene delivery. The two peptides executed their actions at the right space and time, resulting in a synergetic effect. Other combinations of the three peptides did not show the optimal transfection action as shown by peptides 1 and 2.

To verify the synergetic effect of peptides 1 and 2, one of them was replaced with the control peptide 4 for the combination. The control peptide 4 did not possess any function to improve transfection. Moreover, the peptide 4 also could not execute a synergetic effect with either peptide 1 or 2. This demonstrates that peptides 1 and 2 could assist each other exclusively to achieve optimal transgenic action.

It was shown that the optimal transgenic action can be completed at a 3:1 peptide plasmid ratio. This suggests that a lower quantity of peptide could not execute its function to target the cell and nucleus efficiently. Additionally, when the quantity of the peptide is too high, its receptor might be blocked, resulting in a depressed targeting transposition. This phenomenon is the so-called "excess inhibition" of receptors.

Confirmation of the delivery of transposon into the nuclei by LPD was supported by confocal microscopy. This result showed that LPD with peptides 1 and 2 can accumulate into nucleus efficiently but when LPD

was modified with only peptide 1, the plasmid failed to translocate into the nucleus. This fact suggests that the NLS peptide contributes to the efficient nuclear localization of the complexes. The nuclear localization is very important for transposon transfection. Since transposons do not have the transducing abilities of viral vectors, it is necessary to devise a method to deliver this plasmid-based system into cells efficiently. The transposition rate is critically dependent on the efficiency of uptake of the plasmids into the cell nuclei. After being guided into the nucleus by NLS, transposon had a high opportunity to integrate into host genome, causing substantially increased transfection efficiency.

One of the major barriers of non-viral gene delivery is the transient nature of gene expression. Therefore, stable genomic integration is a particularly attractive feature to enable stable transduction of dividing target cells, especially for stem cells, and their differentiated progeny. We performed a time course of gene expression levels using transposon. The levels of gene expression were examined up to 168 h both from pEGFP-N1 and transposon in rMSCs. For the pEGFP-N1, a gradually reduced expression level was observed after 96 h. However, the transposon maintained 90% of its maximum transfection even after 168 h, which appeared to increase the duration of gene expression. The transgenic activity of transposon was also superior to the pEGFP-N1 as 1.43 times.

This suggested that the expression of the SB transposase gene on transposition rates will trigger the activity of SB transposon to increase insertion rates of transgenes into cellular chromosomes.[126] Thus, the transposon system could yield unprecedented stable and durative gene transfer efficiencies that compare favorably to the stable transduction efficiencies of integrating viral vectors.[127,128] This system is expected to facilitate widespread applications in functional genomics and gene therapy.

It was shown that LPD was relatively safer than Lipofectamine 2000. No notable toxicity was observed for LPD among any of the given concentrations. This might result from the biocompatibility of liposomes and peptides. LPD was found to have no negative effect on the differentiation potential of rMSCs. Cells transfected with the LPD were able to differentiate into the osteogenic lineage as were the un-transfected cells. Thus, LPD with various peptides was regarded as a safe gene delivery system. Furthermore, it can be utilized over a larger range of dosages. Accordingly, LPD is a promising gene carrier without any significant adverse effects on the rMSCs.

2.5 Conclusions

In conclusion, we identified an rMSC-targeting peptide by phage display. A liposome protamine/DNA lipoplex (LPD) was constructed by combining the targeting peptide and a nuclear localization signal (NLS) peptide with a Sleeping Beauty transposon delivery system. Our results show that the selected peptide can improve the transfection efficiency due to its rMSC-targeting property. The rMSC transfections mediated by LPD with the targeting peptide and NLS peptide were much more efficient than those mediated by the randomly chosen control peptide. We also found that the targeting peptide and NLS peptide could have a synergetic effect to promote efficient and lasting transfection expression of transposon. Furthermore, LPD neither showed apparent cytotoxicity nor disturbed the osteogenic differentiation of rMSCs. Therefore, a liposome-based nanoparticle combined with NLS and rMSC-homing peptide was developed for targeted delivery of the transposon system to rMSCs, yielding stable and durative gene transfer efficiency, making it a promising gene carrier for future applications.

Chapter 3 Reiterated targeting peptides on the nanoparticle surface significantly promote targeted vascular endothelial growth factor (VEGF) gene delivery to stem cells

3.1 Introduction

Stem cell-based gene therapy is a promising approach to the treatment of many diseases such as myocardial ischemia[129,130], bone defects[131,132] and cancer[133,134]. In this approach, a foreign gene, such as the one encoding vascular endothelial growth factor (VEGF), is carried by stem cells such as mesenchymal stem cells (MSCs) and the transfected stem cells are implanted into the diseased sites (e.g., ischemic heart), followed by the expression of the gene into a functional protein (such as the VEGF that can induce blood vessel formation to repair the ischemic heart). MSCs are considered a good cell carrier in stem cell-based gene therapy because they also have the potential to differentiate into bone, muscle, cartilage and other connective tissues. This multipluripotency makes MSCs attractive candidate for gene therapy[135]. VEGF is essential for vasculogenesis and angiogenesis to regenerate new blood vessels[136]. Hence, it is a good therapeutic protein in treating diseases where new blood vessel formation is the key, such as the healing processes of damaged bones [137]. Study showed that MSCs expressing VEGF hold

potential for treating various disease[138-140]. Study also showed that viruses can carry gene in gene therapy with a high efficiency[3,141-144]. However, they are not ideal carriers because they can potentially induce mutagenesis and immune responses. To overcome such challenges, non-viral vectors such as nanoparticles (NPs)[145-148], cationic lipids[149-151] and polymers[68,152,153] are proposed for gene delivery to MSCs. However, due to the lack of efficient internalization, nuclear translocation and integration of foreign genes into host genome, the non-viral vectors generally have low transfection efficiency (typically lower than 20%), particularly when they are used to deliver the gene into the hard-to-transfect stem cells. Thus there is a pressing need in the development of a biocompatible and efficient non-viral vector for gene delivery to MSCs.

Previously we showed that a peptide (VTAMEPGQ, termed VT-peptide) that can target bone marrow-derived rat MSCs (rMSCs) could be selected from a random peptide library by using phage display technique[154]. We also showed that when the peptide was mechanically mixed with lipids to form liposomes, only leaving a few molecules on the surface, the EGFP gene transfection efficiency could be improved from ~8% to ~12%. We then hypothesized that if the peptide was presented on the surface of nanoparticles by chemical conjugation with the surface molecules, the nanoparticles will have a higher efficiency of recognizing

the rMSCs and becoming internalized, leading to improved efficiency of delivering gene into rMSCs. Moreover, once gene is delivered into the rMSCs, the gene needs to be translocated to the cell nuclei and also inserted into the host genome for gene expression. To assist these two important steps, we adopt two measures. One is to integrate a reported nuclear localization signaling (NLS) peptide (DKKKRKV) with the DNA to be delivered[155,156]. Another is to use a non-traditional special type of plasmid, a sleeping beauty (SB) transposon system, which is a mixture made of a transposon and a transposase[157,158]. The transposon carries the VEGF target gene and the transposase acts as an enzyme that can "cut" the VEGF gene from the transposon and "paste" it into the host genome of rMSCs. The "cut-and-paste" mechanism ensures the target gene to be expressed in a long-lasting manner instead of the undesired transient manner. In essence, to solve the two daunting challenges facing the use of non-viral nanoparticles to transfect MSCs, namely, the low efficiency of delivering gene to the cells and transient production of functional protein, we allow the rMSC-targeting peptide to be chemically conjugated to the surface of lipid-based nanoparticles (LBNs), which deliver a VEGF-encoding SB transposon system complexed with a cationic NLS peptide to rMSCs.

Specifically, we employed a three-fold reiterated rMSC-targeting peptide (VTAMEPGQVTAMEPGQVTAMEPGQC, termed 3VT-peptide) to study if we can observe enhanced transfection effect. Non-reiterated VTAMEPGQC (VT-peptide) was used as a control. A cysteine at the C-terminal of peptide was introduced to facilitate peptide-lipid conjugation. Second, in contrast to the conventional plasmid vectors, the SB system provides efficient and long-term gene expression. Third, in order to overcome the nuclear membrane barrier, we incorporated the NLS peptide to enhance nuclear translocation of DNA. The NLS peptide has been proven to promote gene expression to mammalian cells[156,159]. Fourth, the arginine-rich polycationic protamine is used as a condensation reagent. Studies showed that protamine was able to condense plasmid DNA efficiently to promote gene delivery to several cell types in combination with liposome[160,161]. The fabricated nanoparticles display rMSC-targeting motif on the surface and carry an electrostatically condensed mixture of NLS peptide, protamine and SB system inside, promoting MSC-internalization，nuclear translocation and integration of target gene into MSCs genome, all of which collectively resulted in enhanced sustained gene expression.

3.2 Materials and methods

3.2.1 Materials

All the lipids such as 1,2-dioleoyl-3-trimethylammonium-propane (DOTAP), 1,2-dioleoyl-sn-glycero-3-phosphoethanolamine (DOPE), and 1,2-distearoyl-sn-glycero-3-phosphoethanolamine-N-[maleimide(polyethylene glycol)-2000] (DSPE-PEG2000-MAL), mini extruder and polycarbonate membrane filters were purchased from Avanti Polar Lipids Inc. Cholesterol, protamine and chloroform were purchased from Sigma Aldrich. Fetal bovine serum (FBS), Dulbecco's Modified Eagle Medium (DMEM), SYBR Safe and lipofectamine® 2000 were purchased from Invitrogen.

3.2.2 Construction of VEGF SB transposon system

We obtained the pEGFP-VEGF plasmid containing VEGF and EGFP gene from Professor H. K. Lin (the Health Science Center, University of Oklahoma). The original sleeping beauty transposon pT2/SVNeo (the transposon) and pSB11 (the transposase) were a kind gift from Dr. Perry B. Hackett (University of Minnesota). The neomycin resistance gene in pT2/SVNeo was replaced by VEGF and EGFP gene (Figure 3.13). First, DNA fragments containing VEGF and EGFP gene

72

were amplified by PCR from pEGFP-VEGF plasmid (Primer1: GCC<u>TGATCA</u>ATGAACTTTCTGCTGTCT; Primer2: GCC<u>TTCGAA</u>TTACTTGTACAGCTCGTC), the underlines denote the introduced restriction enzyme sites. Second, both the DNA fragments and pT2/SVNeo plasmids were digested by restriction enzyme BclI and BstBI. Finally, the digested products were purified and ligated to give rise to the recombinant pT2/VEGF plasmid. The purified pT2/VEGF plasmids were verified by DNA sequencing (MCLAB).

3.2.3 Preparation of Liposome

The liposomes consisting of DOTAP, DOPE and cholesterol (1:1:1 molar ratio) were prepared by thin film hydration. Briefly, a thin lipid film was formed by evaporating the lipid solvent with nitrogen gas in a 10 ml round bottom flask. Hydration of the lipid films was done with vigorous vortexing for 1h, followed by sonication for 5 min. The resultant liposomes were repeatedly extruded (9 times) at room temperature through polycarbonate membranes filters of decreasing pore size of 0.2 and 0.1 mm respectively using a mini extruder.

3.2.4 Conjugation of targeting peptide with DSPE-PEG2000-MAL

VTAMEPGQGGGC peptide (VT-peptide, MW=1106.25) or VTAMEPGQVTAMEPGQVTAMEPGQGC (3VT-peptide, MW=2620.01) were synthesized by United BioSystems Inc. The reduction of cysteine residues in the targeting peptide was first performed. Briefly, 5 ml peptide (100 μM, PBS, pH7.5) was first mixed with tris (2-carboxyethyl) phosphine (TCEP) (2 mM) with a 1:2 ratio of peptide/TCEP. The reaction was allowed to proceed at 37 $^\circ$C for 2 h. A 10 μl DSPE-PEG2000-MAL (10 mM) stock solution was reacted with 5 ml (100 μM) of the reduced peptide in PBS buffer (pH 7.5), corresponding to 5:1 molar ratio of reduced peptide to maleimide groups. The conjugation reaction was carried out for 3 h at room temperature. Conjugated peptide-PEG-DSPE was purified by dialysis (500 Da membranes).

3.2.5 Preparation of targeting LBNs

To obtain targeting liposome, the insertion of the peptide conjugated lipid (peptide-PEG-DSPE) into liposomes was performed by employing a post-insertion technique. Targeting liposomes were prepared with varied peptide-PEG-DSPE:liposome molar ratios at 0.1%, 0.5%, 1%, 5% and 10%. For this purpose, liposome (20 mM, as denoted by DOTAP in liposome) in water solution was incubated with a various amount of

peptide-PEG-DSPE for 1 h with vortexing. The resultant solution was kept at 60 ° C for 1 h. As a result, the conjugates became attached to the outer lipid layer of the vesicles via hydrophobic DSPE domain. The size and zeta-potential values of liposome in water solution were determined by dynamic light scattering (DLS) (Zeta Potential Analyzer, Brook haven Instruments Corporation, NY).

3.2.6 Gel retardation of protamine/pDNA polyplexes

The protamine and pDNA (0.25 μg) were mixed at different weight ratios and incubated for 20 min. The resultant complexes were confirmed using gel electrophoresis (1% agarose gel, 105 V, 40 min, with SYBR Safe staining).

3.2.7 Gel retardation of Liposome Protamine/DNA Lipoplexes

The protamine and pDNA (0.25 μg) were mixed at a weight ratio of 2:1 and the complex was incubated for 20 min. Then, the DOTAP/DOPE/Chol (Mole ratio 1:1:1) liposome was added into the complex followed by incubation for 20 min. The resultant complexes were confirmed using gel electrophoresis as shown in Figure 3.5 (1% agarose gel, 105 V, 30 min, with SYBR Safe staining).

3.2.8 Preparation of LBN

Sleeping Beauty plasmids (transposon and transposase plasmids at 2:1 mass ratio) and protamine, NLS peptides were mixed at various weight ratios to form polyplex. The resultant polyplex was allowed to stand at room temperature for 30 min. Then liposome was added into the polypex solution followed by vortexing. The resultant mixture was incubated for 1 h to give rise to LBN.

3.2.9 MTT Assay

The cells were seeded at a concentration of 2×10^4 cells/well in 96-well plates in standard expansion medium for 24 h. PBS was used to wash cells and different concentrations of LBN or Lipofectamine 2000 were used to treat cells for 6 h. Cell viability was evaluated using the 3-(4,5-dimethyl thiazol-2-yl)-2,5-diphenyl tetrazolium bromide (MTT) assay. MSCs were incubated with MTT solution (5 mg/ml, 20 μl, Sigma, USA) for 4 h. After the supernatant was discarded, dimethyl sulfoxide (DMSO, 300 μl) was used to dissolve the formazin crystals. Biotek plate reader was used to quantify cell viability by measuring absorbance at 570 nm.

3.2.10 LBN internalization

LBN was prepared using carboxyfluorescein-labeled DOPE and the rhodamine labeled pDNA. The rMSCs were incubated in 96-well plates at 37 ° C. The cells were then transfected with dye-labeled LBN and incubated for 4 h. The transfection medium was then replaced with fresh expansion medium. MSCs were later fixed with 4% paraformaldehyde for 20 mins. Cell nuclei were stained with DAPI. The LBN particle internalization was visualized with fluorescence microscope.

3.2.11 Gene transfection

Dulbecco's Modified Eagles Medium (DMEM) containing 15% fetal bovine serum (FBS) and 1% antibiotic was prepared as expansion medium for rMSCs and rat dermal fibroblasts. Cells were cultured in the 24-well plate at a density of 1×10^5 cells/well and incubated for 24 h. Cell culture medium was replaced with 500 μl fresh expansion medium and various LBN particles were added with a final 1 μg/ml DNA per well. Lipofectamine 2000 was used as a control. The cells were incubated for another 4 h at 37°C. The transfection medium was then replaced with a fresh expansion medium. GFP expression was visualized with fluorescent microscopy. For flow cytometry evaluation (Becton-Dickinson Biosciences, Franklin Lakes, NJ, USA), the transfected cells detached

from culture flasks by trypsin digestion and fixed in 4% paraformaldehyde for 20 min to prepare single cell suspensions.

3.2.12 Immunofluorescence assay

4% fresh paraformaldehyde was used to fixed rMSCs for 40 min at room temperature. Then PBS was used to wash the cells, followed by incubation of the cells for 1 h in blocking buffer (5% goat serum, 1% BSA, 0.1% Triton X-100 in PBS). After the blocking buffer was removed, the cells were incubated overnight at 4°C in the presence of primary antibody (VEGF, rabbit, abcam) diluted in PBS (5% goat serum). Then PBS was used to wash the cells. The cells were then incubated with the dye-labeled antibody, goat anti-rabbit IgG-TRITC (1:250, Santa Cruz Biotechnology) in PBS (5% goat serum), without light at room temperature for 2 h. After the cells were washed, they were stained with DAPI (0.5 μg/mL, Invitrogen). A fluorescence microscope was then used to image the cells.

3.2.13 Statistical analysis

Statistical analysis was performed using two-tailed unpaired Student's t-test. Data are presented as mean ± SD (standard deviation).

3.3 Results and Discussions

3.3.1 LBN particles characterization

LBN particles were fabricated using a packaging technique as described in Figure 3.1. Briefly, the negatively charged DNA, i.e., the SB transposon system, was condensed via electrostatic interactions with positively charged protamine. The DNA to protamine ratio was tuned to form a slightly negatively charged polyplex. The rMSC-targeting peptides were conjugated to 1,2-distearoyl-sn-glycero-3-phosphoethanolamine-N-[maleimide(polyethylene glycol)-2000] (DSPE-PEG-MAL) lipids (Figure 3.1A). Specifically, the thiol groups on the cysteine residues of 3VT-peptide or VT-peptide were reduced for facilitating the conjugation of the targeting peptide to DSPE-PEG-MAL lipid. The cysteine reduction efficiency was >95% as determined by DTNB assay[162]. The conjugated anionic peptide-lipid complexes were later anchored onto the LBNs. The resultant peptide-lipid conjugates were co-inserted into DOTAP/DOPE/Chol liposomes, which were prepared by a thin film hydration method[114,163], using a post-insertion technique[164,165]. Finally, the positively charged liposome complex was coupled with negative charged protamine/DNA polyplex to give rise to LBNs (Figure 3.1B).
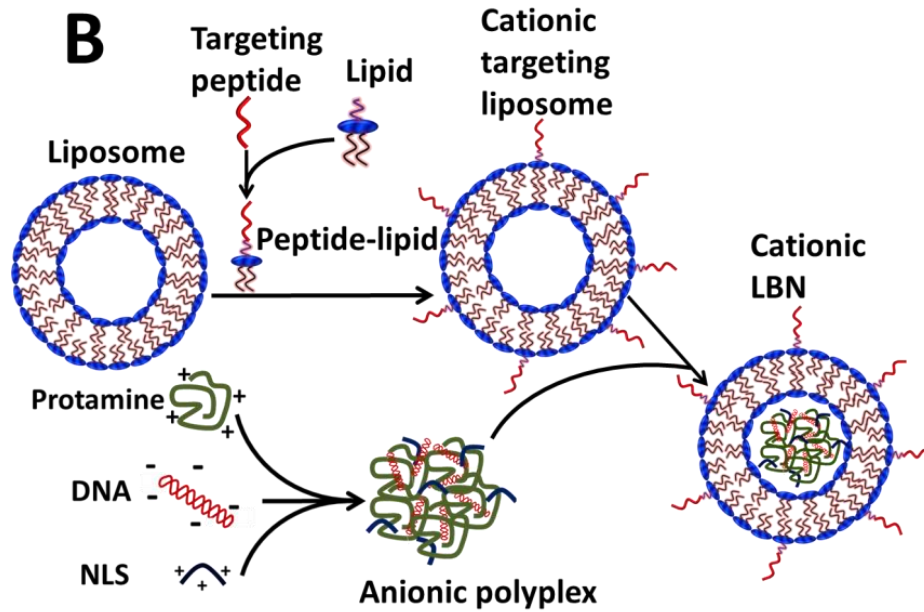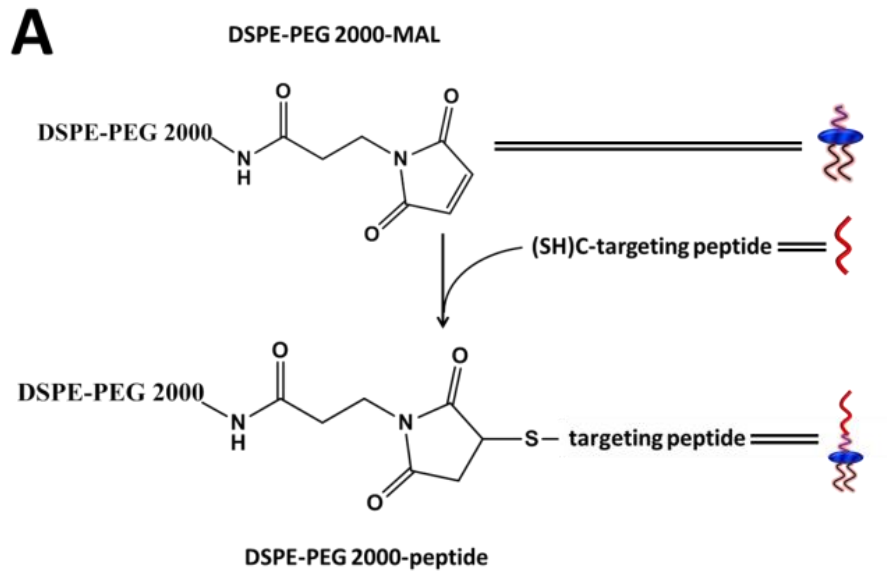
Figure 3.1 The schematic showing the construction of stem cell targeting lipid-based nanoparticles (LBNs). A) Thiol group of cysteine at the

carboxyl-terminus of targeting peptide was conjugated to maleimide (MAL) group of DSPE lipid to form peptide-lipid complexes. B) Peptide-lipid complexes were co-assembled with other lipids (DOTAP, DOPE) and cholesterol to form cationic targeting liposome. Cationic protamine and NLS were collectively used to condense DNA to form anionic protamine/DNA/NLS polyplexs. Finally, the anionic polyplexs were entrapped into cationic targeting liposome to generate cationic targeting LBNs.

The dynamic light scattering of the as-prepared liposomes (with 0% peptide-lipid insertion) showed a size of 110.37 nm with a zeta potential of 77.17 mV (Figure 3.2). The size of the targeted LBN (with 10% 3VT-peptide-lipid insertion) increased to 190.24 nm, with a zeta potential decreased to 62.22 mV (Figure 3.2). As the molar percentage of peptide-lipid in LBNs increased, the size of particles increased and the zeta potential decreased, which indicates the successful insertion of peptide-lipid into the liposomes to form LBNs. The particle size and zeta potential of different percentages of VT-peptide-lipid in LBNs showed a similar pattern (Figure 3.3).
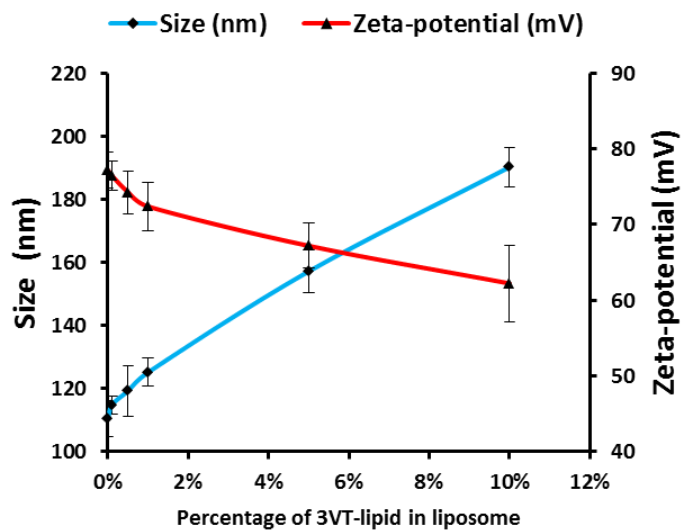
Figure 3.2 Comparison of nanoparticle size and zeta potential between liposomes with different molar percentages of 3VT-peptide-lipid. Data are shown as mean ± SD (n = 3).
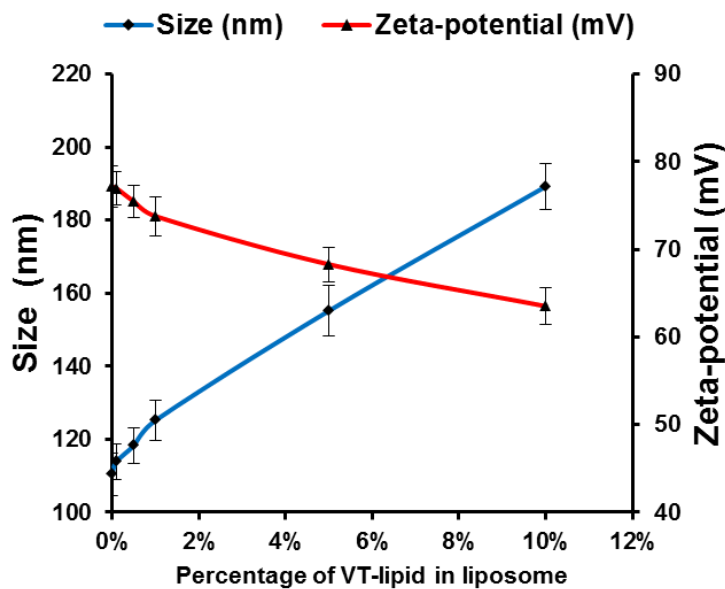
Figure 3.3 Particle size and zeta potential comparison of different percentages of VT-peptide-lipid in liposome. Data are shown as mean ± SD (n = 3).

The DNA loading capability of protamine was determined by gel retardation assay (Figure 3.4). DNA was completely encapsulated when the mass ratio of protamine/DNA reached 4:1. Thus 2:1 ratio was used to render the negative charge of protamine/DNA. DNA loading capacity of liposome was also evaluated (Figure 3.5). The result indicated DNA was completely encapsulated when liposome/DNA mass ratio reached 3:1, which indicated the particle was slightly positively charged. Thus, this ratio was used in the subsequent experiments. The positively charged

nanoparticle will interact with negatively charged cell surface to propel subsequent endocytosis uptake[166,167].
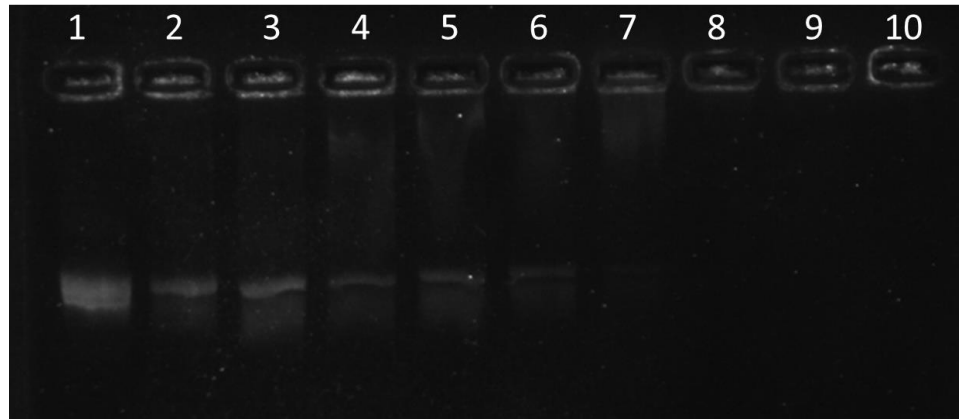
Figure 3.4   The DNA retardation assay to determine the DNA loading in protamine at various weight ratios of Protamine/DNA. (1) 0:1, (2) 0.0625:1, (3) 0.125:1, (4) 0.25:1, (5) 0.5:1, (6) 1:1, (7) 2:1, (8) 4:1, (9) 8:1 and (10) 16:1 respectively. Gel retardation result indicates DNA is completely encapsulated when Protamine/DNA ratio reaches 4:1 on lane 8.
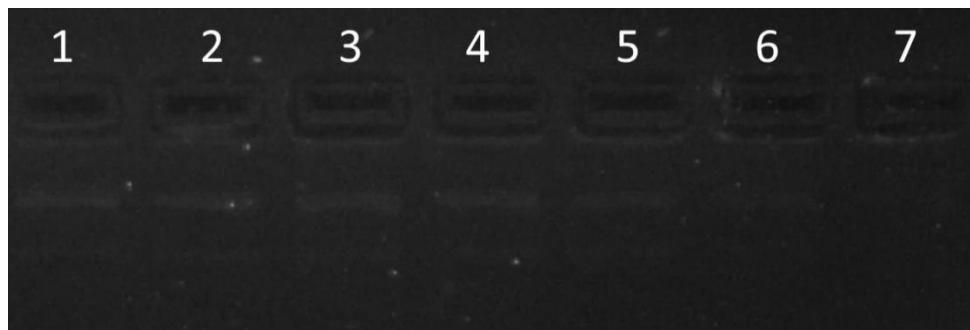
Figure 3.5 Gel retardation assay of LBN at various liposome/DNA mass ratios. (1) 0:1, (2) 0.1875:1, (3) 0.375:1, (4) 0.75:1, (5) 1.5:1, (6) 3:1, and (7) 6:1. Gel retardation result indicated DNA was completely encapsulated when Liposome/DNA ratio reaches 3:1 on lane 6. The mass of liposomes was denoted by the mass of DOTAP in LBN.

3.3.2 Cell cytotoxicity assay

The cytotoxicity of as-prepared LBN was evaluated by MTT assay (Figure 3.6) with Lipofectamine 2000 as a control. At a concentration of 20 μg/ml, rMSCs viability was obviously reduced below 60% with Lipofectamine treatment, whereas all rMSCs remained above 80% viability when treated with different LBN particles. The results clearly demonstrated that our LBN particles are more biocompatible than Lipofectamine. Actually, LBN with a concentration of only 3 μg/ml was used for gene transfection.
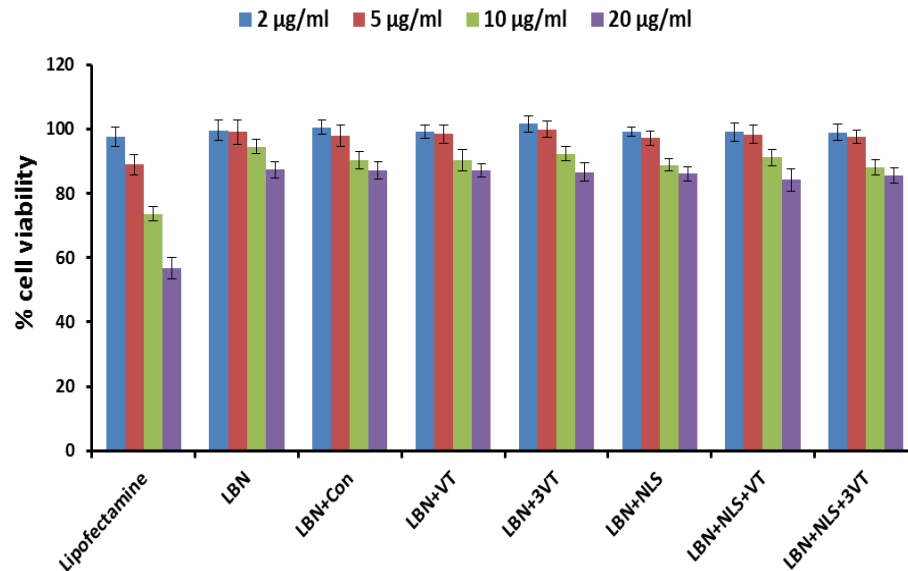
Figure 3.6 MTT assay of MSCs at different concentrations of LBN particles and Lipofectamine 2000. Data are shown as mean ± SD (n = 3).

3.3.3 Cell internalization of LBN

After the successful synthesis of LBN with low toxicity and high DNA-loading capability, we performed cell internalization of LBN in rMSCs (Figure 3.7). To verify the capability of internalization of LBNs in rMSCs due to the presence of rMSC-targeting peptide on the surface, green dye-labeled lipids and red dye-labeled DNA were used to form LBNs, followed by interaction with rMSCs. Green fluorescence from carboxyfluorescein-labeled liposome and red fluorescence from rhodamine-labeled DNA demonstrated that the LBNs were successfully

internalized in rMSCs. LBNs with targeting 3VT-peptide showed higher fluorescence than those without targeting peptide (Figure 3.7). This result indicated that targeting peptides facilitated the cellular internalization of LBNs. Thus the rMSC-targeting peptides on the surface of LBNs facilitated the internalization of LBN in rMSCs, which could lead to enhanced gene delivery to rMSCs.
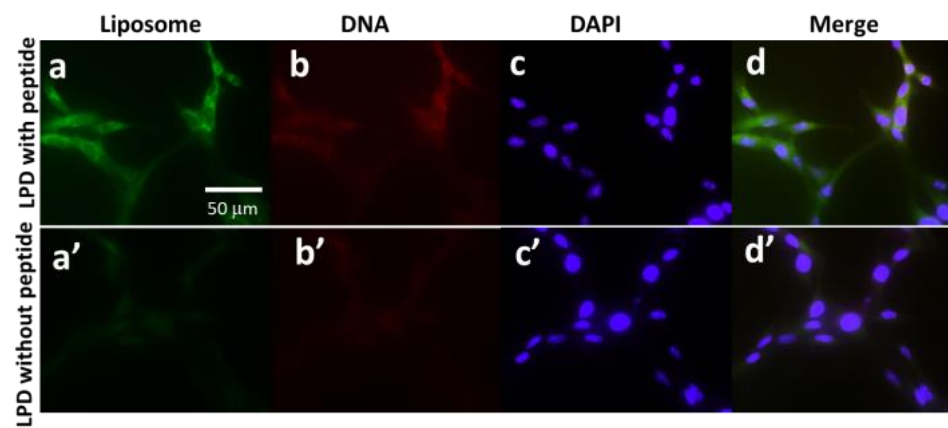
Figure 3.7 Fluorescent images of rMSCs after internalization of LBN with and without 3VT-peptide for 4 h. Lipids, DNA and cell nuclei were labeled with a green dye (carboxylfluorescein, a and a'), a red dye (rhodamine, b and b') and DAPI (c and d'), respectively. d is a merged version of a, b and c. d' is a merged version of a', b' and c'.

3.3.4 Gene transfection

The LBNs containing EGFP-VEGF plasmid and rMSCs-targeting peptide were investigated for targeted gene transfection to rMSCs in vitro. The quantitative EGFP expression was determined by flow cytometry. To determine the optimal gene transfection efficiency of LBNs, various percentages of VT-peptide-lipid (VT-lipid) or 3VT-peptide-lipid (3VT-lipid) in LBNs (without NLS peptide) were evaluated (Figure 3.8A). As the percentage of peptide-lipid increased, the gene transfection efficiencies also increased. At 5% of VT-lipid or 3VT-lipid, the transfection efficiencies plateaued at around 26% or 33%. So 5% VT-lipid or 3VT-lipid was used for the subsequent experiments. The plateau of transfection efficiency might result from the more negative zeta potential of LBN with an increased percentage of peptide-lipid in LBNs, since more negative zeta potential of the nanoparticles will not favour cell internalization. The effect of varying NLS peptide/DNA mass ratio on transfection efficiencies was also monitored with 5% 3VT-lipid prepared liposome. A 2:1 peptide/DNA ratio resulted in the highest gene expression (Figure 3.8B), therefore this ratio was used for the following experiments.
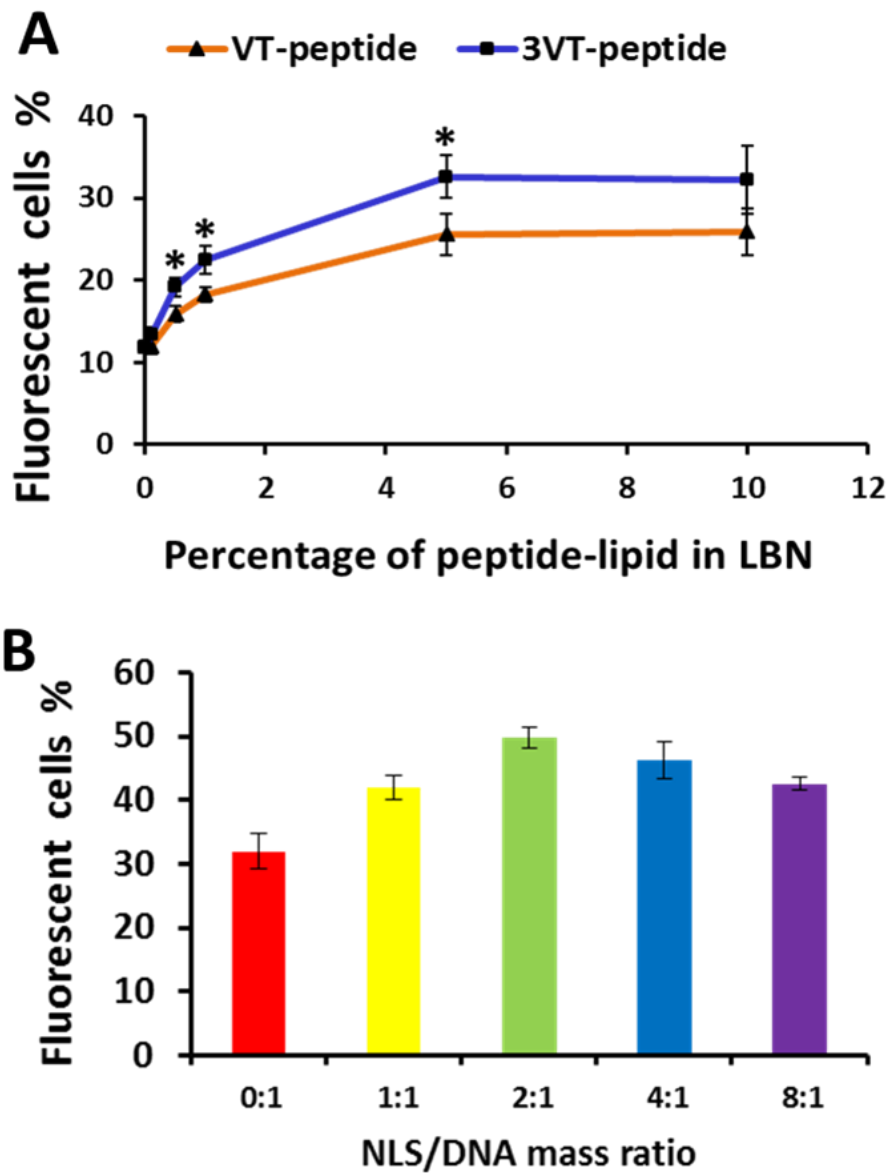
Figure 3.8 Effect of rMSC-targeting and NLS peptides on the transfection efficiency in rMSCs by LBN. A) The EGFP transfection efficiency of LBN with various molar percentages of peptide-lipid.

Asterisk denotes p < 0.05 comparing transfection efficiency of 3VT-peptide-lipid with VT-peptide-lipid at same percentage of peptide-lipid. B) The EGFP gene transfection efficiency of LBN with various NLS peptide/DNA mass ratios. EGFP gene expression was evaluated after 72 h transfection. Data are shown as mean $\pm$ SD (n = 3).

Transfection efficiencies of various LBNs were evaluated (Figure 3.9A). The corresponding EGFP gene expression was visualized with fluorescence microscopy (Figure 3.9B). We find that LBN particles without the surface display of the peptides (13.64%) showed similar transfection efficiency compared with commercially available Lipofectamin 2000 (14.65%). However, when displaying VT-peptide, LBN particles exhibited enhanced transfection efficiency (25.64%). Moreover, LBNs with 3VT-peptide (32.57%) demonstrated even higher transfection efficiency in comparison to those with VT-peptide. Importantly, when LBNs bear both 3VT-peptide and NLS peptide, the highest level of transfection (52.52%) was reached. Our results clearly indicated that both VT-peptide and 3VT-peptide facilitated LBN to efficiently deliver plasmid gene into MSCs. The three-fold reiterated 3VT-peptide demonstrated significantly enhanced transfection efficiency compared with VT-peptide. The targeting peptide and NLS peptide exerted a synergetic effect to promote gene transfection.

A
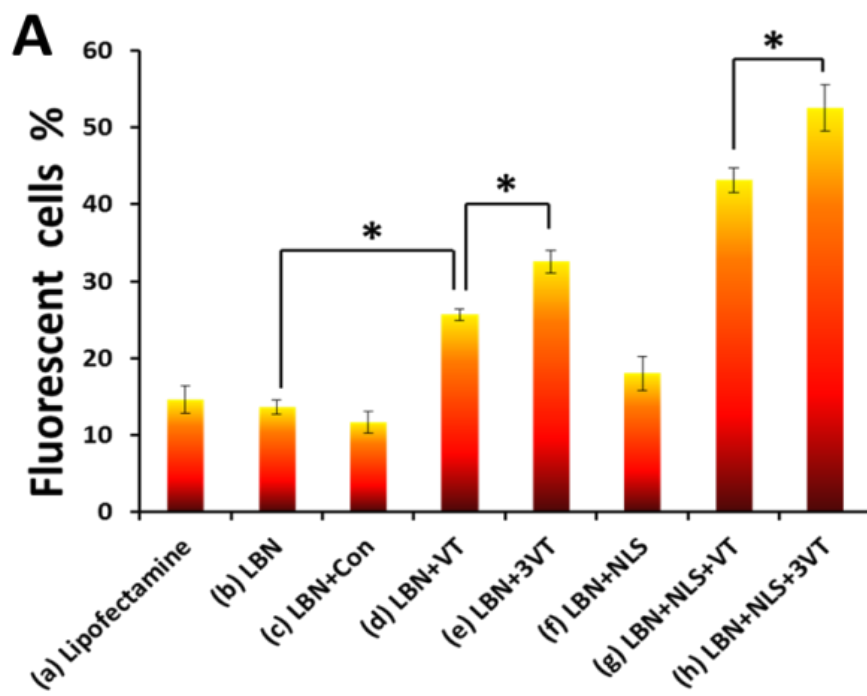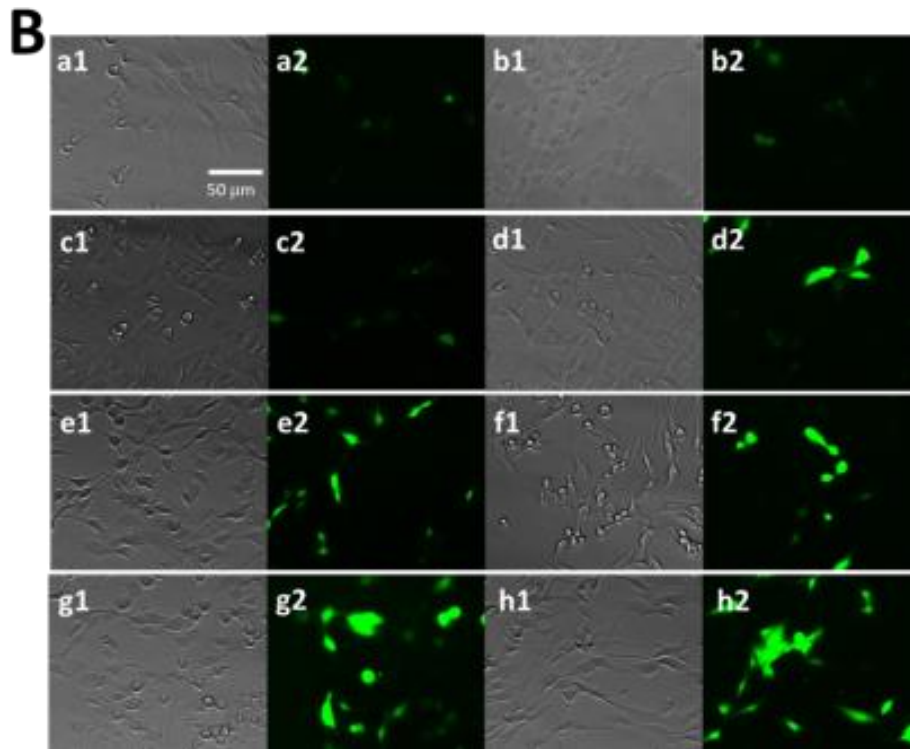
Figure 3.9 Comparison of transfection expression of EGFP in rMSCs by different carriers in 72 h. A) EGFP expression determined by different carriers: (a) Lipofectamine® 2000 (control), (b) LBN without any peptide, (c) LBN with control peptide CGVKYMVM, (d) LBN with VT-peptide, (e) LBN with 3VT-peptide, (f) LBN with NLS peptide, (g) LBN with VT-peptide and NLS peptide, and (h) LBN with 3VT-peptide and NLS peptide. Data are shown as mean ± SD (n = 3). Asterisk denotes $p < 0.05$. B) Fluorescence microscopy showing EGFP expression in rMSCs by carriers shown in A. Image 1 and 2 in (a–h) show the bright-field image and green EGFP expression, respectively.

To evaluate the specificity of LBN particles, rat dermal fibroblasts were used as a control cell for gene transfection (Figure 3.10). Flow cytometry results showed low transfection efficiency and no significant difference between LBNs with (3.34%) and without targeting peptide (3.97%). The results indicated that LBN with rMSCs-targeting peptide has no specificity for rat dermal fibroblasts.
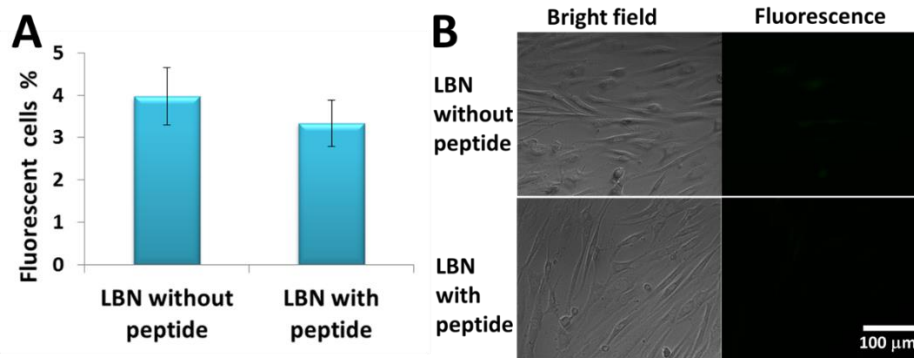
Figure 3.10 Transfection efficiencies of LBN with and without 3VT-peptide on rat dermal fibroblasts were evaluated with flow cytometry (A) and fluorescence microscopy (B). Data are shown as mean ± SD (n = 3).

A time course assessment of gene expression was carried out to compare EGFP-encoding SB transposon system for up to 168 h (Figure 3.11). The expression of EGFP in both EGFP-encoding SB transposon system and traditional (control) EGFP-encoding plasmid (pEGFP-N1)

reached maximum at 72 h. However, the transfection efficiency of control EGFP plasmid later decreased substantially at 168 h. In comparison, the SB system maintained a high transfection level even at 168 h. This result demonstrated the stable and durable gene transfection effect of SB system due to the efficient integration of target gene into rMSCs host genome by the transposase in the SB system.
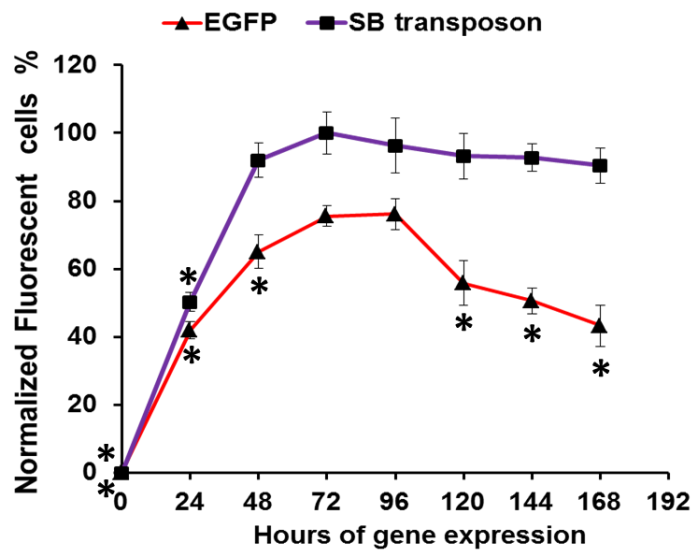
Figure 3.11 Time course comparison of gene expression of SB transposon system and control EGFP plasmid showing the long-lasting EGFP gene expression delivered in the form of SB transposon system. EGFP expression level of SB transposon system in rMSCs reached a maximum in 72 h, which was set as 100%. Data are shown as mean ± SD

(n = 3). Asterisk denotes $p < 0.05$ comparing with maximum expression at 72 h.

Studies indicated that VEGF gene delivery to MSCs improved therapeutic function of MSCs.[168-171] The strategy for constructing EGFP-VEGF-encoding SB transposon system was shown in Figure 3.13. After LBNs carrying the SB transposon system were used to transfect rMSCs, immunofluorescence assay was performed to visualize the VEGF gene expression (Figure 3.12) after 144 h of expression. When rMSCs were transfected with EGFP-VEGF-encoding SB transposon system, high transfection efficiency and co-expression of EGFP and VEGF were observed. In comparison, only EGFP gene expression but no VEGF expression was monitored when control EGFP-encoding SB transposon system was used. This result demonstrated the feasibility of using the LBN system for efficient VEGF gene delivery to rMSCs.
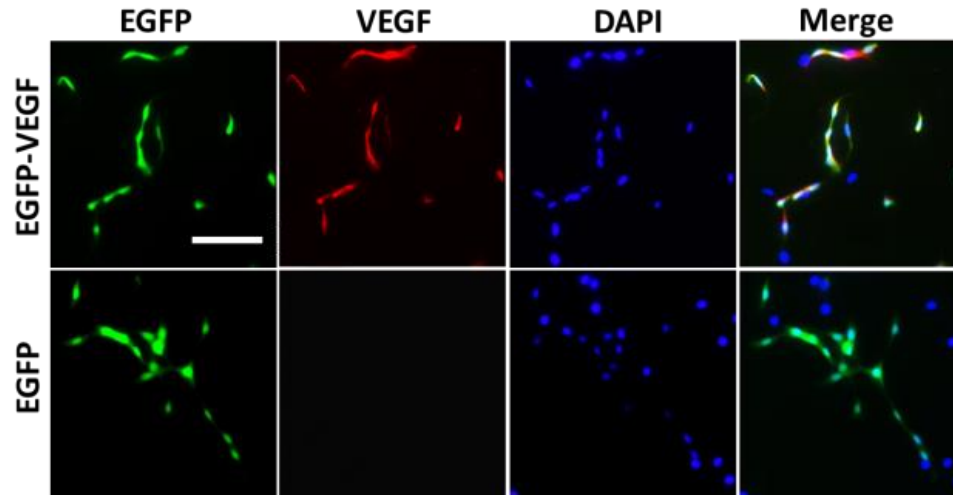
Figure 3.12 Comparison of gene expression of EGFP-VEGF or EGFP in SB transposon system by immunofluorescence assay. EGFP gene expression showed green fluorescence. VEGF gene expression was marked with red fluorescent tetramethylrhodamine (TRITC) labeled antibody. Cell nucleus was labeled with blue DAPI. LBN with 3VT-peptide was used to transfect rMSCs. Scale bar: 50 μm.
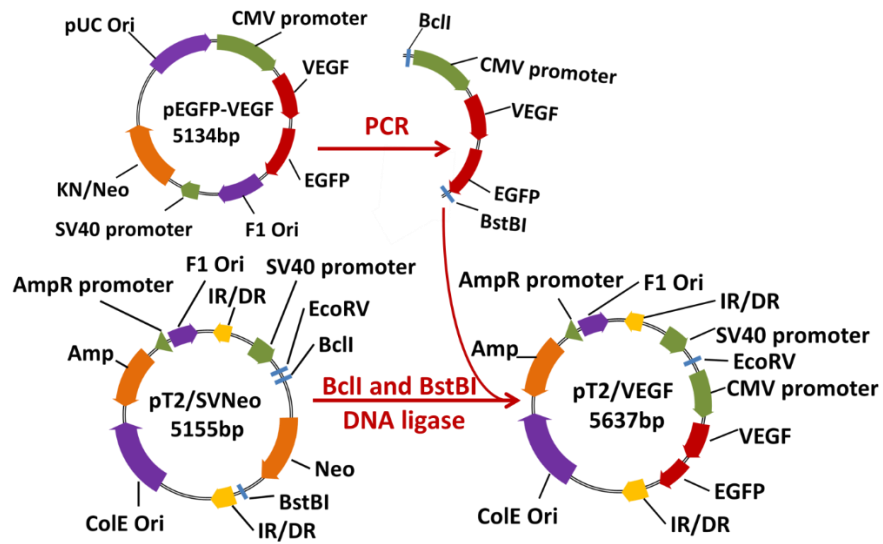
Figure 3.13   Construction of EGFP-VEGF SB transposon system.
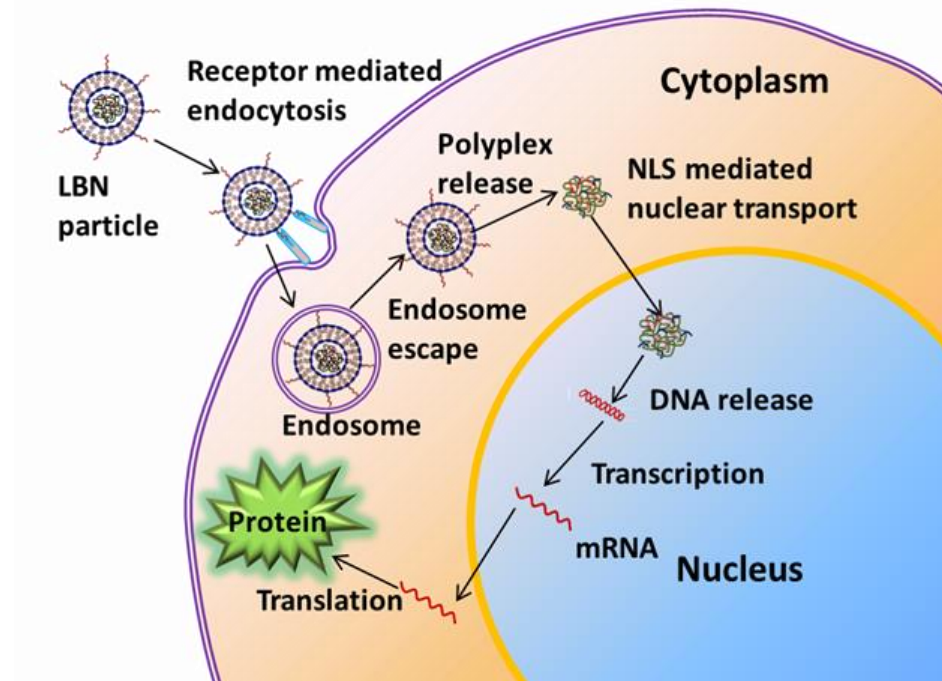
Figure 3.14 A stem cell targeting particle directed targeted gene delivery. This scheme shows the lipid-based nanoparticles (LBNs) endocytosis and gene expression mechanism. LPD particle enters MSCs through receptor mediated endocytosis. In cell cytoplasm, polyplex is released from endosome. Polyplex enters cell nucleus through NLS mediated nuclear transport. In cell nucleus, DNA is released and transcribed. In the end, gene is translated to protein in cell cytoplasm.

3.4 Conclusion

In summary, we developed a LBN system by incorporating the targeting peptides, NLS peptides and a VEGF-encoding SB transposon

system[172]. The resultant targeting LBN demonstrated high gene transfection efficiency and sustained gene expression profile, due to improved MSCs-internalization, nuclear translocation and gene integration. The gene delivery and gene expression mechanism was shown in Figure 3.14. The three-fold reiterated targeting peptide showed much higher capability in improving the transfection efficiency in stem cells than the non-reiterated targeting peptide. Targeting peptide and NLS peptide as well as the use of SB transposon system exerted a synergetic effect to promote efficient and lasting transfection gene expression. The LBNs are shown to efficiently deliver VEGF-encoding SB transposon system into stem cells to enable the cells to efficiently produce VEGF. This targeting LBN complex may have promising applications in clinical stem cell-based gene therapy.

Chapter 4 Virus Mimetic Cytoplasm Cleavable Magnetic/Silica Nanoclusters for Enhanced Gene Delivery to Mesenchymal Stem Cells

4.1 Introduction

Development of non-viral gene delivery vectors for transfecting MSCs will advance the tissue engineering and regenerative medicine to treat several health disparities associated with the heart, brain, spinal cord, bone, and blood vessels.[173-175] In the last decade, there has been remarkable progress in regenerative medicine using the stem cells for therapeutic applications.[176] However, to use these cells more effectively, enabling them to express functional proteins is crucial for rapid formation and repair of tissues and organs. For example, vascular endothelial growth factor (VEGF) is essential for angiogenesis for the progression of new blood vessels. Indeed, efficient VEGF gene expression in mesenchymal stem cells (MSCs) can stimulate the formation of new blood vessels. However, the transfection of VEGF gene into stem cells is complex and challenging because stem cells are hard to transfect. Hitherto, the most efficient gene delivery vectors used in MSCs are genetically engineered viruses encompassed with gene of interest.[177-179] The major limitations in using viral vectors are their inherent toxicity and

ability to induce immune and inflammatory responses. This fact drives research on the development of biocompatible non-viral vectors such as cationic lipids, polymers, hydrogels, and synthetic nanoparticles (NPs).[180-186] But these non-viral vectors are less effective when compared with viral vectors mainly due to the lack of efficient homing and internalization of foreign genes. So there is an urgent need in regenerative medicine to develop safe and efficient non-viral vectors for delivering a foreign gene to MSCs.

4.2 Materials and Methods

4.2.1 Materials

All commercial chemicals and reagents used in this research are used as received without any further purification. Iron (III) acetylacetonate, 1,2-dodecanediol, oleic acid, oleylamine, benzylether, 3-aminopropyltrimethoxysilane, 3-mercaptopropyltrimethoxysilane, tetraethylorthosilicate, hexadecyltrimethylammonium bromide (CTAB), penicillin-G, and streptomycin were all purchased from Sigma Aldrich. Fetal bovine serum (FBS), Lipofection 2000, and primers for PCR were purchased from Invitrogen. DMEM media was purchased from Gibco-BRL. LongAmp® Taq PCR Kit was purchased from NEB Inc.

4.2.2 Hydrophobic magnetic nanoparticles synthesis

10 nm hydrophobic magnetic nanoparticles were synthesized by the seed mediated growth method. First, 4 nm Fe_3O_4 nanoparticles were synthesized by the dissociation of 2 mmol of Fe(AcAc)3 in 10 mmol of 1,2-dodecanediol, 6 mmol of oleic acid, 6 mmol of oleylamine and 20 ml of benzyl ether. The reaction mixture was in reflux (300°C) under nitrogen atmosphere for 1 h. The synthesized nanoparticles were washed several times with ethanol to remove the un-reacted chemicals and finally the precipitated nanoparticles were separated with a magnet. The same procedure was repeated to synthesize the 6 nm and 10 nm nanoparticles by dissolving the 4 nm and 6 nm seed nanoparticles in hexane, respectively.

4.2.3 MSNCs Synthesis

The GSH-cleavable MSNCs were synthesized by in situ hydrolysis of tetraethyl orthosilicate (TEOS) and (3-mercaptopropyl)trimethoxysilane (MTMS) in the presence of superparamagnetic iron oxide nanoparticles (SPIOs) dispersed in Cetyl trimethylammonium bromide (CTAB) at 70 °C for 1 h. The excess CTAB present in the reaction medium was completely removed by centrifugation at 10,000 rpm for 10 min for three times and re-suspended in nanopure water. After complete removal of CTAB, the nanoparticles

solution was aged for 48 h, which resulted in the formation of 80-100 nm spherical MSNCs.

4.2.4 DNA Loading

As-synthesized MSNCs were centrifuged three times to remove excess surfactants, then the purified nanoparticles (8 µg/ml) were incubated overnight at 4°C with 2 µg of DNA before modified with protein conjugated PEI. We have confirmed the successful DNA loading using gel electrophoresis.

4.2.5 Transmission Electron Microscope

Magnetic silica nanoparticles were analyzed in a TEM (JEOL-2000FX). One drop of nanoparticles of each type was placed on a dry carbon-coated copper grid (150 mesh).

4.2.6 Dynamic light scattering (DLS)

The size distribution of MSNCs was measured using DLS in nanopure water. Our result shows that the average hydrodynamic size of MSNCs is ~150 nm.

4.2.7 DTNB assay

DTNB assay was performed as previously described [187]. 4 mg/ml 5,5'-Dithiobis- 2-nitrobenzoic acid (DTNB) solution was prepared in ethanol. 8 ug/ml VMSNCs were treated with 1 mM or 0.1 mM GSH. At predetermined time intervals, the reaction solution (200 ul) is centrifuged to remove GSH in solution. The pellets were resuspended in PBS and incubated with DTNB solution (4 ul) for 5 min at room temperature. The absorbance was measured at 412 nm and free thiol concentration was calculated.

4.2.8   Gel retardation assay

MSNCs were loaded with 0.25 µg of DNA, which is confirmed using gel electrophoresis as shown in Figure 4.8 (1% agarose gel (105V) with ethidium bromide staining).

4.2.9   DNA release assay

In vitro release of the DNA from VMSNCs with or without glutathione (GSH). 1 ml of 8 ug/ml VMSNCs were incubated with 5 ug DNA for 6 h at room temperature. DNA loaded VMSNCs were collected by centrifugation for 20 min at 13000 rpm. MSNCs pellets were resuspended in PBS and incubated with 1 mM GSH. DNA loaded VMSNCs without GSH treatment were used as control.   At

predetermined time intervals, the nanolusters suspension were centrifuged and the amount of DNA released in the supernatant was determined by spectrophotometry at 260 nm.

4.2.10 MTT Assay

The cells were plated at a density of 4×10^3 cells/well in 96-well plates in standard growth medium for 24 h. They were then washed twice in PBS and treated with different concentrations of magnetic silica particles for 72 h. The measurement of cell viability was carried out using the 3-(4,5-dimethyl thiazol-2-yl)-2,5-diphenyl tetrazolium bromide (MTT) assay. MTT was used as an indicator of cell viability as determined by its mitochondrial-dependent reduc¬tion to formazin. Cells were incubated with MTT (5 mg/ml, 20 µl/well, Sigma, USA) in cell culture for 4 h. Finally, the supernatant was removed, followed by the addition of dimethyl sulfoxide (DMSO, 150µl/well, Sigma, USA) and agitated for 10 min to dissolve the formazin crystals completely. The optical density was measured at an absorption maximum of formazin at 570 nm on a Biotek plate reader.

4.2.11 Zeta potential (ξ)

The surface charge of the nanoparticles was measured by the zeta potential in nanopure water using a Zeta pal instrument.

4.2.12   Isolation of major coat protein (pVIII) from phage

We followed a reported procedure[188] to purify pVIII from MSC-targeting phage selected by us previously[189] where pVIII bears MSC-targeting peptide. Equal volumes of Tris-HCl and saturated phenol (pH 8.0) were added to the solution of phage virions. The solution was mixed by vigorously shaking for 8 min; then centrifuged for 10 min at a speed of 3000g. After centrifugation, the aqueous supernatant containing phage DNA was removed and transferred to another tube. The same procedure was repeated 4 more times by adding 1 vol. of Tris-HCl (pH 8.0) to the phenol phase obtained in the previous step to remove the phage DNA completely. The obtained phage protein in phenol was diluted with 2 vol. of methanol and dialyzed against a 1:1 mixture of methanol and 10 mM Tris-HCl (pH 8.0), a 1:3 mixture of methanol and 10 mM Tris-HCl (pH 8.0), only 10 mM Tris-HCl (pH 8.0), and deionized water for 12 h for each dialysis step. Finally, 1 ml PBS was added to the pure phage protein and stored at -20°C for further experiments.

4.2.13   VMSNCs Synthesis

The 1 mM of isolated MSC-targeting pVIII protein was conjugated to the surface of the 1 nM MSNCs to obtain VMNCs. Bio-conjugation was carried out by protecting the –NH$_2$ groups using 2 mM of tert-Butyl carbamate (BOC) in THF/H$_2$O, which was important to stop the self-conjugation of pVIII. The –COOH groups present in pVIII protein were activated using 2 mM of 1-Ethyl-3-[3-dimethylaminopropyl]carbodiimide hydrochloride and N-Hydroxysuccinimide (EDC/NHS). Then the activated pVIII protein was incubated with amine terminated PEI on DNA-loaded MSNCs for 4 h in a buffer at pH 7.5.

4.2.14   MTT Assay

The cells were plated at a density of 4×10^3 cells/well in 96-well plates in standard growth medium for 24 h. They were then washed twice in PBS and treated with different concentrations of magnetic silica particles for 72 h. The measurement of cell viability was carried out using the 3-(4,5-dimethyl thiazol-2-yl)-2,5-diphenyl tetrazolium (MTT) assay. MTT was used as an indicator of cell viability as determined by its mitochondrial-dependent reduction to formazin. Cells were incubated with MTT (5 mg/ml, 20 µl/well, Sigma, USA) in cell culture for 4 h. Finally, the supernatant was removed, followed by the

addition of dimethyl sulfoxide (DMSO, 150μl/well, Sigma, USA) and agitated for 10 min to dissolve the formazin crystals completely. The optical density was measured at an absorption maximum of formazin at 570 nm on a Biotek plate reader.

4.2.15 Gene transfection

MSCs at the third passage were washed with PBS and detached by incubation with 0.25% trypsin-EDTA for 2 to 3 min at 37°C. Complete medium was added to inactivate the trypsin. The cells were centrifuged at 1000g for 3 min, the medium was removed, and the cells were re-suspended in 2 to 5 ml of complete medium. The cells were counted using a hemacytometer and then plated at a density of 1×10^4 cells/well (24 wells plate) for overnight culturing. Then the cells were treated with different concentrations of VMSNCs complexed with DNA (eGFP-VEGF) and MSC-targeting pVIII in the medium without FBS with or without an external magnetic field. After 4 h incubation, the treated solution was removed and then added to the culture medium with FBS. The cells were checked with a fluorescence microscope (Nikon) at the indicated time for the expression of reporter gene.

4.3 Results and discussion

4.3.1 VMSNCs synthesis and characterization

Here, for the first time we demonstrated the virus mimetic magnetic silica nanoclusters (VMSNCs) for gene delivery to MSCs (Figure 4.1). The VMSNCs are designed on the following observations. First, fd-tet phage is a virus that specifically infects bacteria by transferring DNA to cells and is non-toxic to human beings. It is made of DNA encapsulated by a protein coat (Figure 4.1). The protein coat includes ~3900 copies of major coat protein (pVIII) on the side wall of phage and ~5 copies each of four minor coat proteins at the two tips of phage.[190] We have recently used phage display technique to discover fd-tet phage particles that display a MSC-targeting peptide (VTAMEPGQ) as fusion to each of ~3900 copies of pVIII constituting the side wall of phage.[191] We also found that the MSC-targeting peptide could promote the delivery of the gene into MSCs once presented on liposome NPs. Second, embedding superparamagnetic iron oxide (SPIO) NPs in a silica matrix can aid magnetically guided gene delivery, which is crucial for future in vivo applications. Third, porous structure formed due to the aggregation of SPIO and silica NPs in the nanoclusters through S-S bonds (Figure 4.2) can safely hold and protect DNA before gene release and expression.

Fourth, pVIII can be purified from fd-tet phage body,[192] and then chemically conjugated with PEI to ensure the targeting of the cluster to MSCs. Lastly, once the cluster is internalized in the MSCs, the S-S bonds holding the NPs together in the cluster can be cleaved by intracellular glutathione (GSH) (Figure 4.2E) to dissociate the nanocluster, leading to the DNA release and gene expression for improved gene transfection. The VMSNCs mimic phage structure by bearing phage-borne pVIII on the surface and loading DNA inside, can promote their cell-internalization and gene transfection to MSCs.
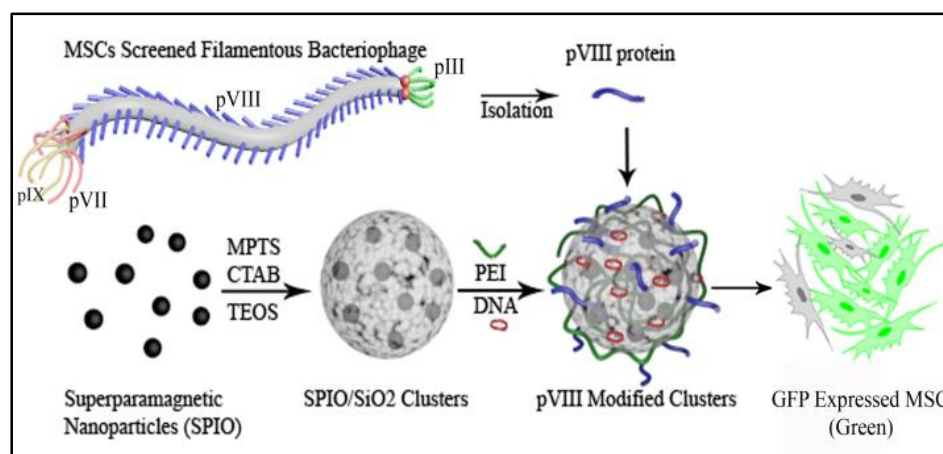
Figure 4.1 Virus Mimetic Magnetic Silica Nanoclusters (VMSNCs) for gene delivery to MSCs. The MSC-targeting phage particle has ~3900 copies of pVIII with the MSC-targeting peptide fused to the solvent-exposed terminal. The MSC-targeting pVIII can be isolated and purified from the phage. Cleavable MSNCs are synthesized by embedding SPIO

NPs in silica network, which is achieved by in situ hydrolysis of tetraethyl orthosilicate (TEOS) and (3-mercaptopropyl)trimethoxysilane (MPTS) in the presence of SPIO NPs dispersed in Cetyl trimethylammonium bromide (CTAB). Then the DNA (red circles) is incorporated into the porous structure of SPIO-embedded silica matrix. The magnetic silica nanoclusters (MSNCs) are modified with polyethyleneimine (PEI), which is conjugated with pVIII (blue) purified from MSC-targeting phage by EDC/NHS chemistry, to form VMSNCs. Bearing phage-borne pVIII on VMNSCs allows the clusters to mimic phage particles, target and enter MSCs to achieve gene delivery. The successful transfection of MSCs using VMSNCs is visualized by green fluorescence from eGFP.

These GSH-cleavable MSNCs were formed by in situ hydrolysis of TEOS and MPTS in the presence of hydrophobic SPIO NPs dispersed in CTAB. The spherical magnetic silica nanoclusters (MSNCs, Figure 4.2A, 4.2B, 4.2D) were synthesized with a diameter of ~80-100 nm. Transmission electron microscopy (TEM) images (Figure 4.2A, 4.2B) clearly verify the magnetic NPs embedded in a silica matrix to form a nanocluster.
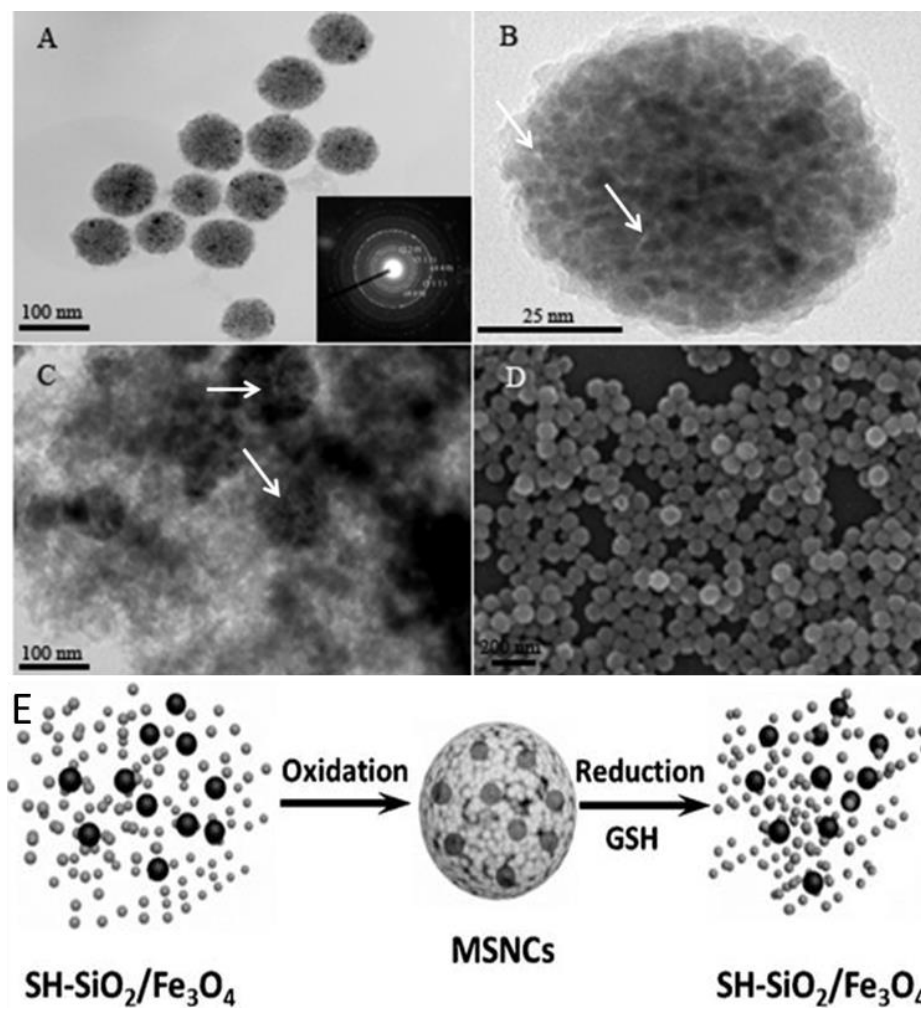
Figure 4.2   MSNCs synthesis mechanism and characterization. (A) TEM image of MSNCs showing the magnetic NPs embedded in silica. (B) High magnification image of an individual nanocluser to show the intrinsic pores inside the cluster (pointed with arrows). (C) TEM images of GSH treated MSNCs, which shows the clusters were dissociated due to the cleavage of S-S bonding between the NPs inside nanoclusters, white

arrows indicates the partially dissociated nanoclusters. (D) Scanning electron microscope (SEM) image of MSNCs to show the large view and morphology of clusters. (E) Mechanism of magnetic/silica nanocluster (MSNC) formation and their subsequent cleavage by oxidation/reduction mechanism of sulfhydryl bonds between the silica/Fe_3O_4 NPs. Specifically, Fe_3O_4 NPs are embedded inside a porous matrix aggregated from silica NPs through S-S bond. The resultant cluster is porous and can hold loaded DNA. In the presence of intracellular GSH, the S-S bond will be broken to dissociate the clusters, favoring the release of gene loaded in the porous silica matrix.
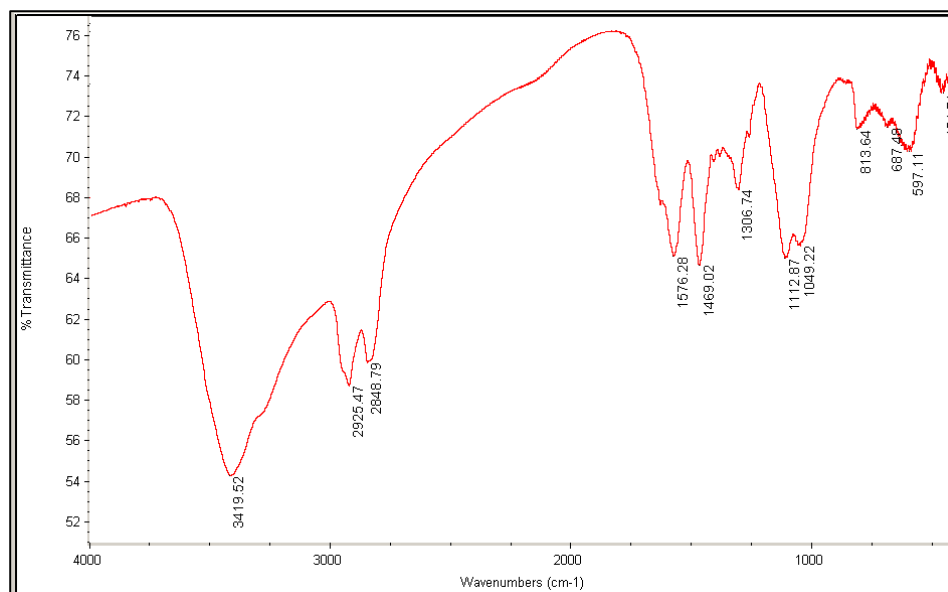
Figure 4.3 FT-IR spectra of PEI modified magnetic/silica nanoclusters.

Elt.	Line	Intensity (c/s)	Error 2-sig	Conc	Units	
Si	Ka	191.24	3.911	88.236	wt.%	
Fe	Ka	5.61	0.670	11.764	wt.%	
				100.000	wt.%	Total

Cursor=15.015 keV   0 cnt ID =
Vert=840   Window 0.005 - 40.955= 23,274 cnt
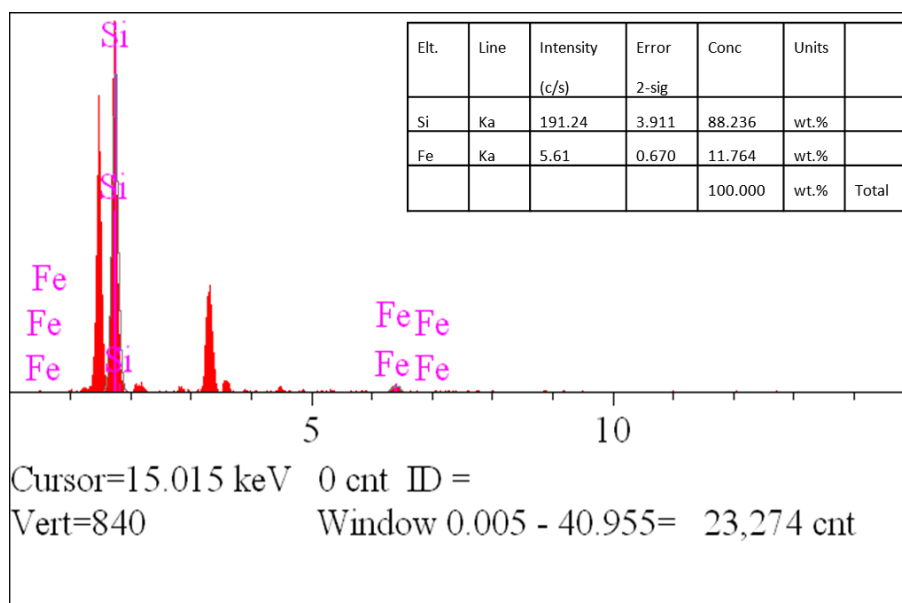
Figure 4.4   Energy dispersive X-ray microanalysis spectrum of nanoclusters measured in JEOL JSM880. Inset shows the approximate elemental composition of Si and Fe at the selected area.
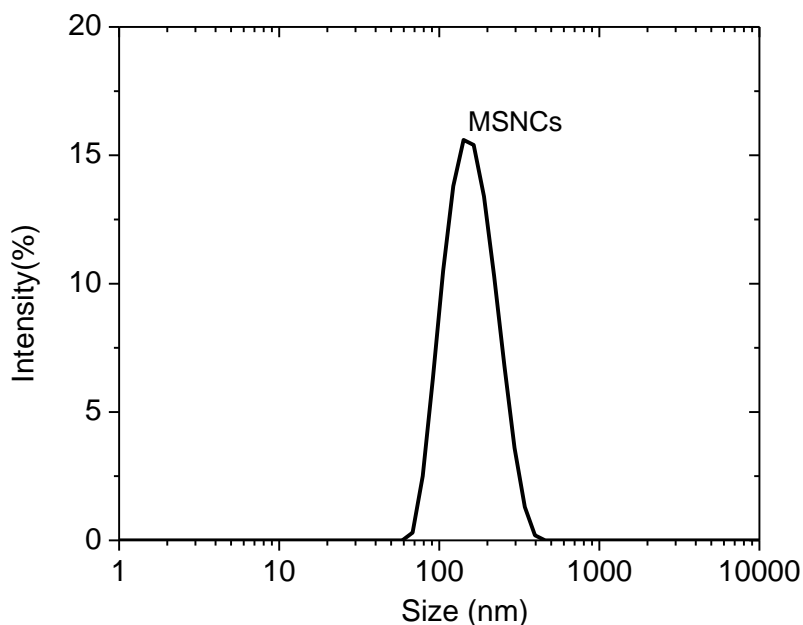
Figure 4.5   Dynamic light scattering (DLS) hydrodynamic size distribution of MSNCs showing an average size of ~150 nm.

During the in situ hydrolysis of TEOS and MTMS in the presence of hydrophobic SPIO NPs, upon aerial oxidation, S-S bonding between the formed thiolated silica colloidal NPs tend to aggregate into MSNCs while the hydrophobic SPIO NPs are being embedded inside the resultant clusters. The inter-particle S-S bonding in the nanoclusters was

confirmed by the fact that incubating the nanolusters (10 nM) in 5 mM GSH for 4 h at 37°C dissociated the nanoclusters into isolated NPs. TEM images (Figure 4.2A, C) clearly show the particle difference before and after GSH treatment, which confirms the presence of S-S bonding and subsequent cleavage upon GSH reduction. The intracellular GSH concentration (1-10 mM) is significantly higher than extracellular levels (2-20 uM)[193,194], providing a mechanism for controlled intracellular release. DTNB assay is used to measure free thiol concentration of VMSNCs in the presence of GSH concentrations at 1 mM and 0.1 mM (Figure 4.6). The addition of GSH triggered the release of free thiol, confirming that cellular GSH can indeed cleave the disulfide bond to release DNA. These kinds of thiol-fused MSNCs can be used as molecular switches for triggered release of therapeutics in cytoplasm by reducing the inter-particle disulfide bonding in the presence of GSH available in the living cells.
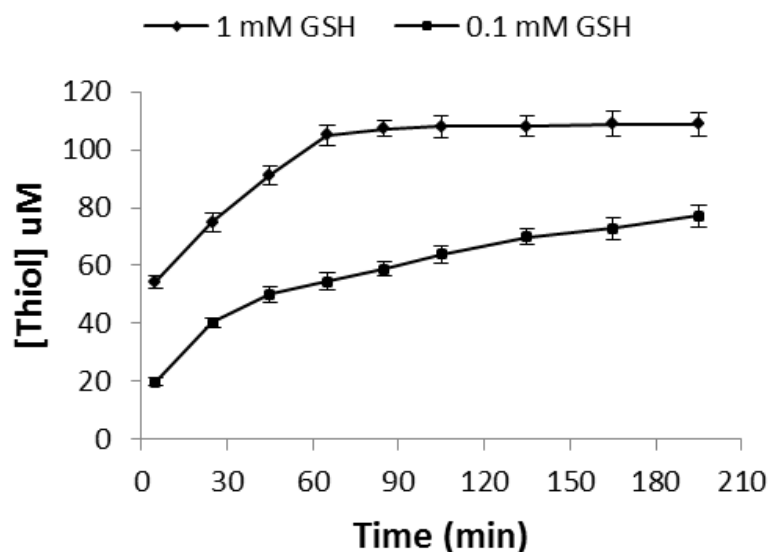
Figure 4.6   Time course of in vitro free thiol release from 8 ug/ml

VMSNCs in the presence of GSH concentrations at 1 mM and 0.1 mM.

The addition of GSH triggered the release of free thiol. The profile in the

figure exhibited a rapid thiol release, due to enhanced VMSNCs

dissociation in the presence of a high concentration of GSH (1mM). In

contrast, the thiol release is relatively slow at a low GSH concentration

(0.1 mM).

Magnetic measurement at 300 K using a magnetometer[195] showed

that both SPIO NPs and MSNCs were superparamagnetic (Figure 4.7).

However, the paramagnetic strength of clusters was determined to be 4.0

Am^2/kg at 1.0 tesla, which is 10 folds lesser than SPIO NPs. This is

117

mainly due to the weight percentage of SPIO NPs present in MSNCs. The magnetic measurement confirmed the superparamagnetic nature of our nanoclusters, which is crucial for magnetically guide the delivery of the gene-loaded nanoclusters into cells (magnetofection).
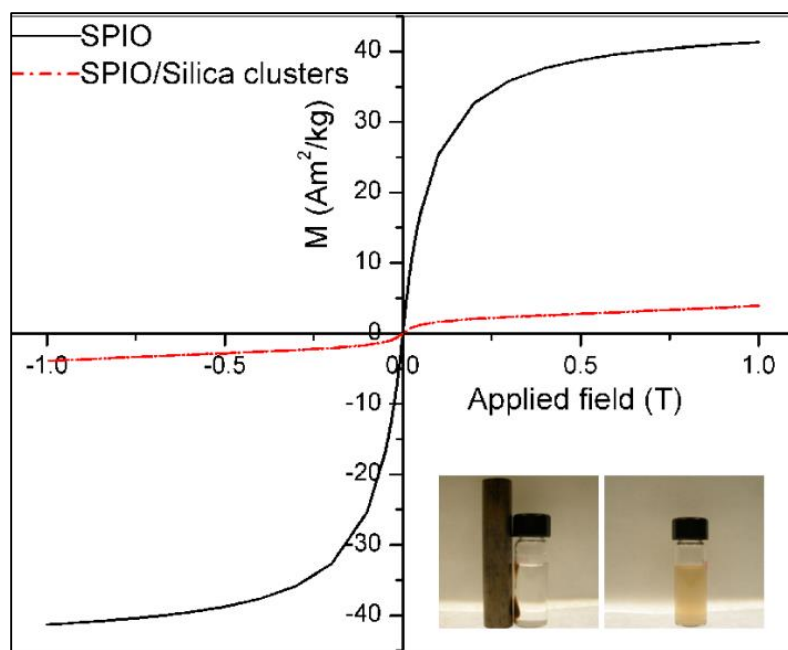
Figure 4.7   Magnetic Properties: Hysteresis loops of SPIO (straight line) and cleavable MSNCs (dotted line) measured in SQUID. Inset shows the magnetic strength of the MSNCs in water with (left) and without (right) a magnetic bar.

4.3.2 DNA loading capacity

118

The DNA loading capability of the MSNCs before modification with PEI was estimated by gel electrophoresis. Figure 4.8 shows DNA is completely encapsulated at NP/DNA ratio 1:1. In fact, only 2 µg of DNA was used to complex with 8 ug/ml of MSNCs for transfection studies in MSCs in this work. These MSNCs were further modified with low molecular weight PEI (MW= 8 kDa). The FTIR spectrum (Figure 4.3) confirms the presence of PEI, SiO2, and Fe_3O_4 in the nanoclusters. The zeta potential of the PEI modified MSNCs was determined to be 26±2 mV. This positive charge will promote the efficient gene transfection.
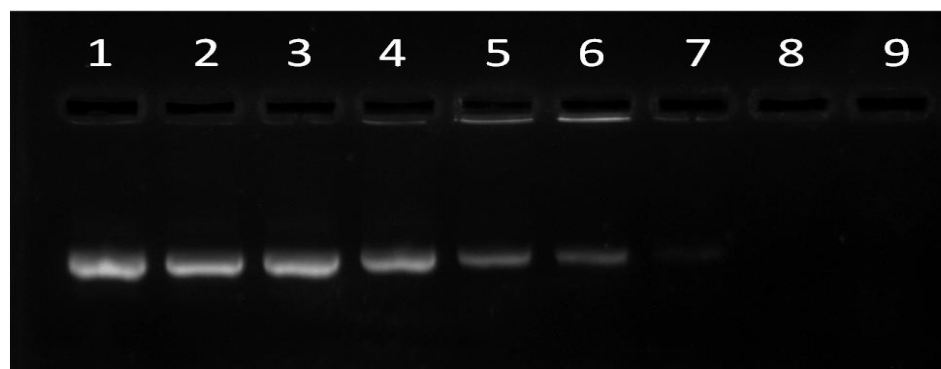
Figure 4.8 The DNA retardation assay of DNA loading in nanoparticles at various weight ratios of NP/DNA. (1) 0:1, (2) 0.015625:1, (3) 0.03125:1, (4) 0.0625:1, (5) 0.125:1, (6) 0.25:1, (7) 0.5:1, (8) 1:1 and (9) 2:1 respectively. 0.25 ug DNA is used per lane. Gel retardation result indicates DNA is completely encapsulated at NP/DNA ratio 1:1 on lane 8.

The pVIII was isolated from the MSC-targeting filamentous fd-tet phage, which was identified by us recently and had ~3900 copies of MSC-homing pVIII,[191] by phenol extraction following a reported protocol.[192] The MSC-homing pVIII purified from the MSC-targeting phage can favor the MSC-homing of the NPs modified with the pVIII. Towards this end, the isolated pVIII is conjugated to the PEI on the surface of the nanoclusters so that the nanoclusters can home to MSCs. Bio-conjugation between the C terminal end of pVIII and $-NH_2$ in PEI was carried out using 1-Ethyl-3-[3-dimethylaminopropyl] carbodiimide hydrochloride and N-Hydroxysuccinimide (EDC/NHS) conjugation chemistry. The resultant VMSNCs exhibited both magnetic and fusogenic properties.

4.3.3 Cleavage of VMSNCs and DNA release

A DTNB assay was used to measure the concentration of thiol groups present in NPs formed owing to the cleavage of VMSNCs in the presence of GSH with a concentration of 1 mm or 0.1 mm (Figure 4.9). The addition of GSH triggered the cleavage of disulfide bond in the nanoclusters and the concurrent formation of free thiol groups (Figure 4.9), suggesting that thiol-fused MSNCs can be used as molecular switches for triggered release of therapeutics in cytoplasm by reducing

120

the interparticle disulfide bonding in the presence of GSH available in the living cells.
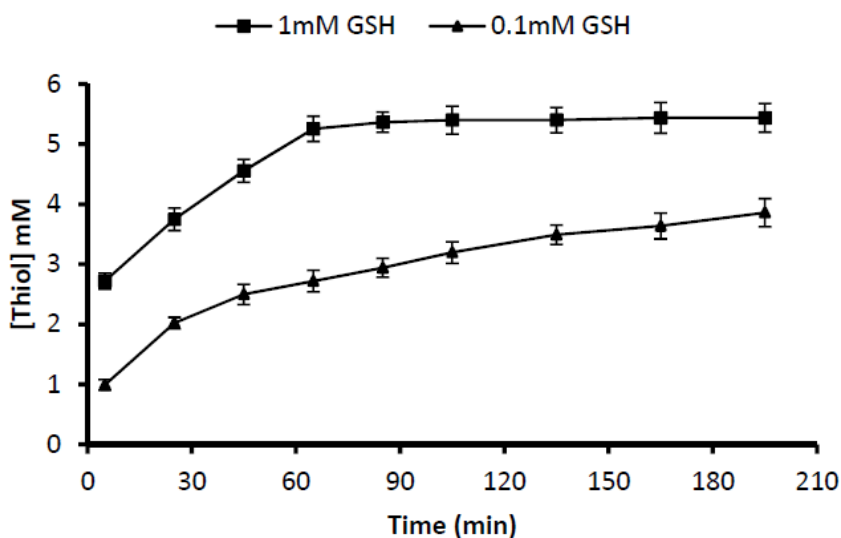
Figure 4.9 Time course of the concentration of free thiols present on the nanoparticles as a result of the cleavage of disulfide bonds in VMSNCs by GSH at 1 mM and 0.1 mM. The addition of GSH triggered the cleavage of disulfide bond to form free thiol groups. The profile shows that thiol groups are formed over time and then level off after 60 min at 1 mM GSH, and a higher GSH concentration promoted the formation of free thiol groups (and thus the cleavage of nanoclusters).

We later examined DNA release from VMSNCs in the presence and absence of GSH at physiological concentration (1mM) (Figure 4.10). Our data showed that GSH-treated VMSNCs demonstrated sustained release

of DNA whereas the VMSNCs in the absence of GSH showed minimum DNA release. The results suggested that GSH at an intracellular concentration can cleave the disulfide bond in the VMSNCs and consequently lead to the release of DNA from the nanoparticles.
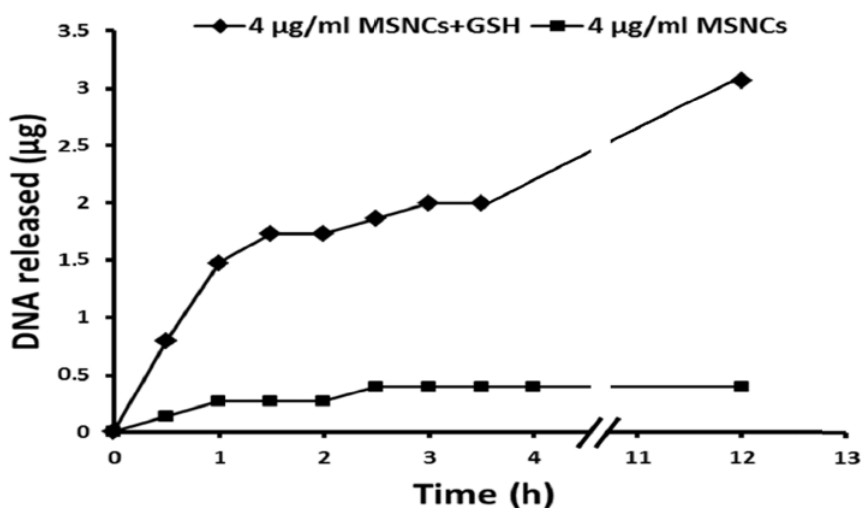
Figure 4.10   GSH-treated VMSNCs demonstrated a sustained release of DNA. 2.27 ug of DNA was released in the first 4 h and 3.07 ug DNA was released in 12 h. VMSNCs without GSH treatment in the absence of GSH shows significantly lower DNA release.

4.3.4 MTT assay

3-(4,5-Dimethylthiazol-2-yl)-2,5-diphenyltetrazolium bromide (MTT) assay was done to evaluate cytotoxicity at different concentrations of VMSNCs. At a concentration of 20 ug/ml, VMSNCs still showed high cell viability at around 96% (Figure 4.11). However, lipofectamine 2000 at the same concentration showed less than 70% cell viability (Figure 4.12). This fact shows that VMSCNs are more biocompatible than the widely-used commercial transfection reagent (lipofectamine 2000).
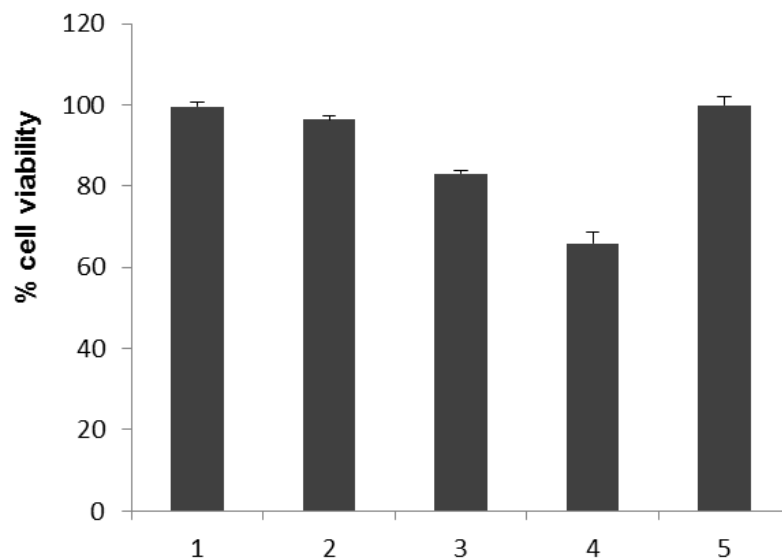
Figure 4.11　Cell viability studies: MTT assay of MSCs at different concentrations of VMSNCs. Bars 1 to 4 shows the % viability of MSCs with 10, 20, 40, and 80 ug/ml of nanoclusters in 500 µl of Fetal bovine serum (FBS) free Dulbecco's Modified Eagle Medium (DMEM) incubated for 4 h, respectively. Bar 5 is the control cells viability. After incubated

with nanoclusters for 4 h, cells were washed twice with PBS and fresh DMEM medium with 10 % FBS was added.
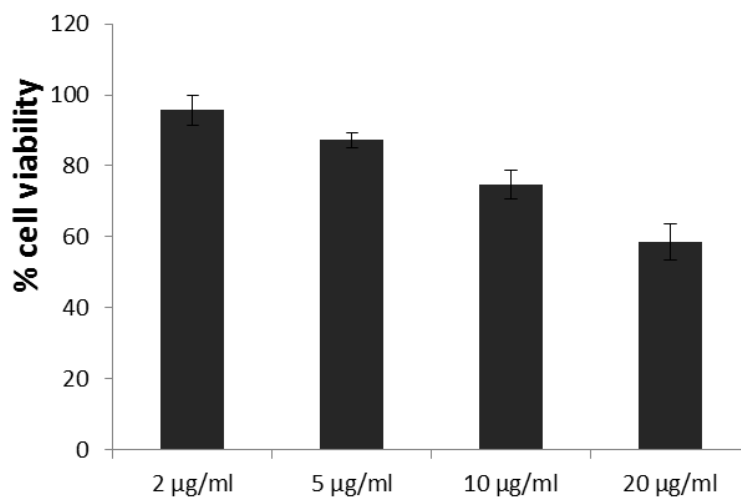
Figure 4.12   Cell viability studies: MTT assay of MSCs at different concentrations of lipofectamine 2000. MSCs were treated with different concentration of lipofectamine in 500 µl of Fetal bovine serum (FBS) free Dulbecco's Modified Eagle Medium (DMEM) incubated for 4 h. Cell viability is reduced below 80% at 10 µg/ml lipofectamine.

4.3.5 Cell internalization

After the successful synthesis of desired VMSNCs with low toxicity, high gene loading capability and sufficient paramagnetic strength, we conducted cell internalization studies in MSCs (Figure 4.13). The VMSNCs with FITC-labeled DNA loaded were incubated with MSCs at

37°C. After incubation for 2 h, the cells were washed three times with PBS. Green fluorescence images confirmed that the VMSNCs were successfully internalized in MSCs. Our previous studies showed that a pVIII with cell-targeting peptide fused to its N-terminal could facilitate the cell-internalization of phage particles that bear the same pVIII.[196] Thus the internalization of VMSNCs in MSCs might be promoted by the MSC-homing pVIII on the surface of VMSNCs, which would facilitate the delivery of gene to MSCs.
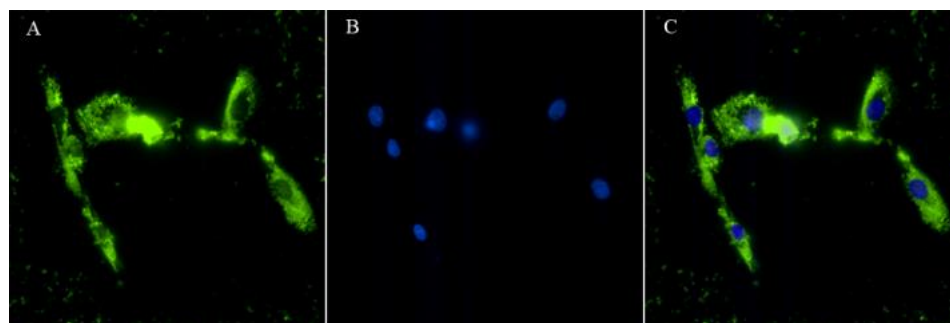
Figure 4.13 Internalization studies of VMSNCs carrying a dye-labeled DNA. All images were captured at 40X optical zoom. (A) Green fluorescence of FITC-labeled DNA entrapped in nanoclusters in MSCs to confirm the cell internalization capabilities of VMSNCs. (B) DAPI-stained MSCs to show the cell nuclei. (C) Merged images of A and B.

4.3.6 Gene transfection

The VMSNCs containing eGFP-VEGF plasmid and cell-targeting pVIII were dispersed in 500 µl of DMEM to transfect the MSCs in vitro. After 24 h of incubation, eGFP-VEGF gene was successfully delivered to MSCs by VMSNCs and expressed (Figure 4.14). The gene expression was visualized with the reporter eGFP gene expression by green fluorescence (Figure 4.14A). The quantitative eGFP expression is evaluated by flow cytometry (Figure 4.14B). We tested the transfection efficiency of VMSNCs at different transfection conditions (with or without pVIII or magnetic field), with lipofectamine 2000 as a control. The transfection efficiency of our novel cleavable VMSNCs was significantly better than the commercially available transfection reagent lipofectamin 2000 (7.66%). VMSNCs in the presence of magnet (at a 1.0 Tesla external magnetic field) shows highest levels of transfection (40.01%) compared to VMSNCs in the absence of magnet (25.80%), MSNCs in the presence of magnet (14.64%), and MSNCs alone (6.05%). When control nanoparticles (MSNCs without any protein or with wild-type pVIII modified) are used, the transfection efficiency is very low (less than 10%) and similar to that by lipofectamine. . Our results clearly indicate that both MSCs homing phage protein and magnetic strength help the VMSNCs to carry the eGFP-VEGF gene into MSCs. At the same time, in the absence of the magnet VMSNCs transfection efficiency

is lower than the presence of the magnet, possibly due to the faster internalization and lower endosomal DNA degradation in the presence of an external magnetic field.
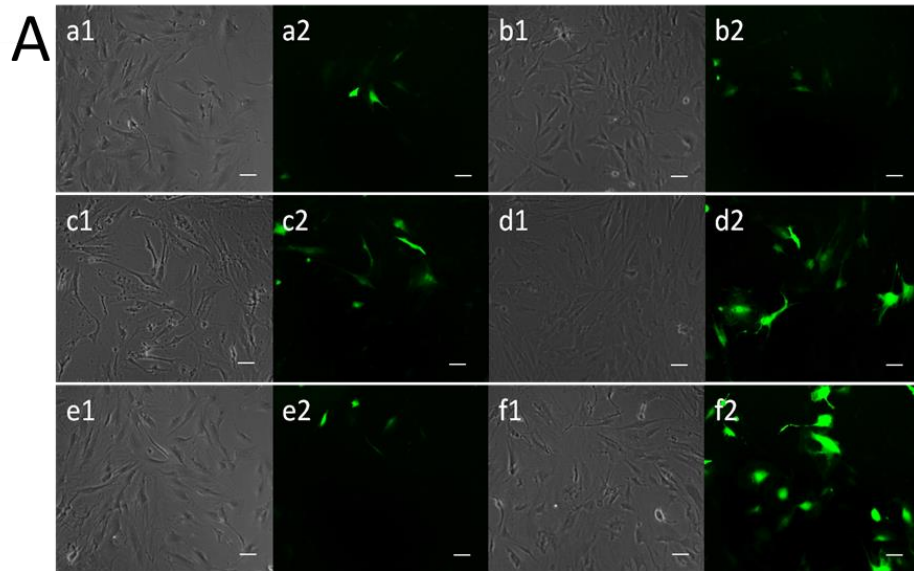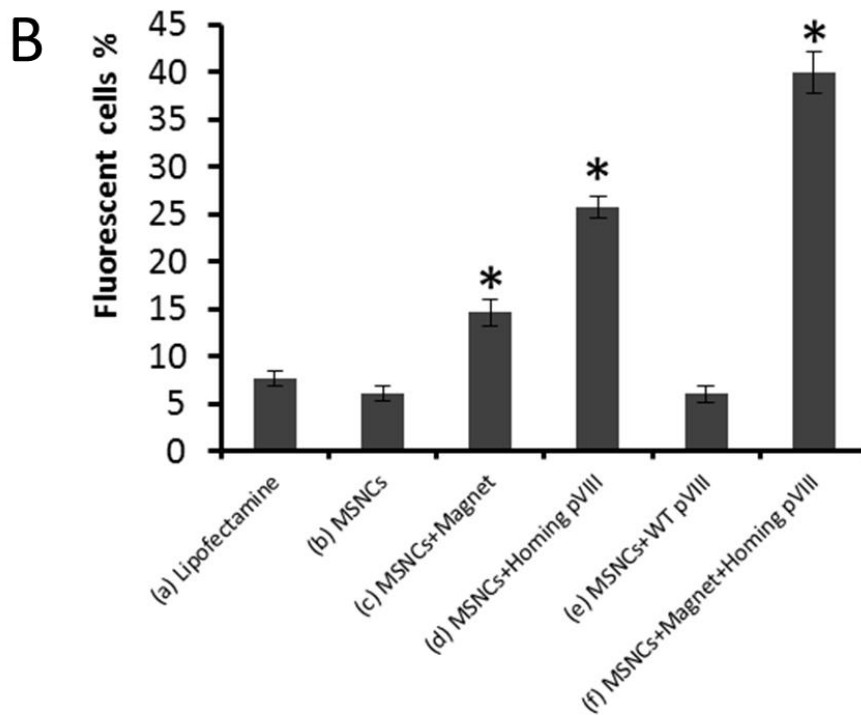
Figure 4.14 Effect of the magnetic field and MSC-homing pVIII protein on eGFP-VEGF gene transfection in MSCs. Lipofectamine 2000 was the control. A) Comparison of transfection expression of EGFP (a) Lipofectamine 2000. (b) Transfection with MSNCs in the absence of magnetic field. (c) Transfection with MSNCs (i.e., the clusters with no pVIII on the surface) under 1T magnetic field. (d) The VMSNCs had MSC-homing pVIII with magnetic field. (e) The VMSNCs with wild-type phage pVIII without magnetic field. (f) The VMSNCs with MSC-homing pVIII under 1T magnetic field. Image 1 in (a–f) is bright-field light image and image 2 is the corresponding fluorescence image. B) Corresponding

EGFP expression after transfection was examined by flow cytometry. Data are shown as mean ± SD (n = 3). Asterisk denotes P < 0.01 with Lipofectamine 2000 as a reference. (Scale bar, 50 μm.)

4.4 Conclusion

In summary, we developed novel VMSNCs for gene delivery to MSCs. We transferred the MSC-targeting pVIII from phage to nanoclusters to enable cell internalization. These VMSNCs are ideal gene therapy vectors owing to their MSC-homing capability and controlled release at the target site. Even in the absence of the magnetic field, the VMSNCs can deliver gene to MSCs at a higher efficiency than commercially available vectors. The dual nature of virus mimicking and superparamagnetism make these vectors an ideal tool for the magnetically guided targeted delivery and possibly an ideal contrast enhancement agent for the magnetic resonance imaging in future in vivo applications.

Chapter 5 MSC-binding peptide induces osteoblastic differentiation of mesenchymal stem cells

5.1 Introduction

In the body, stem cells reside in a special microenvironment termed the "niche," which supports and regulates stem cells to maintain tissue homeostasis[17,197]. Extracellular matrix (ECM) in the niche provides biochemical and biophysical cues to regulate stem cell fate in a temporal and spatial manner[198-200]. Biophysical cues (such as mechanical and topographical properties) have been demonstrated to govern various cellular processes including morphology, adhesion, migration, proliferation and differentiation[14,15,89,201-206]. Biochemical cues (such as growth factors, cytokines and ECM molecules) have also been extensively explored as cellular stimuli [207-210]. Peptides as biochemical cues have been well studied and some peptide differentiation inducers or regulators were identified[211-215]. However, how the binding affinity of a peptide influences stem cell differentiation is not well studied.

Here we show that peptides with different affinities to mesenchymal stem cells (MSCs), which were evolutionarily selected from a random peptide library by phage display technique, could show different capabilities in inducing the osteogenic differentiation of MSCs. To

achieve this goal, we employ fd filamentous bacteriophage (also termed phage), which is a bio-nanofiber with about 7 nm in width and 890 nm in length[216]. It is advantageous as a promising biomaterial based on the following facts. First, it is made of DNA encapsulated by a protein coat. Inserting a foreign gene into phage genome leads to the display of a foreign peptide as biochemical cues at high density (~3900 copies of major coat protein) on the side wall of phage[110,217]. Second, it can easily self-assemble into ordered biomimetic nanostructures that effectively mimic natural ECM fibers to provide biophysical cues[189,205,218]. Third, it is non-toxic to human cells [219,220]. These unique properties enable us to use phage as a building block to construct matrix for regulating stem cell fate.

Recently we have utilized phage display technique to successfully select several peptide sequences including VTAMEPGQ (termed VT), AFNPEPGQ (termed AF) and DTPPGWDQ (termed DT) with high affinity to rat mesenchymal stem cells (rMSCs)[189]. These binding peptides have a degree of binding affinity of 28/51, 11/51 and 5/51, respectively. The degree of binding affinity is defined as the number of occurrences of a particular peptide displayed on a phage clone divided by the total number of randomly chosen phage clones displaying different peptides during biopanning. These peptides hold the potential to facilitate targeted rMSCs delivery due to the high affinity against rMSCs [172,189]. We assemble

phages displaying these peptides into the matrix with similar nanotopography and then study the effect of these different binding peptides on the osteogenic differentiation of rMSCs.

5.2 Methods and experiments

5.2.1 Phage film formation

Nanofibrous phage films were prepared following a layer-by-layer self-assembly technique developed by our group[221,222]. Briefly, pre-cleaned cover glass slides were immersed into a poly-lysine solution for 20 min, allowing for the adsorption of the first cationic poly-lysine layer onto the glasses. The substrates were washed with water and dried in 24-well plates. Then a phage solution with different concentrations was added to form the secondary layer. This process was repeated three times. The phage film was terminated with a phage layer.

5.2.2 Scanning Electron Microscopy (SEM)

SEM was used to evaluate the morphology of rMSCs seeded on the phage film. The rMSCs on the phage films were fixed with 4% paraformaldehyde. The cells were then dehydrated in a graded series of ethanol (40%, 70%, 90%, and 100%) for 20 min each. The samples were dried by a critical point carbon dioxide. The dried samples were sputter-

coated with palladium later. The morphology of the phage films and the attached cells was imaged by SEM (Zeiss Neon). Cell surface area was measured using the ImageJ program with fifty cells examined in each experiment.

5.2.3 MTT proliferation assay

3-(4,5-dimethyl thiazol-2-yl)-2,5-diphenyl tetrazolium bromide (MTT) assay was used to evaluate proliferation. The rMSCs were cultured on the phage films in 96 well plates for 72 h. MTT (5 mg/ml, 15 μl/well, Sigma, USA) was then added to MSCs and incubated at 37 $^{\circ}$ C for 4 h. The supernatant was removed and dimethyl sulfoxide (DMSO, 100 μl/well) was added to dissolve the precipitates. The absorbance results were quantified at 560 nm with a plate reader (Biotek, USA).

5.2.4 Real-time PCR

Total RNA was purified with RNeasy Mini Kit (Qiagen). Reverse transcription was prepared with cells-to-cDNA kit (Invitrogen). Real-time PCR using Power SYBR Green PCR master mix (Applied Biosystems) was carried out in a mini Fast real-time PCR system (BIORAD) according to the manufacturer's instructions. Data were analyzed using the $\Delta\Delta Ct$ method with GAPDH as a housekeeping gene. The PCR reaction

conditions utilized include: 50 cycles of PCR, 95 °C for 15 s, 60 °C for 1 min. The sequences of gene primers were listed as follows:

OPN

Forward primer, 5'- GACGGCCGAGGTGATAGCTT -3'

Reverse primer, 5'- CATGGCTGGTCTTCCCGTTGC -3';

OCN

Forward primer, 5'- AAAGCCCAGCGACTCT-3'

Reverse primer, 5'- CTAAACGGTGGTGCCATAGAT -3';

SOX2

Forward primer, 5'- GAACGCCTTCATGGTATGG -3'

Reverse primer, 5'- AGCCGTTCATGTAGGTCTGC -3';

GAPDH (Housekeeping gene),

Forward primer, 5' -CGATCCCGCTAACATCAAAT -3',

Reverse primer, 5' -GGATGCAGGGATGATGTTCT -3'.

5.2.5 Immunofluorescence assay

The MSCs on the phage films were first fixed with 4% paraformaldehyde for 40 min at room temperature. Then the cells were incubated for 1 h in a blocking buffer (5% goat serum, 1% BSA, 0.1% Triton X-100 in PBS). The blocking buffer was discarded and cells were incubated overnight at 4°C with primary antibody anti-osteocalcin (OCN) antibody (1:1000, Abcam) and anti-osteopontin (OPN) antibody (1:1000, Abcam) developed from rabbit. Phosphate-buffered saline (PBS) was then used to wash the sample. Cells were incubated with goat anti-rabbit IgG-Alexa Fluor®488 (1:300, abcam) or goat anti-rabbit IgG-TRITC (1:250, Santa Cruz) in PBS (5% goat serum) at 37°C for 1 h. Cell nuclei were stained with DAPI. The samples were visualized with fluorescence microscope (Nikon Eclipse Ti).

5.2.6 Mineralization assay

MSCs were cultured on the phage films in 96-well plates. Cells were fixed with 4% paraformaldehyde and mineralized nodules were stained with Alizarin red S for 20 min[222,223]. The Alizarin Red S-calcium complex product was dissolved in 0.2 N sodium hydroxide and absorbance was measured at 548 nm on a plate reader (Biotek, USA).

5.2.7 Propagation of phages.

Phage nanofibers were amplified and purified according to the protocol with modifications[110]. First, 20 µl of phage containing *E. coli* solution was added into 10 ml LB medium (20 µg/mL tetracycline) and incubated at 37°C overnight. Next the overnight culture was introduced into 1 L LB medium (20 µg/mL tetracycline) and incubated for 10 h in a shaking incubator. The culture solution was centrifuged at 3000g for 15 min and then at 8200g for 15 min to remove the *E. coli*. 150 ml of PEG/NaCl solution (500 mL of water, 116.9 g of NaCl and 100 g of PEG) was added to the resultant clear supernatant and the mixture was kept at 4°C for 4 h. The phages were precipitated by centrifugation at 8200g for 1 h. 30 ml of Tris buffered saline (TBS) was used to re-suspend phage precipitates and then the suspension was centrifuged again at 11000g for 10 min. 5 ml of PEG/NaCl solution was added to the supernatant and kept at 4°C overnight. The phages were precipitated at 11000g and re-suspended in TBS. Phage concentration was evaluated with a spectrophotometer using the formula: 1 absorbance unit (AU) $_{269nm}$=6.5 $\times 10^{12}$ pfu/ml.

5.2.8 Statistical analysis.

Statistical analysis was performed using two-tailed unpaired Student's t-test. Data are presented as mean $\pm$ SD (standard deviation).

5.3 Results
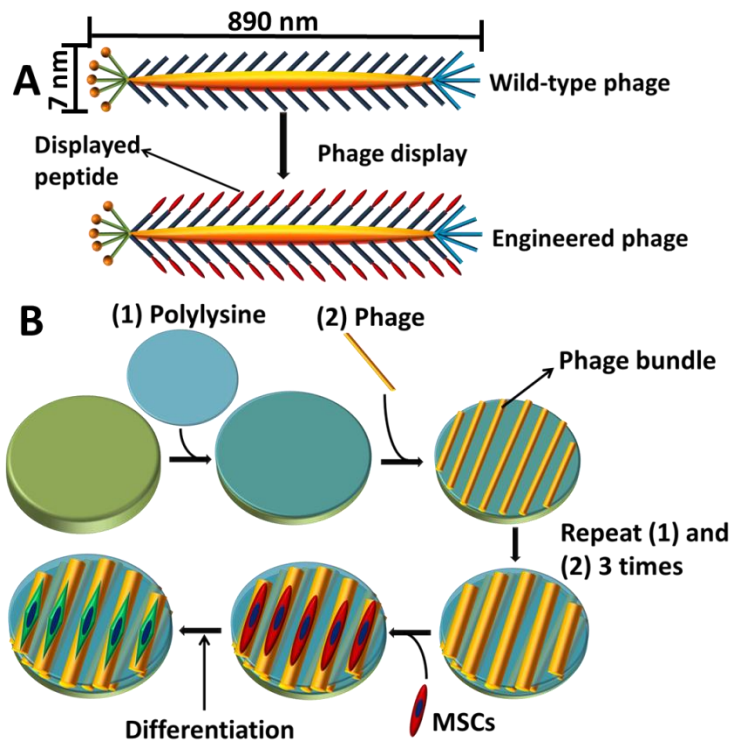
Figure 5.1 Schematics showing phage display technique (A) and the construction of phage-based film through a layer-by-layer self-assembly technique (B). A) Display of peptides on phage: Foreign peptides (e.g VTAMEPGQ) were introduced to the N-terminal of the major coat protein of filamentous Fd phage by phage display technique. In this study, the engineered phage was selected from a random library by biopanning process. B) Assembly of phage into films: Polylysine was first deposited on the glass substrate, then phage nanofibers were introduced as the

second layer. This procedure was repeated three times to form the phage-based films. The as-formed films were found to support the proliferation and differentiation of MSCs.

5.3.1 Characterization of phage film

The phage nanofibers were first assembled into a film by our previously reported layer-by-layer technique[189]. Schematic in Figure 5.1 shows phage display technique. Wild-type (WT) phage was used as a control. In the layer-by-layer assembly technique, the liquid crystalline phase transitions and interaction between negatively charged phage and positively charged polylysine provide driving force for the formation of highly ordered supramolecular phage film. The self-assembled phage film exhibited a rough surface made of parallel bundles (ridges) separated by grooves (Figure 5.2). Our study shows that phage concentration determines the size of the ridge/groove property. At a high phage concentration (10^{14} pfu/ml), phage formed bundles with a diameter of around 4 μm (Figure 5.2). In comparison, phage bundles were around 2 μm in diameter at a medium phage concentration (10^{13} pfu/ml). We didn't observe phage bundle formation at a low phage concentration (10^{12} pfu/ml) under optical microscope. However, we were able to monitor phage bundles under

transmission electron microscopy (TEM) at a concentration of 10^{13} pfu/ml

and 10^{10} pfu/ml (Figure 5.3).
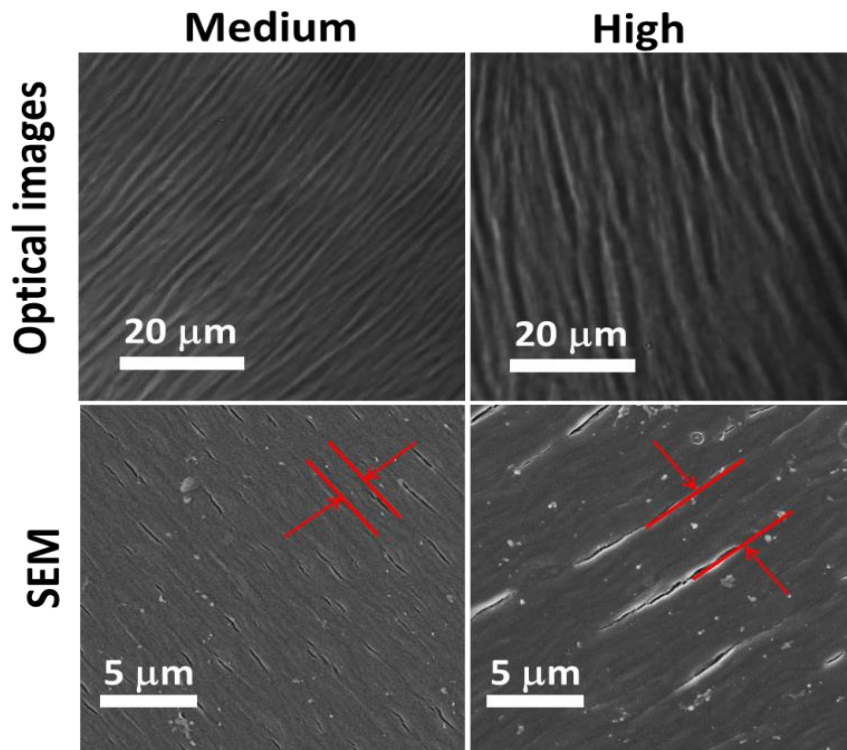
Figure 5.2 Characterization of phage film with optical microscopy and SEM. The phage film was derived from phages with medium concentration (10^{13} pfu/ml) and high concentration (10^{14} pfu/ml). The red arrows indicate the width of a single phage bundle. The phage bundles exhibit linear and parallel orientation with ridges/grooves structure.

10¹³ pfu/ml
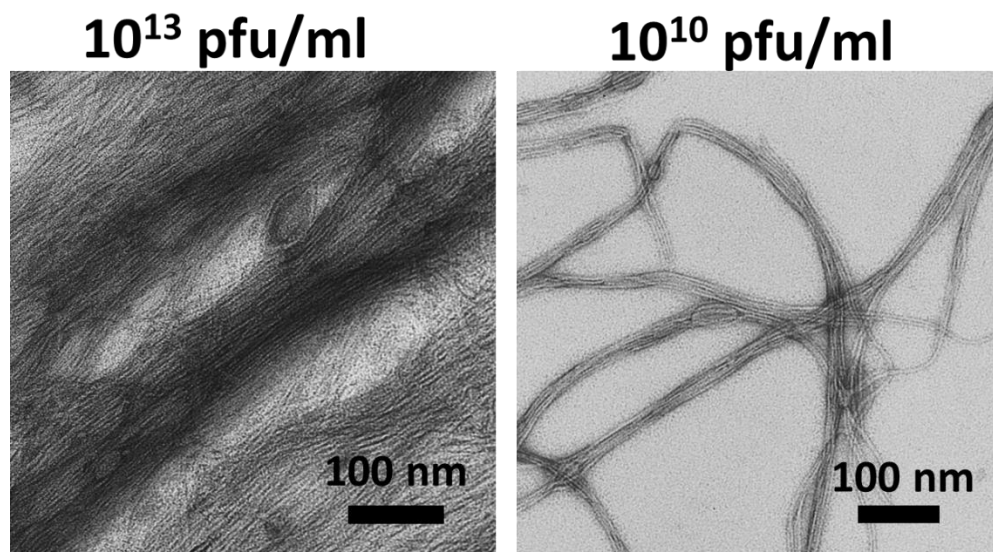
10¹⁰ pfu/ml

Figure 5.3 TEM images of phage bundles formed at different phage concentrations. Higher phage concentration (10^{13} pfu/ml) induced the formation of thicker and rigid phage bundles. Lower phage concentration (10^{10} pfu/ml) resulted in the formation of thinner and flexible phage bundles.

5.3.2 Morphology of rMSCs on phage films

We studied the rMSCs morphologies on the phage films with polylysine coated substrate as a control. As shown in Figure 5.4 and Figure 5.5, rMSCs on the films assembled from phage at a medium concentration (10^{13} pfu/ml) showed elongation and alignment along the phage ridges/grooves. The high magnification images of rMSCs were

demonstrated in Figure 5.6. MSCs on the films assembled form phage at a

high concentration (10^{14} pfu/ml) demonstrated enhanced spatial elongation.

In comparison, rMSCs on the control poly-lysine substrate exhibited

random orientation and didn't show elongation. On the phage substrate

with low concentration, rMSCs exhibited random orientation, but also

showed stretches along different directions. Cell surface areas were also

dependent on the phage concentrations (Figure 5.7). The films derived

from high phage concentration (10^{14} pfu/ml) induced significantly

decreased cell surface areas comparing with the control polylysine

substrates. These results demonstrated that rMSCs morphologies are

significantly influenced by the phage concentrations. However, we didn't

observe significant changes in rMSCs morphology on the phage films with

different displayed peptide sequences.
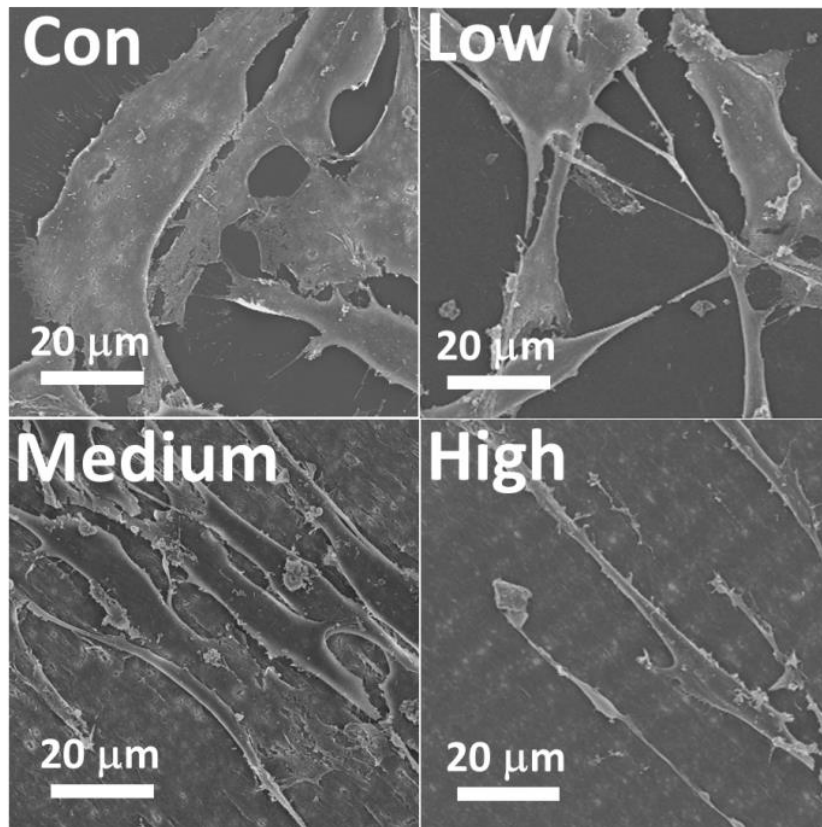
Figure 5.4 Scanning electron microscopy (SEM) analysis showing the effects of phage concentrations on the morphology of MSCs cultured for five days. Con: polylysine coating. Low: phage films assembled from phage at a low concentration (10^{10} pfu/ml). Medium: phage films assembled from phage at a medium concentration (10^{13} pfu/ml). High: phage films assembled from phage at a high concentration (10^{14} pfu/ml). MSCs show alignment and elongation on the phage films derived from the medium and high phage concentrations.
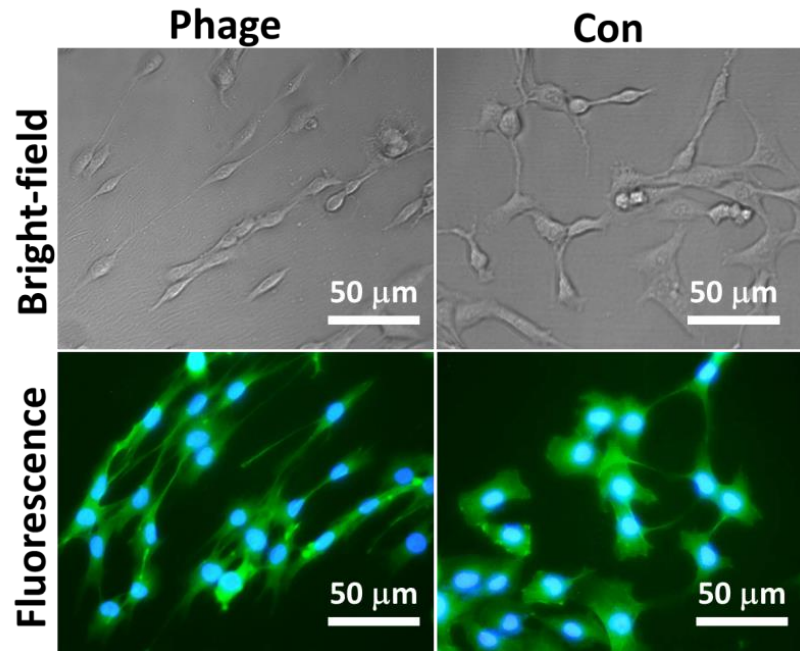
Figure 5.5 Bright-field images showing the morphology of live MSCs cultured for three days and fluorescence images showing the morphology of stained MSCs cultured for five days on control and phage substrates. Phage substrates are the phage films prepared with a concentration of 10^{13} pfu/ml. Control (Con) substrates are the polylysine-coated plates. Cell nuclei were stained with DAPI (blue). F-actin was stained with FITC-labeled phalloidin (green).
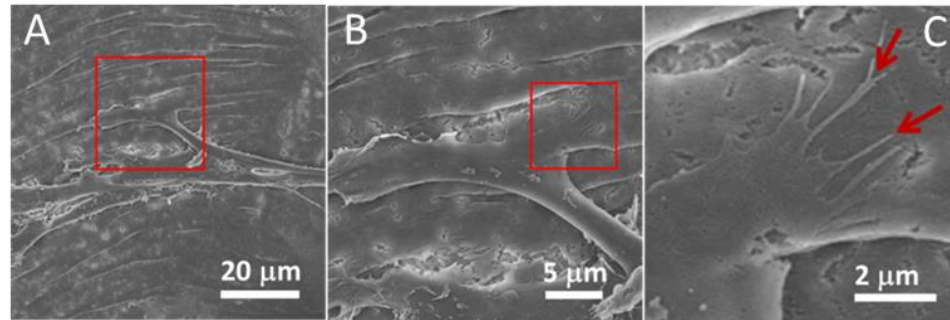
Figure 5.6 (A-C) SEM images at different magnifications showing rMSCs adhesion to phage bundles generated from VT-Phage (5×10^{13} pfu/ml). B) High magnification inset region in red box of image A. C) Higher magnification of the region in red box in image B. Red arrows indicate filopodium adhesion to phage bundles.
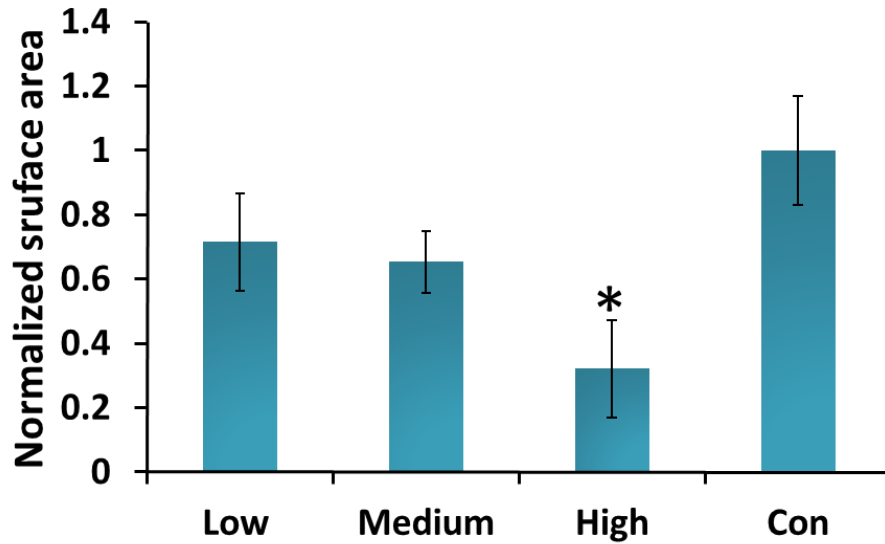
Figure 5.7 MSCs surface areas on the phage films generated from different phage concentrations. Data were normalized to cells grown on control (Con) polylysine coated substrates. Asterisk denotes $p < 0.05$ when compared with control.

5.3.3 Proliferation of rMSCs on phage film

We proceeded to investigate rMSCs proliferation on the phage films with different concentrations and displayed peptide motifs (Figure 5.8). 3-(4,5-dimethyl thiazol-2-yl)-2,5-diphenyl tetrazolium bromide (MTT) proliferation assay demonstrated that rMSCs proliferation was regulated by both the concentrations of phages and the peptide motifs displayed on the phage nanofibers. As the concentration of WT-phage

increased, the rMSCs proliferation rate decreased (Figure 5.8a). rMSCs seeded on the VT-phage film demonstrated higher proliferation rate than those on AF, DT or WT-phage films (Figure 5.8b). There is no significant difference between the growth rate of MSCs on AF, DT or WT-phage film.
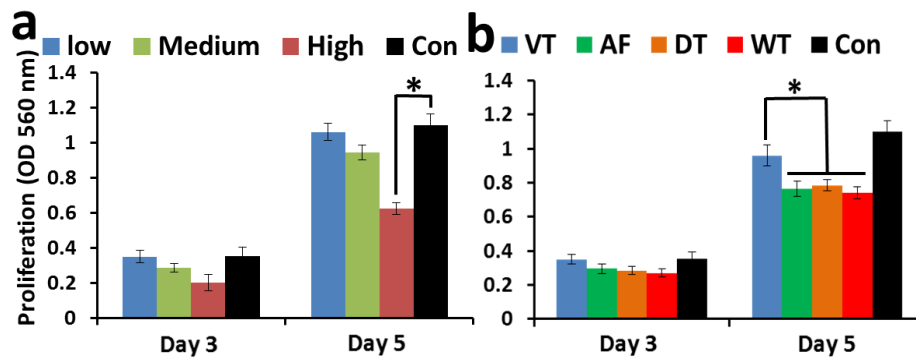
Figure 5.8 MSCs proliferation on the phage films assembled from phage at different concentrations (a) or displaying different peptide motifs (b). a) MSCs were seeded on the wild-type phage films assembled from phages of a low concentration (10^{10} pfu/ml), medium concentration (10^{13} pfu/ml), and high concentration (10^{14} pfu/ml). Polylysine-coated substrate was used as a control. Asterisk denotes $p < 0.05$ when a group was compared with the control, n = 3. b) MSCs grown on the phage film (10^{13} pfu/ml) displaying various peptide sequences . VT, AF, and DT denoted films assembled from phage displaying VTAMEPGQ, AFNPEPGQ, and DTPPGWDQ, respectively. WT denoted films assembled from wild-type

phage. Con denoted polylysine coated control substrate. Asterisk denotes p< 0.05 when compared with VT group, n = 3.

5.3.4 rMSCs differentiation on phage films

To investigate how these phage-displayed peptide sequences regulate rMSCs differentiation, we employed real-time PCR to evaluate the osteogenic differentiation of rMSCs on the phage films (Figure 5.9). rMSCs were cultured in primary non-osteogenic medium for three weeks before the assay. Various genetic markers associated with cell differentiation including osteocalcin (OCN), osteopontin (OPN) and pluripotency sex-determining region Y-box 2 (SOX2) were evaluated. VT-phage significantly induced and promoted osteogenesis by up-regulating OCN and OPN gene expression comparing with polylysine coated control groups (p<0.01) (Figure 5.9A). AF and DT-phage also demonstrated enhanced osteogenesis comparing with the control substrate (p<0.05). The immunofluorescence assay also demonstrated that VT-phage induced osteogenesis with enhanced OCN and OPN protein expression (Figure 5.9B). For pluripotency RT-PCR assay, VT-phage significantly down-regulated SOX2 gene expression (Figure 5.10). This decreased pluripotency property indicated the enhanced differentiation of MSCs. The real-time PCR and immunofluorescence assay collectively

show a direct relationship between the rMSC-binding affinity and the rMSC differentiation induction capability of the peptides.

To further evaluate the osteogenic mineralization property of rMSCs, alizarin red S staining was used to detect the calcium deposit formation (Figure 5.9C). The calcium deposits were dissolved in sodium hydroxide and quantified with absorbance at 548 nm[222,224] (Figure 5.9D). Our results indicated that VT-phage significantly induced and promoted osteoblastic differentiation of MSCs.
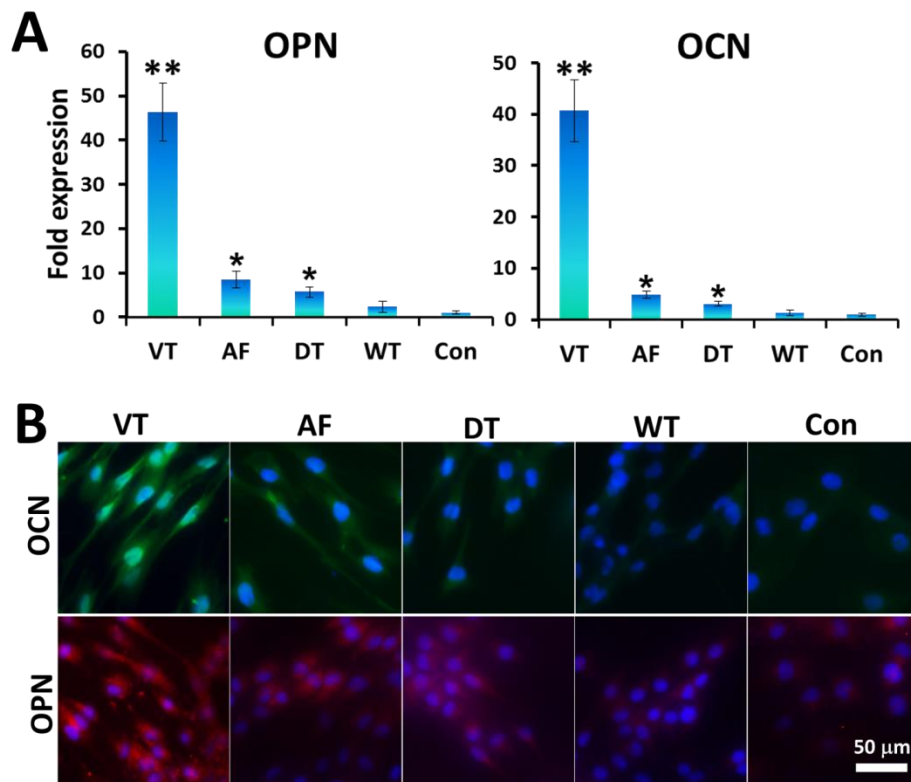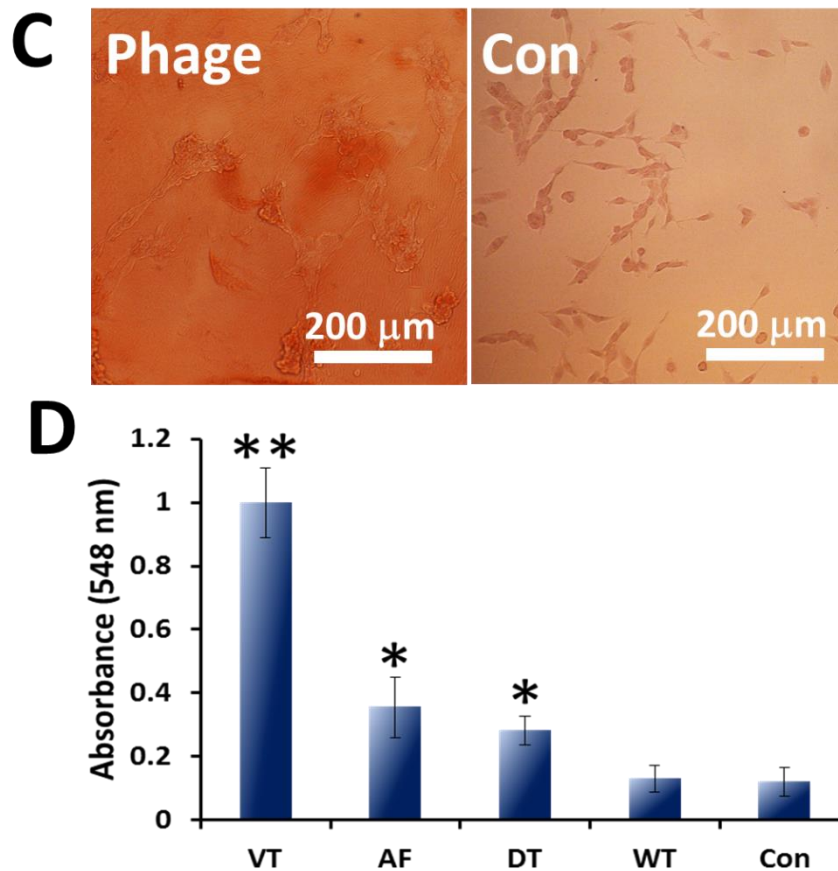
Figure 5.9 Osteogenic differentiation of MSCs on the phage films after MSCs were cultured in basal media for three weeks. A) Real-time PCR analysis of OCN and OPN mRNA expression (n=3). B) Immunofluorescence assay of OCN (green) and OPN (red) expression of MSCs on the phage films. OCN was marked with green fluorescent Alexa Fluor® 488 labeled antibody. OPN was marked with red fluorescent tetramethylrhodamine (TRITC) labeled antibody. Cell nuclei were stained with DAPI (blue). C) Alizarin red S staining of MSCs on the VT-phage

film and control polylysine substrate.   D) Quantitative analysis of mineralization of MSCs on the phages films (n=3). * denotes p<0.05, ** denotes p<0.01 compared with control.
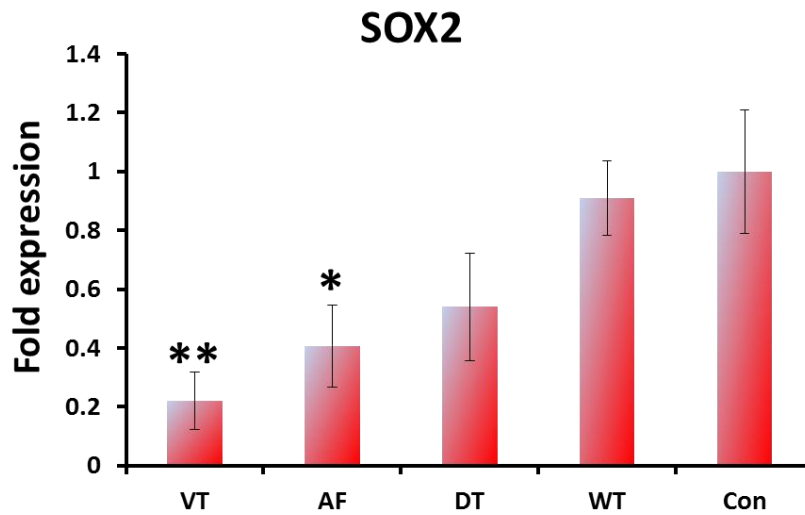
Figure 5.10   Real-time PCR analysis for pluripotency marker SOX2 mRNA expression (n=3). VT-phage down-regulated SOX2 gene expression when compared with control phage. * denotes p<0.05, ** denotes p<0.01 compared with control.
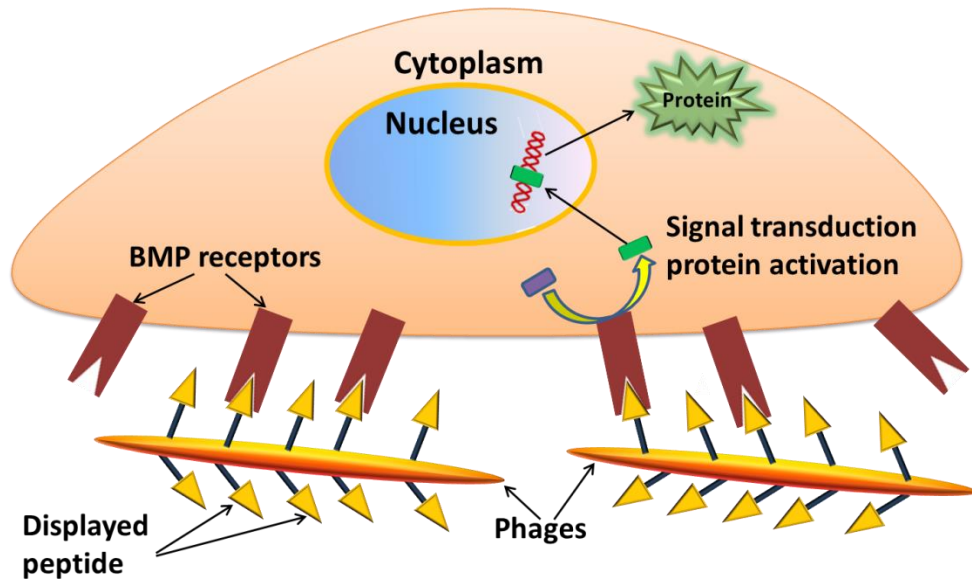
Figure 5.11 Schematic showing proposed mechanism of rMSCs differentiation induced by phage matrix. Displayed VT-peptide binds to BMP receptors. Specific signal transduction proteins are activated, then translocate to the cell nucleus and bind to DNA to regulate gene transcription. This results in osteogenic protein expression upregulation.

Amino acid of VT-Peptide	Amino acid of BMP-8A that shows similarity with VT-peptide
$_3$AMEPG$_7$	$_2$AMRPG$_6$
$_4$MEPG$_7$	$_{225}$MDPG$_{228}$

Table 5.1 Similarity between VT-peptide and BMP-8A (protein ID: P34821.1) revealed by BLAST.

Amino acid of VT-Peptide	Amino acid of BMP-11 that shows similarity with VT-peptide
$_1$VTAMEPG$_7$	$_{269}$VTSLGPG$_{275}$

Table 5.2 Similarity between VT-peptide and BMP-11 (protein ID: Q9Z1W4.1) revealed by BLAST.

5.4 Discussion

Peptide sequences as biochemical cues had been reported to influence proliferation and osteoblastic differentiation of stem cells. For example, osteogenic growth peptide (OGP) is a 14-amino acid peptide that mainly regulates proliferation, bone minerization and alkaline phosphatase activity[225,226]. OGP could bind to OGP-receptor so as to activate Gi protein mitogen-activated protein (MAP) kinases signaling cascade. In the meantime, MAP kinase has a pivotal role in the proliferation and osteogenic differentiation of human MSCs[225,227]. Miao *et al* reported a parathyroid hormone-related peptide enhanced rat bone marrow

osteogenic cell proliferation through activation of the Ras/MAP kinase signaling pathway[228]. Yang *et al* demonstrated that RGD peptide-tethered biomaterial stimulated osteogenesis of bone marrow-derived marrow stromal cells with enhanced alkaline phosphatase and OCN expression in a dose-dependent fashion[229]. Kiessling et al identified peptides binding to human embryonal carcinoma cells (ECs) using phage display and then found that these peptides, once immobilized on gold substrates, support the proliferation of undifferentiated human embryonal stem cells[99].

Our results indicate that there is a direct relationship between the rMSCs binding affinity of peptides identified by rMSCs and the osteogenic differentiation inducing capability of the rMSCs. Namely, the higher binding affinity results in better inducing capability of a peptide. VT-peptide displayed on the phage films significantly induced and promoted osteoblastic differentiation of rMSCs by up-regulating OCN and OPN gene expression, while down-regulating SOX2 gene expression. Other studies also showed that SOX2 down-regulation led to the loss of pluripotency and subsequent differentiation of MSCs[230].

To further understand the role of these peptides in inducing the osteogenic differentiation of MSCs, we carried protein blast of these sequence on national center for biotechnology information (NCBI)

database. Surprisingly, we found that amino acid position 2-6 and 225-228 of bone morphogenetic protein 8A (BMP8A), which is also known as osteogenic protein 2 (OP-2), are similar to the amino acid position 4-7 and 3-7 of the VT-peptide, respectively (Table 5.1). BMP8A is a growth factor that induces cartilage and bone formation and plays an important role in bone homeostasis and calcium regulation [231,232]. We also found that the amino acid position 1-7 of the VT-peptide is similar to the amino acid position 269-275 of another BMP, bone morphogenetic protein 11 (BMP11), also known as growth differentiation factor 11 (GDF11) (Table 5.2). It is known that BMP11 regulates axial skeletal patterning and limb skeletal formation [233-235]. Namely, the VT-peptide shows similarity with two BMPs that can regulate osteogenic differentiation. Interestingly, we did not find any similarity between other peptides (AF and DT) and these two BMPs.

Hence, we propose that VT-peptide binds to BMP receptors to initiate osteogenic differentiation pathway (Figure 5.11). Specific signal transduction proteins are then activated and translocate to the rMSCs nucleus. Osteogenic transcription factors are then recruited to regulate gene transcription. This results in OCN and OPN protein expression upregulation as well as calcium deposit formation. The future goal of our

study is to verify the signal transduction pathway on VT-peptide mediated

osteogenic induction.

Chapter 6

6.1 Summary of this dissertation

Stem cells hold great potential for the regenerative medicine and tissue engineering. Controlled delivery of specific genes to stem cells presents a promising strategy to alter the differentiation fate of stem cells. In this thesis, we developed non-viral vectors with efficient gene delivery and low toxicity to hard-to-transfect MSCs. MSCs demonstrated capacity to differentiate into cell types including osteogenic, chondrogenic, myogenic and adipogenic lineages. Also, they are easy to isolate and demonstrated significant expansion capability. As a result, MSCs are promising candidates for the regenerative medicine.

In chapter 2, we employed phage display technique and identified a peptide (VTAMEPGQ) that can home to rat mesenchymal stem cells (rMSCs). A nanoparticle, called liposome protamine/DNA lipoplex (LPD), is electrostatically assembled from cationic liposomes and an anionic complex of protamine, DNA and targeting peptides. Various peptides are enveloped inside the LPD to improve its targeting capability for rMSCs and nuclei. The rMSC-targeting peptide and nuclear localization signal (NLS) peptide can execute the synergetic effect to promote transfection action of LPD. The homing peptide directs the LPD

to target the MSCs, whereas the NLS peptide directs transposon to accumulate into nuclei once LPD is internalized inside the cells, leading to increased gene expression. This suggests that rMSC-targeting peptide and NLS peptide within LPD can target to rMSCs and then guide transposon uptake into nuclei. After entering the nuclei, the SB transposon increases the insertion rates into cellular chromosomes. The targeting LPD does not show obvious cell toxicity and influence on the differentiation potential of rMSCs. Therefore, the integration of SB transposon and LPD system may represent a promising non-viral gene delivery vector in stem cell therapy.

In chapter 3, we continued to improve the LPD based gene delivery system on rMSCs. We re-synthesized the LPD particle using a chemically defined faction. Also, we introduced three-folds reiterated targeting peptides and a vascular endothelial growth factor (VEGF) reporter gene. Overall, we developed a non-viral vector integrating lipids, sleeping beauty transposon system and 8-mer stem cell targeting peptides for safe and efficient gene delivery to MSCs. The 8-mer MSC-targeting peptides, when synthetically reiterated in three-folds and chemically presented on the surface, significantly promoted the resultant lipid-based nanoparticles (LBNs) to deliver VEGF gene into MSCs with a high transfection efficiency and long-lasting gene expression when compared

to non-reiterated peptides. However, the reiterated stem cell targeting peptides do not enable the highly efficient gene transfer to other control cells. This work suggests that the surface presentation of the reiterated stem cell-targeting peptides on the non-viral vectors is a promising method for improving the efficiency of cell-specific non-viral gene transfection in stem cells.

In chapter 4, we developed a non-viral vector integrating fusogenic and magnetic properties for safe and efficient gene delivery to MSCs. Glutathione (GSH) cleavable magnetic/silica nanoclusters are synthesized, where magnetic nanoparticles (NPs) are dispersed in a porous silica matrix by S-S bond. The porous structure can hold DNA with the aid of polyethyleneimine (PEI), which is further conjugated with MSC-homing major coat protein (pVIII) purified from the MSC-homing phage identified by using phage display technique. Due to the presence of pVIII on the surface, the resultant virus mimetic magnetic silica nanoclusters (VMSNCs) can transfect rat MSCs in a higher efficiency than commercially available non-viral vectors. The intracellular GSH is responsible for cleaving the S-S bond to dissociate the nanoclusters to release DNA. The VMSNCs bear MSC-homing phage-borne protein on the surface and encapsulate DNA inside, promoting the transfer of DNA into MSCs.

158

In chapter 5, we studied the osteogenic differentiation induction of rMSCs by rMSC-binding peptides with different binding affinities using phage-based matrix. The phage-based matrix has nearly constant architecture but different rMSC-binding peptides, enabling us to focus on and reveal a direct relationship between rMSC-binding affinities and osteogenic differentiation induction capabilities of the peptides. VTAMEPGQ, with the highest rMSC-binding affinity, was verified to most efficiently induce the osteogenic differentiation of rMSCs. Surprisingly, we found that VTAMEPGQ peptide shares good similarity in sequence with two BMPs. This result encourages us to hypothesize that the peptide binds to BMP receptor to initiate the osteogenic differentiation pathway.

In summary, first we discovered MSCs-targeting peptide sequence. Then we developed non-viral MSCs-targeting gene delivery vector with high gene transfection efficiency and sustained gene expression profile using the MSCs-targeting peptide or MSCs-targeting phage protein. We also discovered that the peptide (VTAMEPGQ) induced the osteogenic differentiation of MSCs efficiently. These specific targeting complexes may demonstrate promising applications in clinical stem cell-based therapy.

References

1   Thomson, J. A. *et al.* Embryonic stem cell lines derived from human blastocysts. *science* **282**, 1145-1147 (1998).

2   Chambers, I. & Smith, A. Self-renewal of teratocarcinoma and embryonic stem cells. *Oncogene* **23**, 7150-7160 (2004).

3   Takahashi, K. & Yamanaka, S. Induction of pluripotent stem cells from mouse embryonic and adult fibroblast cultures by defined factors. *Cell* **126**, 663-676 (2006).

4   Pera, M. F. & Tam, P. P. Extrinsic regulation of pluripotent stem cells. *Nature* **465**, 713-720 (2010).

5   Shah, N. M., Groves, A. K. & Anderson, D. J. Alternative Neural Crest Cell Fates Are Instructively Promoted by TGF Superfamily Members. *cell* **85**, 331-344 (1996).

6   Niwa, H., Miyazaki, J.-i. & Smith, A. G. Quantitative expression of Oct-3/4 defines differentiation, dedifferentiation or self-renewal of ES cells. *Nature genetics* **24**, 372-376 (2000).

7   Nichols, K., Black, D. L., Blake, S. & Baker, F. Definition of the differentiated services field (DS field) in the IPv4 and IPv6 headers. (1998).

8   Avilion, A. A. *et al.* Multipotent cell lineages in early mouse development depend on SOX2 function. *Genes & development* **17**, 126-140 (2003).

9   Masui, S. *et al.* Pluripotency governed by Sox2 via regulation of Oct3/4 expression in mouse embryonic stem cells. *Nature cell biology* **9**, 625-635 (2007).

10   Mitsui, K. *et al.* The homeoprotein Nanog is required for maintenance of pluripotency in mouse epiblast and ES cells. *cell* **113**, 631-642 (2003).

11   Shenghui, H., Nakada, D. & Morrison, S. J. Mechanisms of stem cell self-renewal. *Annual Review of Cell and Developmental* **25**, 377-406 (2009).

12   Takahashi, K. *et al.* Induction of pluripotent stem cells from adult human fibroblasts by defined factors. *cell* **131**, 861-872 (2007).

13   Schofield, R. The relationship between the spleen colony-forming cell and the haemopoietic stem cell. *Blood Cells* **4**, 7-25 (1978).

14   Lutolf, M. P., Gilbert, P. M. & Blau, H. M. Designing materials to direct stem-cell fate. *Nature* **462**, 433-441 (2009).

15   Discher, D. E., Mooney, D. J. & Zandstra, P. W. Growth factors, matrices, and forces combine and control stem cells. *Science* **324**, 1673-1677 (2009).

16   Guilak, F. *et al.* Control of stem cell fate by physical interactions with the extracellular matrix. *Cell Stem Cell* **5**, 17 (2009).

17   Li, L. & Xie, T. Stem cell niche: structure and function. *Annu. Rev. Cell Dev. Biol.* **21**, 605-631 (2005).

18   Moore, K. A., Ema, H. & Lemischka, I. R. In vitro maintenance of highly purified, transplantable hematopoietic stem cells. *Blood* **89**, 4337-4347 (1997).

19   Dexter, T., Moore, M. & Sheridan, A. Maintenance of hemopoietic stem cells and production of differentiated progeny in allogeneic and semiallogeneic bone marrow chimeras in vitro. *The Journal of experimental medicine* **145**, 1612-1616 (1977).

20   Brinster, R. L. & Zimmermann, J. W. Spermatogenesis following male germ-cell transplantation. *Proceedings of the National Academy of Sciences* **91**, 11298-11302 (1994).

21   Collins, C. A. *et al.* Stem cell function, self-renewal, and behavioral heterogeneity of cells from the adult muscle satellite cell niche. *cell* **122**, 289-301 (2005).

22   Morrison, S. J. & Spradling, A. C. Stem cells and niches: mechanisms that promote stem cell maintenance throughout life. *cell* **132**, 598-611 (2008).

23   Cotsarelis, G., Sun, T.-T. & Lavker, R. M. Label-retaining cells reside in the bulge area of pilosebaceous unit: implications for follicular stem cells, hair cycle, and skin carcinogenesis. *cell* **61**, 1329-1337 (1990).

24   Fuchs, E., Tumbar, T. & Guasch, G. Socializing with the neighbors: stem cells and their niche. *cell* **116**, 769-778 (2004).

25   Doetsch, F. A niche for adult neural stem cells. *Current opinion in genetics & development* **13**, 543-550 (2003).

26   Kiel, M. J. *et al.* SLAM family receptors distinguish hematopoietic stem and progenitor cells and reveal endothelial niches for stem cells. *cell* **121**, 1109-1121 (2005).

27   Yin, T. & Li, L. The stem cell niches in bone. *Journal of Clinical Investigation* **116**, 1195-1201 (2006).

28   Dong-Dong, W., Lin, W. & Chuanbin, M. in *Encyclopedia of Biomedical Polymers and Polymer Biomaterials* Vol. 11   7565-7576 (Taylor & Francis, 2015).

29   Friedenstein, A. J., Gorskaja, J. & Kulagina, N. Fibroblast precursors in normal and irradiated mouse hematopoietic organs. *Experimental hematology* **4**, 267-274 (1976).

30   Chamberlain, G., Fox, J., Ashton, B. & Middleton, J. Concise review: mesenchymal stem cells: their phenotype, differentiation capacity, immunological features, and potential for homing. *Stem cells* **25**, 2739-2749 (2007).

31   Ashton, B. A. *et al.* Formation of bone and cartilage by marrow stromal cells in diffusion chambers in vivo. *Clinical orthopaedics and related research* **151**, 294-307 (1980).

32   Moore, M. *et al.* Characterization of human bone marrow fibroblast colony-forming cells. *Blood* **56**, 289 (1980).

33   Scherjon, S. A. *et al.* Amniotic fluid as a novel source of mesenchymal stem cells for therapeutic transplantation. *Blood* **102**, 1548-1549 (2003).

34   Campagnoli, C. *et al.* Identification of mesenchymal stem/progenitor cells in human first-trimester fetal blood, liver, and bone marrow. *Blood* **98**, 2396-2402 (2001).

35   Pittenger, M. F. *et al.* Multilineage potential of adult human mesenchymal stem cells. *science* **284**, 143-147 (1999).

36   Mackay, A. M. *et al.* Chondrogenic differentiation of cultured human mesenchymal stem cells from marrow. *Tissue engineering* **4**, 415-428 (1998).

37   Wakitani, S., Saito, T. & Caplan, A. I. Myogenic cells derived from rat bone marrow mesenchymal stem cells exposed to 5‐azacytidine. *Muscle & nerve* **18**, 1417-1426 (1995).

38   Dezawa, M. *et al.* Specific induction of neuronal cells from bone marrow stromal cells and application for autologous transplantation. *Journal of Clinical Investigation* **113**, 1701 (2004).

39   Pack, D. W., Hoffman, A. S., Pun, S. & Stayton, P. S. Design and development of polymers for gene delivery. *Nature Reviews Drug Discovery* **4**, 581-593 (2005).

40   Van Deutekom, J. C. & Van Ommen, G.-J. B. Advances in Duchenne muscular dystrophy gene therapy. *Nature Reviews Genetics* **4**, 774-783 (2003).

41   Ferrari, S., Geddes, D. M. & Alton, E. W. Barriers to and new approaches for gene therapy and gene delivery in cystic fibrosis. *Advanced drug delivery reviews* **54**, 1373-1393 (2002).

42   Burton, E., Glorioso, J. & Fink, D. Gene therapy progress and prospects: Parkinson's disease. *Gene Therapy* **10**, 1721-1727 (2003).

43   Tuszynski, M. H. Growth-factor gene therapy for neurodegenerative disorders. *The Lancet Neurology* **1**, 51-57 (2002).

44   Dzau, V. J., Beatt, K., Pompilio, G. & Smith, K. Current perceptions of cardiovascular gene therapy. *The American journal of cardiology* **92**, 18-23 (2003).

45   Vile, R., Russell, S. & Lemoine, N. Cancer gene therapy: hard lessons and new courses. *Gene Therapy* **7**, 2-8 (2000).

46   Cavazzana-Calvo, M. *et al.* Gene therapy of human severe combined immunodeficiency (SCID)-X1 disease. *Science* **288**, 669-672 (2000).

47   L Santos, J. *et al.* Non-viral gene delivery to mesenchymal stem cells: methods, strategies and application in bone tissue engineering and regeneration. *Current gene therapy* **11**, 46-57 (2011).

48   Zwaka, T. P. Use of genetically modified stem cells in experimental gene therapies. *Regenerative medicine*, 45 (2006).

49   Pittenger, M., Vanguri, P., Simonetti, D. & Young, R. Adult mesenchymal stem cells: potential for muscle and tendon regeneration and use in

gene therapy. *Journal of Musculoskeletal and Neuronal Interactions* **2**, 309-320 (2002).

50   Saraf, A. & Mikos, A. G. Gene delivery strategies for cartilage tissue engineering. *Advanced drug delivery reviews* **58**, 592-603 (2006).

51   Edelstein, M. L., Abedi, M. R. & Wixon, J. Gene therapy clinical trials worldwide to 2007—an update. *The journal of gene medicine* **9**, 833-842 (2007).

52   Li, S.-D. & Huang, L. Non-viral is superior to viral gene delivery. *Journal of controlled release* **123**, 181-183 (2007).

53   Mastrobattista, E., Bravo, S. A., van der Aa, M. & Crommelin, D. J. Nonviral gene delivery systems: from simple transfection agents to artificial viruses. *Drug Discovery Today: Technologies* **2**, 103-109 (2005).

54   Winn, S. R., Hu, Y., Sfeir, C. & Hollinger, J. O. Gene therapy approaches for modulating bone regeneration. *Advanced drug delivery reviews* **42**, 121-138 (2000).

55   Hamm, A., Krott, N., Breibach, I., Blindt, R. & Bosserhoff, A. K. Efficient transfection method for primary cells. *Tissue engineering* **8**, 235-245 (2002).

56   Felgner, P. L. *et al.* Lipofection: a highly efficient, lipid-mediated DNA-transfection procedure. *Proceedings of the National Academy of Sciences* **84**, 7413-7417 (1987).

57   Duzgunes, N. *et al.* Cationic liposomes for gene delivery: novel cationic lipids and enhancement by proteins and peptides. *Current medicinal chemistry* **10**, 1213-1220 (2003).

58   Hoekstra, D., Rejman, J., Wasungu, L., Shi, F. & Zuhorn, I. Gene delivery by cationic lipids: in and out of an endosome. *Biochemical Society Transactions* **35**, 68 (2007).

59   Hoelters, J. *et al.* Nonviral genetic modification mediates effective transgene expression and functional RNA interference in human mesenchymal stem cells. *The journal of gene medicine* **7**, 718-728 (2005).

60   Ko, B., Chang, T., Shyue, S., Chen, Y. & Liou, J. An efficient transfection method for mouse embryonic stem cells. *Gene Therapy* **16**, 154-158 (2009).

61   Park, J. *et al.* The effect on bone regeneration of a liposomal vector to deliver BMP-2 gene to bone grafts in peri-implant bone defects. *Biomaterials* **28**, 2772-2782 (2007).

62   Park, J. *et al.* Bone regeneration in critical size defects by cell-mediated BMP-2 gene transfer: a comparison of adenoviral vectors and liposomes. *Gene Therapy* **10**, 1089-1098 (2003).

63   Luten, J., van Nostrum, C. F., De Smedt, S. C. & Hennink, W. E. Biodegradable polymers as non-viral carriers for plasmid DNA delivery. *Journal of controlled release* **126**, 97-110 (2008).

64   Dang, J. M. & Leong, K. W. Natural polymers for gene delivery and tissue engineering. *Advanced drug delivery reviews* **58**, 487-499 (2006).

65   Behr, J.-P. The proton sponge: a trick to enter cells the viruses did not exploit. *CHIMIA International Journal for Chemistry* **51**, 34-36 (1997).

66   Fischer, D., Bieber, T., Li, Y., Elsässer, H.-P. & Kissel, T. A novel non-viral vector for DNA delivery based on low molecular weight, branched polyethylenimine: effect of molecular weight on transfection efficiency and cytotoxicity. *Pharmaceutical research* **16**, 1273-1279 (1999).

67   Godbey, W., Wu, K. K. & Mikos, A. G. Size matters: molecular weight affects the efficiency of poly (ethyleneimine) as a gene delivery vehicle. *Journal of biomedical materials research* **45**, 268-275 (1999).

68   Ahn, H. H. *et al.* Polyethyleneimine-mediated gene delivery into human adipose derived stem cells. *Biomaterials* **29**, 2415-2422 (2008).

69   Abdelhady, H. G. *et al.* Direct real‑time molecular scale visualisation of the degradation of condensed DNA complexes exposed to DNase I. *Nucleic acids research* **31**, 4001-4005 (2003).

70   Schaffer, D. V., Fidelman, N. A., Dan, N. & Lauffenburger, D. A. Vector unpacking as a potential barrier for receptor‑mediated polyplex gene delivery. *Biotechnology and bioengineering* **67**, 598-606 (2000).

71   Dash, P., Read, M., Barrett, L., Wolfert, M. & Seymour, L. Factors affecting blood clearance and in vivo distribution of polyelectrolyte complexes for gene delivery. *Gene Therapy* **6**, 643-650 (1999).

72   Ogris, M., Brunner, S., Schüller, S., Kircheis, R. & Wagner, E. PEGylated DNA/transferrin-PEI complexes: reduced interaction with blood components, extended circulation in blood and potential for systemic gene delivery. *Gene Therapy* **6**, 595-605 (1999).

73   Toncheva, V. *et al.* Novel vectors for gene delivery formed by self-assembly of DNA with poly (L-lysine) grafted with hydrophilic polymers. *Biochimica et Biophysica Acta (BBA)-General Subjects* **1380**, 354-368 (1998).

74   Bettinger, T., Remy, J.-S. & Erbacher, P. Size reduction of galactosylated PEI/DNA complexes improves lectin-mediated gene transfer into hepatocytes. *Bioconjugate chemistry* **10**, 558-561 (1999).

75   Zanta, M.-A., Boussif, O., Adib, A. & Behr, J.-P. In vitro gene delivery to hepatocytes with galactosylated polyethylenimine. *Bioconjugate chemistry* **8**, 839-844 (1997).

76   Leamon, C. P., Weigl, D. & Hendren, R. W. Folate copolymer-mediated transfection of cultured cells. *Bioconjugate chemistry* **10**, 947-957 (1999).

77   Kircheis, R. *et al.* Coupling of cell-binding ligands to polyethylenimine for targeted gene delivery. *Gene Therapy* **4**, 409-418 (1997).

78   Schaffer, D. V., Neve, R. L. & Lauffenburger, D. A. Use of the green fluorescent protein as a quantitative reporter of epidermal growth factor receptor-mediated gene delivery. *Tissue engineering* **3**, 53-63 (1997).

79   Harbottle, R. P. *et al.* An RGD-oligolysine peptide: a prototype construct for integrin-mediated gene delivery. *Human gene therapy* **9**, 1037-1047 (1998).

80   Mukherjee, S., Ghosh, R. N. & Maxfield, F. R. Endocytosis. *Physiological reviews* **77**, 759-803 (1997).

81   Mislick, K. A. & Baldeschwieler, J. D. Evidence for the role of proteoglycans in cation-mediated gene transfer. *Proceedings of the National Academy of Sciences* **93**, 12349-12354 (1996).

82   Haensler, J. & Szoka Jr, F. C. Polyamidoamine cascade polymers mediate efficient transfection of cells in culture. *Bioconjugate chemistry* **4**, 372-379 (1993).

83   Boussif, O. *et al.* A versatile vector for gene and oligonucleotide transfer into cells in culture and in vivo: polyethylenimine. *Proceedings of the National Academy of Sciences* **92**, 7297-7301 (1995).

84   Lechardeur, D. *et al.* Metabolic instability of plasmid DNA in the cytosol: a potential barrier to gene transfer. *Gene Therapy* **6**, 482-497 (1999).

85   Subramanian, A., Ranganathan, P. & Diamond, S. L. Nuclear targeting peptide scaffolds for lipofection of nondividing mammalian cells. *Nature biotechnology* **17**, 873-877 (1999).

86   Kalderon, D., Roberts, B. L., Richardson, W. D. & Smith, A. E. A short amino acid sequence able to specify nuclear location. *Cell* **39**, 499-509 (1984).

87   Zanta, M. A., Belguise-Valladier, P. & Behr, J.-P. Gene delivery: a single nuclear localization signal peptide is sufficient to carry DNA to the cell

nucleus. *Proceedings of the National Academy of Sciences* **96**, 91-96 (1999).

88   Soen, Y., Mori, A., Palmer, T. D. & Brown, P. O. Exploring the regulation of human neural precursor cell differentiation using arrays of signaling microenvironments. *Molecular systems biology* **2** (2006).

89   Engler, A. J., Sen, S., Sweeney, H. L. & Discher, D. E. Matrix elasticity directs stem cell lineage specification. *Cell* **126**, 677-689 (2006).

90   Liao, S., Chan, C. K. & Ramakrishna, S. Stem cells and biomimetic materials strategies for tissue engineering. *Materials Science and Engineering: C* **28**, 1189-1202 (2008).

91   Li, Z., Leung, M., Hopper, R., Ellenbogen, R. & Zhang, M. Feeder-free self-renewal of human embryonic stem cells in 3D porous natural polymer scaffolds. *Biomaterials* **31**, 404-412 (2010).

92   Lutolf, M. *et al.* Synthetic matrix metalloproteinase-sensitive hydrogels for the conduction of tissue regeneration: engineering cell-invasion characteristics. *Proceedings of the National Academy of Sciences* **100**, 5413-5418 (2003).

93   Lutolf, M. P. *et al.* Repair of bone defects using synthetic mimetics of collagenous extracellular matrices. *Nature biotechnology* **21**, 513-518 (2003).

94   Willerth, S. M. & Sakiyama-Elbert, S. E. Combining stem cells and biomaterial scaffolds for constructing tissues and cell delivery. (2008).

95   Lampe, K. J. & Heilshorn, S. C. Building stem cell niches from the molecule up through engineered peptide materials. *Neuroscience Letters* **519**, 138-146 (2012).

96   Smith, G. P. Filamentous fusion phage: novel expression vectors that display cloned antigens on the virion surface. *Science* **228**, 1315-1317 (1985).

97   Ma, K. *et al.* Synergetic Targeted Delivery of Sleeping‐Beauty Transposon System to Mesenchymal Stem Cells Using LPD Nanoparticles Modified with a Phage‐Displayed Targeting Peptide. *Advanced Functional Materials* (2012).

98   Pasqualini, R. & Ruoslahti, E. Organ targeting in vivo using phage display peptide libraries. *Nature* **380**, 364-366 (1996).

99 Derda, R. *et al.* High-throughput discovery of synthetic surfaces that support proliferation of pluripotent cells. *Journal of the American Chemical Society* **132**, 1289-1295 (2010).

100 Caprini, A. *et al.* A Novel Bioactive Peptide: Assessing its Activity Over Murine Neural Stem Cells and its Potential for Neural Tissue Engineering. *New biotechnology* (2013).

101 Balian, G. *et al.* Peptides from Phage Display Library Modulate Gene Expression in Mesenchymal Cells and Potentiate Osteogenesis in Unicortical Bone Defects. *Journal of visualized experiments: JoVE* (2010).

102 Snyder, R. O. Adeno‐associated virus‐mediated gene delivery. *The Journal of Gene Medicine* **1**, 166-175 (1999).

103 Marshall, E. Gene therapy a suspect in leukemia-like disease. *Science* **298**, 34-35 (2002).

104 Verma, I. M. & Somia, N. Gene therapy-promises, problems and prospects. *Nature* **389**, 239-242 (1997).

105 Nishikawa, M. & Huang, L. Nonviral vectors in the new millennium: delivery barriers in gene transfer. *Human gene therapy* **12**, 861-870 (2001).

106   Arap, M. A. Phage display technology: applications and innovations. *Genetics and Molecular Biology* **28**, 1-9 (2005).

107   Yoo, M.-K. *et al.* Targeted delivery of chitosan nanoparticles to Peyer's patch using M cell-homing peptide selected by phage display technique. *Biomaterials* **31**, 7738-7747 (2010).

108   Gafni, Y. *et al.* Stem cells as vehicles for orthopedic gene therapy. *Gene therapy* **11**, 417-426 (2004).

109   Kalervo Väänänen, H. Mesenchymal stem cells. *Annals of medicine* **37**, 469-479 (2005).

110   Abbineni, G., Modali, S., Safiejko-Mroczka, B., Petrenko, V. A. & Mao, C. Evolutionary selection of new breast cancer cell-targeting peptides and phages with the cell-targeting peptides fully displayed on the major coat and their effects on actin dynamics during cell internalization. *Molecular pharmaceutics* **7**, 1629-1642 (2010).

111   Pi, Y. *et al.* Targeted delivery of non-viral vectors to cartilage in vivo using a chondrocyte-homing peptide identified by phage display. *Biomaterials* **32**, 6324-6332 (2011).

112   Kelly, K. A. *et al.* Targeted nanoparticles for imaging incipient pancreatic ductal adenocarcinoma. *PLoS medicine* **5**, e85 (2008).

113   Li, S.-D., Chono, S. & Huang, L. Efficient gene silencing in metastatic tumor by siRNA formulated in surface-modified nanoparticles. *Journal of Controlled Release* **126**, 77-84 (2008).

114   Masuda, T. *et al.* Envelope-type lipid nanoparticles incorporating a short PEG-lipid conjugate for improved control of intracellular trafficking and transgene transcription. *Biomaterials* **30**, 4806-4814 (2009).

115   LI, S. D. & Huang, L. Surface‐Modified LPD Nanoparticles for Tumor Targeting. *Annals of the New York Academy of Sciences* **1082**, 1-8 (2006).

116   Belur, L. R., Podetz-Pedersen, K., Frandsen, J. & McIvor, R. S. Lung-directed gene therapy in mice using the nonviral Sleeping Beauty transposon system. *Nature protocols* **2**, 3146-3152 (2007).

117   Hoare, M. *et al.* Enhanced lipoplex‐mediated gene expression in mesenchymal stem cells using reiterated nuclear localization sequence peptides. *The journal of gene medicine* **12**, 207-218 (2010).

118   Ivics, Z., Hackett, P. B., Plasterk, R. H. & Izsvák, Z. Molecular Reconstruction of< i> Sleeping Beauty</i>, a< i> Tc1</i>-like Transposon from Fish, and Its Transposition in Human Cells. *Cell* **91**, 501-510 (1997).

119   Izsvák, Z. & Ivics, Z. Sleeping beauty transposition: biology and applications for molecular therapy. *Molecular Therapy* **9**, 147-156 (2004).

120   Yant, S. R. *et al.* High-resolution genome-wide mapping of transposon integration in mammals. *Molecular and cellular biology* **25**, 2085-2094 (2005).

121   Geurts, A. M. *et al.* Structure-based prediction of insertion-site preferences of transposons into chromosomes. *Nucleic acids research* **34**, 2803-2811 (2006).

122   Berry, C., Hannenhalli, S., Leipzig, J. & Bushman, F. D. Selection of target sites for mobile DNA integration in the human genome. *PLoS computational biology* **2**, e157 (2006).

123   Hackett, P. B., Largaespada, D. A. & Cooper, L. J. A transposon and transposase system for human application. *Molecular Therapy* **18**, 674-683 (2010).

124   Hackett, P. B. Integrating DNA vectors for gene therapy. *Molecular therapy: the journal of the American Society of Gene Therapy* **15**, 10 (2007).

125   Oh, E. *et al.* Cellular uptake and fate of PEGylated gold nanoparticles is dependent on both cell-penetration peptides and particle size. *ACS Nano* **5**, 6434-6448 (2011).

126   Belur, L. R. *et al.* Gene insertion and long-term expression in lung mediated by the Sleeping Beauty transposon system. *Molecular Therapy* **8**, 501-507 (2003).

127   Bell, J. B., Aronovich, E. L., Schreifels, J. M., Beadnell, T. C. & Hackett, P. B. Duration of expression and activity of Sleeping Beauty transposase in mouse liver following hydrodynamic DNA delivery. *Molecular Therapy* **18**, 1796-1802 (2010).

128   Lin, E.-H. *et al.* Lifelong reporter gene imaging in the lungs of mice following polyethyleneimine-mediated sleeping-beauty transposon delivery. *Biomaterials* **32**, 1978-1985 (2011).

129   Jackson, K. A. *et al.* Regeneration of ischemic cardiac muscle and vascular endothelium by adult stem cells. *Journal of Clinical Investigation* **107**, 1395 (2001).

130   van der Bogt, K. E. *et al.* Comparison of different adult stem cell types for treatment of myocardial ischemia. *Circulation* **118**, S121-S129 (2008).

131   Arinzeh, T. L. *et al.* Allogeneic mesenchymal stem cells regenerate bone in a critical-sized canine segmental defect. *J. Bone Joint Surg.* **85**, 1927-1935 (2003).

132   Dupont, K. M. *et al.* Human stem cell delivery for treatment of large segmental bone defects. *Proc. Natl. Acad. Sci. USA* **107**, 3305-3310 (2010).

133   Reya, T., Morrison, S. J., Clarke, M. F. & Weissman, I. L. Stem cells, cancer, and cancer stem cells. *nature* **414**, 105-111 (2001).

134   Tang, C., Ang, B. T. & Pervaiz, S. Cancer stem cell: target for anti-cancer therapy. *The FASEB Journal* **21**, 3777-3785 (2007).

135   Caplan, A. Why are MSCs therapeutic? New data: new insight. *J. Pathol.* **217**, 318-324 (2009).

136   Ferrara, N., Gerber, H.-P. & LeCouter, J. The biology of VEGF and its receptors. *Nature Med.* **9**, 669-676 (2003).

137   Arinzeh, T. L. *et al.* Allogeneic mesenchymal stem cells regenerate bone in a critical-sized canine segmental defect. *The Journal of Bone & Joint Surgery* **85**, 1927-1935 (2003).

138   Wang, Y. *et al.* Combining pharmacological mobilization with intramyocardial delivery of bone marrow cells over-expressing VEGF is

more effective for cardiac repair. *Journal of molecular and cellular cardiology* **40**, 736-745 (2006).

139   Matsumoto, R. *et al.* Vascular endothelial growth factor–expressing mesenchymal stem cell transplantation for the treatment of acute myocardial infarction. *Arteriosclerosis, thrombosis, and vascular biology* **25**, 1168-1173 (2005).

140   Xiong, N. *et al.* VEGF-expressing human umbilical cord mesenchymal stem cells, an improved therapy strategy for Parkinson's disease. *Gene Therapy* **18**, 394-402 (2011).

141   Naldini, L. *et al.* In vivo gene delivery and stable transduction of nondividing cells by a lentiviral vector. *Science* **272**, 263-267 (1996).

142   Xia, H., Mao, Q., Paulson, H. L. & Davidson, B. L. siRNA-mediated gene silencing in vitro and in vivo. *Nature Biotechnol.* **20**, 1006-1010 (2002).

143   Huang, F., Dempsey, C., Chona, D. & Suh, J. Quantitative nanoparticle tracking: applications to nanomedicine. *Nanomedicine* **6**, 693-700 (2011).

144   Thomas, C. E., Ehrhardt, A. & Kay, M. A. Progress and problems with the use of viral vectors for gene therapy. *Nature Rev. Genetics* **4**, 346-358 (2003).

145   Chen, X. *et al.* Nanoparticle delivery of stable miR-199a-5p agomir improves the osteogenesis of human mesenchymal stem cells via the HIF1a pathway. *Biomaterials* **53**, 239-250 (2015).

146   Hsu, S.-h., Ho, T.-T. & Tseng, T.-C. Nanoparticle uptake and gene transfer efficiency for MSCs on chitosan and chitosan-hyaluronan substrates. *Biomaterials* **33**, 3639-3650 (2012).

147   Corsi, K., Chellat, F., Yahia, L. H. & Fernandes, J. C. Mesenchymal stem cells, MG63 and HEK293 transfection using chitosan-DNA nanoparticles. *Biomaterials* **24**, 1255-1264 (2003).

148   Deng, W. W. *et al.* Delivery of a transforming growth factor β-1 plasmid to mesenchymal stem cells via cationized Pleurotus eryngii polysaccharide nanoparticles. *International journal of nanomedicine* **7**, 1297 (2012).

149   Madeira, C. *et al.* Nonviral gene delivery to mesenchymal stem cells using cationic liposomes for gene and cell therapy. *J. Biomed. Biotechnol.* **2010** (2010).

150   KC, R. B., Kucharski, C. & Uludağ, H. Additive nanocomplexes of cationic lipopolymers for improved non-viral gene delivery to mesenchymal stem cells. *Journal of Materials Chemistry B* **3**, 3972-3982 (2015).

151   Cui, Z.-K. *et al.* Delivery of siRNA via cationic Sterosomes to enhance osteogenic differentiation of mesenchymal stem cells. *Journal of Controlled Release* **217**, 42-52 (2015).

152   Santos, J. L. *et al.* Functionalization of poly (amidoamine) dendrimers with hydrophobic chains for improved gene delivery in mesenchymal stem cells. *Journal of Controlled Release* **144**, 55-64 (2010).

153   Miao, T., Rao, K. S., Spees, J. L. & Oldinski, R. A. Osteogenic differentiation of human mesenchymal stem cells through alginate-graft-poly (ethylene glycol) microsphere-mediated intracellular growth factor delivery. *Journal of Controlled Release* **192**, 57-66 (2014).

154   Ma, K. *et al.* Synergetic Targeted Delivery of Sleeping‐Beauty Transposon System to Mesenchymal Stem Cells Using LPD Nanoparticles Modified with a Phage‐Displayed Targeting Peptide. *Adv. Funct. Mater.* (2012).

155   Tkachenko, A. G. *et al.* Cellular trajectories of peptide-modified gold particle complexes: comparison of nuclear localization signals and peptide transduction domains. *Bioconj. Chem.* **15**, 482-490 (2004).

156   Zanta, M. A., Belguise-Valladier, P. & Behr, J.-P. Gene delivery: a single nuclear localization signal peptide is sufficient to carry DNA to the cell nucleus. *Proc. Natl. Acad. Sci. USA* **96**, 91-96 (1999).

157   Mátés, L. *et al.* Molecular evolution of a novel hyperactive Sleeping Beauty transposase enables robust stable gene transfer in vertebrates. *Nature genetics* **41**, 753-761 (2009).

158   Dupuy, A. J., Akagi, K., Largaespada, D. A., Copeland, N. G. & Jenkins, N. A. Mammalian mutagenesis using a highly mobile somatic Sleeping Beauty transposon system. *nature* **436**, 221-226 (2005).

159   Hoare, M. *et al.* Enhanced lipoplex‐mediated gene expression in mesenchymal stem cells using reiterated nuclear localization sequence peptides. *J. Gene Med.* **12**, 207-218 (2010).

160   Sorgi, F., Bhattacharya, S. & Huang, L. Protamine sulfate enhances lipid-mediated gene transfer. *Gene Therapy* **4**, 961-968 (1997).

161   Li, S., Rizzo, M., Bhattacharya, S. & Huang, L. Characterization of cationic lipid-protamine-DNA (LPD) complexes for intravenous gene delivery. *Gene Therapy* **5**, 930 (1998).

162   Gandra, N., Wang, D. D., Zhu, Y. & Mao, C. Virus‐Mimetic Cytoplasm‐Cleavable Magnetic/Silica Nanoclusters for Enhanced Gene Delivery to Mesenchymal Stem Cells. *Ang. Chem. Int. Ed.* **125**, 11488-11491 (2013).

184

163   Chono, S., Li, S.-D., Conwell, C. C. & Huang, L. An efficient and low immunostimulatory nanoparticle formulation for systemic siRNA delivery to the tumor. *J. Control. Release* **131**, 64-69 (2008).

164   Iyer, A. K. *et al.* The effect of internalizing human single chain antibody fragment on liposome targeting to epithelioid and sarcomatoid mesothelioma. *Biomaterials* **32**, 2605-2613 (2011).

165   Iden, D. L. & Allen, T. M. In vitro and in vivo comparison of immunoliposomes made by conventional coupling techniques with those made by a new post-insertion approach. *Biochim. Biophys. Acta* **1513**, 207-216 (2001).

166   Aoyama, T., Hosseinkhani, H., Yamamoto, S., Ogawa, O. & Tabata, Y. Enhanced expression of plasmid DNA–cationized gelatin complex by ultrasound in murine muscle. *Journal of controlled release* **80**, 345-356 (2002).

167   Hosseinkhani, H. & Tabata, Y. Ultrasound enhances in vivo tumor expression of plasmid DNA by PEG-introduced cationized dextran. *Journal of Controlled Release* **108**, 540-556 (2005).

168   Deuse, T. *et al.* Hepatocyte growth factor or vascular endothelial growth factor gene transfer maximizes mesenchymal stem cell–based

myocardial salvage after acute myocardial infarction. *Circulation* **120**, S247-S254 (2009).

169   Pons, J. *et al.* VEGF improves survival of mesenchymal stem cells in infarcted hearts. *Biochem. Biophys. Res. Comm.* **376**, 419-422 (2008).

170   Liu, B., Li, X., Liang, G. & Liu, X. VEGF expression in mesenchymal stem cells promotes bone formation of tissue-engineered bones. *Mol. Med. Rep.* **4**, 1121-1126 (2011).

171   Moon, H.-H. *et al.* MSC-based VEGF gene therapy in rat myocardial infarction model using facial amphipathic bile acid-conjugated polyethyleneimine. *Biomaterials* **35**, 1744-1754 (2014).

172   Wang, D.-D., Yang, M., Zhu, Y. & Mao, C. Reiterated Targeting Peptides on the Nanoparticle Surface Significantly Promote Targeted Vascular Endothelial Growth Factor Gene Delivery to Stem Cells. *Biomacromolecules* (2015).

173   Kocher, A. A. *et al.* Neovascularization of ischemic myocardium by human bone-marrow-derived angioblasts prevents cardiomyocyte apoptosis, reduces remodeling and improves cardiac function. *Nat. Med.* **7**, 430-436 (2001).

174   Woodbury, D., Schwarz, E. J., Prockop, D. J. & Black, I. B. Adult rat and human bone marrow stromal cells differentiate into neurons. *J. Neurosci. Res.* **61**, 364-370 (2000).

175   Hofstetter, C. P. *et al.* Marrow stromal cells form guiding strands in the injured spinal cord and promote recovery. *Proc. Natl. Acad. Sci. U.S.A.* **99**, 2199-2204, doi:10.1073/pnas.042678299 (2002).

176   Chen, F. M., Zhang, M. & Wu, Z. F. Toward delivery of multiple growth factors in tissue engineering. *Biomaterials* **31**, 6279-6308, doi:10.1016/j.biomaterials.2010.04.053 (2010).

177   Naldini, L. *et al.* In vivo gene delivery and stable transduction of nondividing cells by a lentiviral vector. *Science* **272**, 263-267 (1996).

178   Xia, H. B., Mao, Q. W., Paulson, H. L. & Davidson, B. L. siRNA-mediated gene silencing in vitro and in vivo. *Nat. Biotechnol.* **20**, 1006-1010, doi:10.1038/nbt739 (2002).

179   He, T. C. *et al.* A simplified system for generating recombinant adenoviruses. *P Natl Acad Sci USA* **95**, 2509-2514, doi:10.1073/pnas.95.5.2509 (1998).

180   Corsi, K., Chellat, F., Yahia, L. & Fernandes, J. C. Mesenchymal stem cells, MG63 and HEK293 transfection using chitosan-DNA nanoparticles. *Biomaterials* **24**, 1255-1264 (2003).

181   Dobson, J. Gene therapy progress and prospects: magnetic nanoparticle-based gene delivery. *Gene Ther* **13**, 283-287, doi:10.1038/sj.gt.3302720 (2006).

182   Prabha, S., Zhou, W. Z., Panyam, J. & Labhasetwar, V. Size-dependency of nanoparticle-mediated gene transfection: studies with fractionated nanoparticles. *Int. J. Pharm.* **244**, 105-115 (2002).

183   de Lima, M. C. P., Simoes, S., Pires, P., Faneca, H. & Duzgunes, N. Cationic lipid-DNA complexes in gene delivery: from biophysics to biological applications. *Adv. Drug Delivery Rev.* **47**, 277-294 (2001).

184   Wasungu, L. & Hoekstra, D. Cationic lipids, lipoplexes and intracellular delivery of genes. *J. Controlled Release* **116**, 255-264, doi:10.1016/j.jconrel.2006.06.024 (2006).

185   Park, T. G., Jeong, J. H. & Kim, S. W. Current status of polymeric gene delivery systems. *Adv. Drug Delivery Rev.* **58**, 467-486, doi:10.1016/j.addr.2006.03.007 (2006).

186   Wieland, J. A., Houchin-Ray, T. L. & Shea, L. D. Non-viral vector delivery from PEG-hyaluronic acid hydrogels. *J. Controlled Release* **120**, 233-241, doi:10.1016/j.jconrel.2007.04.015 (2007).

187   Ellman, G. L. Tissue sulfhydryl groups. *Archives of biochemistry and biophysics* **82**, 70-77 (1959).

188   Knippers, R. & Hoffmann-Berling, H. A coat protein from bacteriophage fd: I. Hydrodynamic measurements and biological characterization. *Journal of molecular biology* **21**, 281-292 (1966).

189   Ma, K. *et al.* Synergetic Targeted Delivery of Sleeping‐Beauty Transposon System to Mesenchymal Stem Cells Using LPD Nanoparticles Modified with a Phage‐Displayed Targeting Peptide. *Advanced functional materials* **23**, 1172-1181 (2013).

190   Gandra, N. *et al.* Bacteriophage Bionanowire as a Carrier for Both Cancer-Targeting Peptides and Photosensitizers and its use in Selective Cancer Cell Killing by Photodynamic Therapy. *Small*, doi: 10.1002/smll.201202090, doi:10.1002/smll.201202090 (2012).

191   Ma, K. *et al.* Synergetic Targeted Delivery of Sleeping-Beauty Transposon System to Mesenchymal Stem Cells Using LPD Nanoparticles Modified with a Phage-Displayed Targeting Peptide. *Adv. Funct. Mater.*, doi: 10.1002/adfm.201102963, doi:10.1002/adfm.201102963 (2012).

192   Knippers, R. & Hoffmann-Berling, H. A coat protein from bacteriophage fd: I. Hydrodynamic measurements and biological characterization. *J. Mol. Biol.* **21**, 281-292, doi:10.1016/0022-2836(66)90099-4 (1966).

193   Hong, R. *et al.* Glutathione-mediated delivery and release using monolayer protected nanoparticle carriers. *Journal of the American Chemical Society* **128**, 1078-1079 (2006).

194   Cheng, R. *et al.* Glutathione-responsive nano-vehicles as a promising platform for targeted intracellular drug and gene delivery. *Journal of Controlled Release* **152**, 2-12 (2011).

195   Cheng, F. Y. *et al.* Characterization of aqueous dispersions of Fe3O4 nanoparticles and their biomedical applications. *Biomaterials* **26**, 729-738, doi:10.1016/j.biomaterials.2004.03.016 (2005).

196   Abbineni, G., Modali, S., Safiejko-Mroczka, B., Petrenko, V. A. & Mao, C. Evolutionary Selection of New Breast Cancer Cell-Targeting Peptides and Phages with the Cell-Targeting Peptides Fully Displayed on the Major Coat and Their Effects on Actin Dynamics during Cell Internalization. *Mol. Pharmaceutics* **7**, 1629-1642, doi:10.1021/mp100052y (2010).

197   Lutolf, M. P. & Blau, H. M. Artificial stem cell niches. *Advanced Materials* **21**, 3255-3268 (2009).

198   Reilly, G. C. & Engler, A. J. Intrinsic extracellular matrix properties regulate stem cell differentiation. *Journal of biomechanics* **43**, 55-62 (2010).

199   Trappmann, B. *et al.* Extracellular-matrix tethering regulates stem-cell fate. *Nature materials* **11**, 642-649 (2012).

200   Watt, F. M. & Huck, W. T. Role of the extracellular matrix in regulating stem cell fate. *Nature Reviews Molecular Cell Biology* **14**, 467-473 (2013).

201   McBeath, R., Pirone, D. M., Nelson, C. M., Bhadriraju, K. & Chen, C. S. Cell shape, cytoskeletal tension, and RhoA regulate stem cell lineage commitment. *Developmental cell* **6**, 483-495 (2004).

202   Chowdhury, F. *et al.* Material properties of the cell dictate stress-induced spreading and differentiation in embryonic stem cells. *Nature materials* **9**, 82-88 (2009).

203   Patel, S. *et al.* Bioactive nanofibers: synergistic effects of nanotopography and chemical signaling on cell guidance. *Nano letters* **7**, 2122-2128 (2007).

204   Oh, S. *et al.* Stem cell fate dictated solely by altered nanotube dimension. *Proceedings of the National Academy of Sciences* **106**, 2130-2135 (2009).

205   Chung, W.-J. *et al.* Biomimetic self-templating supramolecular structures. *Nature* **478**, 364-368 (2011).

206   Gilbert, P. M. *et al.* Substrate elasticity regulates skeletal muscle stem cell self-renewal in culture. *Science* **329**, 1078-1081 (2010).

207   Hu, B.-Y. *et al.* Neural differentiation of human induced pluripotent stem cells follows developmental principles but with variable potency. *Proceedings of the National Academy of Sciences* **107**, 4335-4340 (2010).

208   Murphy, C. M., Haugh, M. G. & O'Brien, F. J. The effect of mean pore size on cell attachment, proliferation and migration in collagen–glycosaminoglycan scaffolds for bone tissue engineering. *Biomaterials* **31**, 461-466 (2010).

209   Kubota, H., Avarbock, M. R. & Brinster, R. L. Growth factors essential for self-renewal and expansion of mouse spermatogonial stem cells. *Proceedings of the National Academy of Sciences of the United States of America* **101**, 16489-16494 (2004).

210   Calvi, L. *et al.* Osteoblastic cells regulate the haematopoietic stem cell niche. *Nature* **425**, 841-846 (2003).

211   López-Noriega, A. *et al.* Thermally triggered release of a pro-osteogenic peptide from a functionalized collagen-based scaffold using

thermosensitive liposomes. *Journal of controlled release* **187**, 158-166 (2014).

212   Sun, W. *et al.* Viability and neuronal differentiation of neural stem cells encapsulated in silk fibroin hydrogel functionalized with an IKVAV peptide. *Journal of tissue engineering and regenerative medicine* (2015).

213   Jabbari, E. Osteogenic peptides in bone regeneration. *Current pharmaceutical design* **19**, 3391-3402 (2013).

214   Kim, H. K. *et al.* Osteogenesis induced by a bone forming peptide from the prodomain region of BMP-7. *Biomaterials* **33**, 7057-7063 (2012).

215   He, X., Ma, J. & Jabbari, E. Effect of grafting RGD and BMP-2 protein-derived peptides to a hydrogel substrate on osteogenic differentiation of marrow stromal cells. *Langmuir* **24**, 12508-12516 (2008).

216   Prisco, A. & De Berardinis, P. Filamentous bacteriophage fd as an antigen delivery system in vaccination. *International journal of molecular sciences* **13**, 5179-5194 (2012).

217   Gandra, N., Wang, D. D., Zhu, Y. & Mao, C. Virus‐Mimetic Cytoplasm‐Cleavable Magnetic/Silica Nanoclusters for Enhanced Gene Delivery to Mesenchymal Stem Cells. *Angewandte Chemie* **125**, 11488-11491 (2013).

218   Yoo, P. J. *et al.* Spontaneous assembly of viruses on multilayered polymer surfaces. *Nature materials* **5**, 234-240 (2006).

219   Housby, J. N. & Mann, N. H. Phage therapy. *Drug discovery today* **14**, 536-540 (2009).

220   Moradpour, Z. & Ghasemian, A. Modified phages: novel antimicrobial agents to combat infectious diseases. *Biotechnology advances* **29**, 732-738 (2011).

221   Wang, J., Wang, L., Li, X. & Mao, C. Virus activated artificial ECM induces the osteoblastic differentiation of mesenchymal stem cells without osteogenic supplements. *Scientific reports* **3** (2013).

222   Zhu, H. *et al.* Controlled growth and differentiation of MSCs on grooved films assembled from monodisperse biological nanofibers with genetically tunable surface chemistries. *Biomaterials* **32**, 4744-4752 (2011).

223   Dalby, M. J. *et al.* The control of human mesenchymal cell differentiation using nanoscale symmetry and disorder. *Nature materials* **6**, 997-1003 (2007).

224   Molinuevo, M. S. *et al.* Effect of metformin on bone marrow progenitor

cell differentiation: in vivo and in vitro studies. *Journal of Bone and*

Mineral Research **25**, 211-221 (2010).

225   Gabarin, N. *et al.* Mitogenic Gi protein‐MAP kinase signaling cascade in

MC3T3‐E1 osteogenic cells: Activation by C‐terminal pentapeptide of

osteogenic growth peptide [OGP (10–14)] and attenuation of

activation by cAMP. *Journal of cellular biochemistry* **81**, 594-603 (2001).

226   Robinson, D., Bab, I. & Nevo, Z. Osteogenic growth peptide regulates

proliferation and osteogenic maturation of human and rabbit bone

marrow stromal cells. *Journal of Bone and Mineral Research* **10**, 690-696

(1995).

227   Jaiswal, R. K. *et al.* Adult human mesenchymal stem cell differentiation

to the osteogenic or adipogenic lineage is regulated by mitogen-

activated protein kinase. *Journal of Biological Chemistry* **275**, 9645-9652

(2000).

228   Miao, D. *et al.* Parathyroid hormone-related peptide stimulates

osteogenic cell proliferation through protein kinase C activation of the

Ras/mitogen-activated protein kinase signaling pathway. *Journal of*

Biological Chemistry **276**, 32204-32213 (2001).

229 Yang, F. *et al.* The effect of incorporating RGD adhesive peptide in polyethylene glycol diacrylate hydrogel on osteogenesis of bone marrow stromal cells. *Biomaterials* **26**, 5991-5998 (2005).

230 Park, S. *et al.* SOX2 has a crucial role in the lineage determination and proliferation of mesenchymal stem cells through Dickkopf-1 and c-MYC. *Cell Death & Differentiation* **19**, 534-545 (2012).

231 Carreira, A. C., Alves, G. G., Zambuzzi, W. F., Sogayar, M. C. & Granjeiro, J. M. Bone morphogenetic proteins: Structure, biological function and therapeutic applications. *Archives of biochemistry and biophysics* **561**, 64-73 (2014).

232 Lories, R. J. & Luyten, F. P. Bone morphogenetic protein signaling in joint homeostasis and disease. *Cytokine & growth factor reviews* **16**, 287-298 (2005).

233 Li, Z. *et al.* Transgenic overexpression of bone morphogenetic protein 11 propeptide in skeleton enhances bone formation. *Biochemical and biophysical research communications* **416**, 289-292 (2011).

234 McPherron, A. C., Lawler, A. M. & Lee, S.-J. Regulation of anterior/posterior patterning of the axial skeleton by growth/differentiation factor 11. *Nature genetics* **22**, 260-264 (1999).

235   Gamer, L. W., Cox, K. A., Small, C. & Rosen, V. Gdf11 is a negative regulator of chondrogenesis and myogenesis in the developing chick limb. *Developmental biology* **229**, 407-420 (2001).